REPORT DOCUMENTATION PAGE

Form Approved OMB NO. 0704-0188

1. REPORT DATE (DD-MM-YYYY)	2. REPORT TYPE	3. DATES COVERED (From - To)
15-07-2015	Final Report	18-Apr-2011 - 17-Apr-2015

4. TITLE AND SUBTITLE
Final Report: Research and Education in Development of Multifunctional Sensors and MEMS Devices

5a. CONTRACT NUMBER
W911NF-11-1-0133

5b. GRANT NUMBER

5c. PROGRAM ELEMENT NUMBER
206022

6. AUTHORS
Bahoura Messaoud, Pradhan Aswini, Williams Frances, Skuza Jonathan, Xiao Bo, Geddis Demetris

5d. PROJECT NUMBER

5e. TASK NUMBER

5f. WORK UNIT NUMBER

7. PERFORMING ORGANIZATION NAMES AND ADDRESSES
Norfolk State University
700 Park Avenue
McDemmond Center for Applied Research, Suite 601
Norfolk, VA 23504 -8060

8. PERFORMING ORGANIZATION REPORT NUMBER

9. SPONSORING/MONITORING AGENCY NAME(S) AND ADDRESS (ES)
U.S. Army Research Office
P.O. Box 12211
Research Triangle Park, NC 27709-2211

10. SPONSOR/MONITOR'S ACRONYM(S)
ARO

11. SPONSOR/MONITOR'S REPORT NUMBER(S)
58990-EL-REP.28

12. DISTRIBUTION AVAILIBILITY STATEMENT
Approved for Public Release; Distribution Unlimited

13. SUPPLEMENTARY NOTES
The views, opinions and/or findings contained in this report are those of the author(s) and should not contrued as an official Department of the Army position, policy or decision, unless so designated by other documentation.

14. ABSTRACT
We have investigated the growth of a family of lead zirconate titanate (PZT) type materials for MEMS and sensors applications. We successfully demonstrated the growth of high quality (011) PZT single perovskite phase films on ZnO/glass substrates with an MgO buffer seed layer. A butterfly shape of the capacitance curves were exhibited in the capacitance-voltage measurements. We demonstrated several flexible ways to produce three-dimensional nanostructure stacking with ultrathin film deposition to achieve high degree of freedom in fabrication and high sensitivity detection. We developed a three-dimensional SnO2–ZnO hybrid nanostructures composites that is

15. SUBJECT TERMS
MEMS, Actuators, Unmanned Aerial Vehicles (UAVs), perovskite, PZT, ZnO, Barium strontium titanate (BST), Barium Titanate (BTO), Al doped ZnO (AZO), Silicon dioxide, GaN, MgO, Tin Oxides (SnO2), Oxide Semiconductors, nanodots and nanowires,

16. SECURITY CLASSIFICATION OF:			17. LIMITATION OF ABSTRACT	15. NUMBER OF PAGES	19a. NAME OF RESPONSIBLE PERSON
a. REPORT	b. ABSTRACT	c. THIS PAGE			Messaoud Bahoura
UU	UU	UU	UU		19b. TELEPHONE NUMBER 757-823-2672

Report Title

Final Report: Research and Education in Development of Multifunctional Sensors and MEMS Devices

ABSTRACT

We have investigated the growth of a family of lead zirconate titanate (PZT) type materials for MEMS and sensors applications. We successfully demonstrated the growth of high quality (011) PZT single perovskite phase films on ZnO/glass substrates with an MgO buffer seed layer. A butterfly shape of the capacitance curves were exhibited in the capacitance-voltage measurements. We demonstrated several flexible ways to produce three-dimensional nanostructure stacking with ultrathin film deposition to achieve high degree of freedom in fabrication and high sensitivity detection. We developed a three-dimensional SnO2–ZnO hybrid nanostructures composites that is suitable for vapor/gas sensing.

We fabricated Flexural Plate Wave that is highly sensitive to surface perturbations and indirectly sense analytes by detecting mass changes on the sensing plate surface with a sensitivity of 0.0424 m2/g. In addition, we fabricated thin-film bulk acoustic resonator, where we investigated the influence of the PZT layer thinness on the system's resonance frequency. A functionally modified bimorph actuator with enhanced UAV aerodynamics and maneuverability was fabricated.

Many graduate and undergraduate underrepresented minority students were supported and trained on MEMS and materials growth, synthesis and characterization. Several seminars and professional development were organized. Our STEM outreach activities reached over 6,000 K-12 students.

Enter List of papers submitted or published that acknowledge ARO support from the start of the project to the date of this printing. List the papers, including journal references, in the following categories:

(a) Papers published in peer-reviewed journals (N/A for none)

Received		Paper
05/13/2013	3.00	Rajeh M. Mundle, Hampton S. Terry, Kevin Santiago, Dante Shaw, Messaoud Bahoura , Aswini K. Pradhan. Electrical conductivity and photoresistance of atomic layer depositedAl-doped ZnO films, Journal of Vacuum Science and Technology A, (12 2012): 146. doi:
05/13/2013	4.00	Kevin Santiago, Rajeh Mundle, Chandan B. Samantaray, M. Bahoura, A. K. Pradhan. Nanopatterning of atomic layer depositedAl:ZnO films using electron beam lithographyfor waveguide applications in the NIR region, Optical Materials Express, (12 2012): 1743. doi:
06/07/2013	7.00	R. B. Konda, C. White, D. Thomas, Q. Yang, A. K. Pradhan. Electrical characteristics of ZrO2/GaAs MOS capacitor fabricated by atomic layer deposition, Journal of Vacuum Science and Technology A, (05 2013): 41505. doi:
06/07/2013	9.00	R. Mundle, T. Holloway, K. Zhang, M. Bahoura, A. K. Pradhan. Effects of Surface Potential on Growth of ZnO Nanorod Arrays Investigated by Electric Force Microscopy, Journal of Nanoscience and Nanotechnology, (05 2012): 3938. doi:
06/07/2013	8.00	Bo Xiao, Qiguang Yang, Brandon Walker, Casey A. Gonder, Gari C. Romain, Rajeh Mundle, Messaoud Bahoura, A. K. Pradhan. Competition between (001) and (111) MgO thin film growth on Al-doped ZnO by oxygen plasma assisted pulsed laser deposition, Journal of Applied Physics, (06 2013): 214102. doi:
07/13/2015	22.00	A. K. Pradhan, R. M. Mundle, Kevin Santiago, J. R. Skuza, Bo Xiao, K. D. Song, M. Bahoura, Ramez Cheaito, Patrick E. Hopkins. Extreme tunability in aluminum doped Zinc Oxide plasmonic materials for near-infrared applications, Scientific Reports, (09 2014): 0. doi: 10.1038/srep06415
07/13/2015	23.00	Aswini K. Pradhan, Bo Xiao, Brandon Walker. Low temperature fabrication of high performance ZnO thin film transistors with high-k dielectrics, Solid-State Electronics, (09 2015): 0. doi: 10.1016/j.sse.2015.05.004
08/20/2014	12.00	C. White, T. Donovan, I. Cashwell, R. B. Konda, D. R. Sahu, B. Xiao, M. Bahoura, A. K. Pradhan. Self-Cleaning and Electrical Characteristics of ZrO2 (HfO2)/GaAs MOS Capacitor Fabricated by Atomic Layer Deposition, ECS Transactions, (10 2013): 0. doi: 10.1149/05810.0325ecst
08/20/2014	13.00	C. White, J. Smak, R. Mundle, M. Bahoura, A.K. Pradhan, R.B. Konda. High-k ZrO2 dielectric thin films on GaAs semiconductor with reduced regrowth of native oxides by atomic layer deposition, Chemical Physics Letters, (09 2013): 0. doi: 10.1016/j.cplett.2013.08.012
08/20/2014	14.00	C. White, D. Thomas, Q. Yang, D. Sahu, A. K. Pradhan, R. B. Konda. (Invited) Frequency Dispersion and Band Alignments in ZrO2/n-GaAs MOS Capacitor, ECS Transactions, (05 2014): 0. doi: 10.1149/06102.0125ecst
08/20/2014	15.00	Kevin Santiago, Rajeh Mundle, Chandan B. Samantaray, M. Bahoura, A. K. Pradhan. Nanopatterning of atomic layer deposited Al:ZnO films using electron beam lithography for waveguide applications in the NIR region, Optical Materials Express, (11 2012): 0. doi: 10.1364/OME.2.001743

08/20/2014 16.00 A. K. Pradhan, R. Mundle. Electrical response in atomic layer deposited Al:ZnO with varying stack thickness,
Journal of Applied Physics, (05 2014): 0. doi: 10.1063/1.4875536

08/20/2014 17.00 Hareesh Dondapati, Duc Ha, Erin Jenrette, Bo Xiao, A. K. Pradhan. High-performance chemical-bath deposited CdS thin-film transistors with ZrO2 gate dielectric,
Applied Physics Letters, (08 2014): 0. doi: 10.1063/1.4892578

08/20/2014 18.00 Bo Xiao, Brandon Walker, Aswini K Pradhan. Influence of an MgO interfacial layer on the properties of Pb (Zr,Ti)O,
Journal of Physics D: Applied Physics, (05 2014): 0. doi: 10.1088/0022-3727/47/18/185303

08/20/2014 19.00 Hampton Terry, M Bahoura, A K Pradhan, R Mundle. Ozone-assisted atomic layer deposited ZnO thin films for multifunctional device applications,
Journal of Physics D: Applied Physics, (11 2013): 0. doi: 10.1088/0022-3727/46/47/475101

08/20/2014 20.00 C. Snow-Davis, R. Mundle, A. K. Pradhan, C. G. Carvajal. VLS Growth of Highly Oriented SnO2 Nanorods and ZnO Hybrid Films for Gas Sensing Measurements,
Journal of the Electrochemical Society, (01 2014): 0. doi: 10.1149/2.021402jes

TOTAL: **16**

Number of Papers published in peer-reviewed journals:

(b) Papers published in non-peer-reviewed journals (N/A for none)

Received	Paper

TOTAL:

Number of Papers published in non peer-reviewed journals:

(c) Presentations

- Chineyere Wills, Frances R. Williams, and Demetris Geddis, “Fabrication of MEMS Flexural Plate Wave Bio-Chemical Sensors,” Poster presented at the 2011 Chemical and Biological Defense Science and Technology (CBD S&T) Conference, November 2011, Las Vegas, NV.

- Sha'La Fletcher, Brandon Walker, Casey Gonder, R. M. Mundle, M. Bahoura, and A. K. Pradhan, "Mechanical properties of multilayer ultrathin film of BTO/LSMO on STO and LaO," poster # AA4.18 at 2012 MRS Fall Meeting, Symposium AA: Oxide Nanoelectronics and Multifunctional Dielectrics, 2012 MRS Fall Meeting & Exhibit November 25 - 30, 2012, Boston, MA.

- Doyle Baker and Frances Williams, “Design and Performance of Perovskite-based Microelectromechanical Systems Devices,” 2012 ASME International Mechanical Engineering Congress and Exposition, November 2012, Houston, TX.

- Curtis White, Thomas Donovan, Irving Cashwell, R.B. Konda, D.R. Sahu , Bo Xiao , M. Bahoura , A.K. Pradhan. Self-Cleaning and Electrical Characteristics of ZrO2 (HfO2)/GaAs MOS Capacitor Fabricated by Atomic Layer Deposition, Electrochemical Society Transactions (07 2013)

- R.M. Mundle, H.S. Terry, K. Santiago, D. Shaw, K. Dasari, R. Palai, M. Bahoura, A.K. Pradhan. Atomic Layer Deposited Al-doped ZnO Films: Effects of Cycle Ratio on Electrical Conductivity and Photo-Resistance, Advanced Functional materials (05 2012)

- Aswini Pradhan, “Nanotechnology and beyond,” Invited Talk, Institute of Materials, India, Jan 7 2015.

- Aswini Pradhan, “Nanomaterials & Nanotechnology for various Applications: Biotechnology to Energy,” Key Note Speaker: SPIE, Smart Materials &NDE, March 8-12, 2015, San Diego.

- Aswini Pradhan, “II-VI Quantum-dot based Semiconductor Thin Films and Devices for Optoelectronic Applications,” Invited Talk: MRS conference, April 6-10, 2015, San Francisco, CA.

- Lumu Manandhar & Aswini Pradhan, “CdTe Quantum-dot based Solar cells,” MRS conference, April 6-10, 2015, San Francisco, CA.

- G Rutherford, M Farrell, B Xiao, CG Carvajal, K Santiago, AK Pradhan, “A New Kind of SERS Active Substrate Using a Film of Densely Packed Gold Nanoparticles,” ECS, Chicago, 2015, Meeting Abstracts, pp.2125-2125, 2015.

- CG Carvajal, K Kadri, G Rutherford, AK Pradhan, “Photochemical Decoration of Metal/Metal-Oxide Nanoparticles on SnO2 Nanorods for Improved Hybrid Gas Sensors and Photodetectors for Environmental Applications,” ECS, Chicago, 2015, Meeting Abstracts, pp. 2143-2143, 2015.

- F. Williams, A. Komirisetty, D. Baker, A.K. Pradhan, “Using Nanotechnology for Biosensor Applications,” Invited Talk, ECS, Chicago, 2015, Meeting Abstracts, 1884-1884, 2015.

- M. Farrell, G. Rutherford, A.K. Pradhan, “Effects of 3-Aminopropyl Triethoxysilane (APTES) on Stability, Optical Properties and Morphology of Gold Nanoparticles,” ECS, Chicago, 2015, Meeting Abstracts, 2279-2279, 2015.

- A. K. Pradhan, “Artificially Tailored Plasmonic Nanostructures for High-Performance Biosensing Devices,” Invited talk, ECS, Chicago, 2015, Meeting Abstracts, 2101-2101.

Number of Presentations: 0.00

Non Peer-Reviewed Conference Proceeding publications (other than abstracts):

Received	Paper

TOTAL:

Number of Non Peer-Reviewed Conference Proceeding publications (other than abstracts):

Peer-Reviewed Conference Proceeding publications (other than abstracts):

Received	Paper	
07/13/2015	24.00	Johnson Fujamade, Frances Williams, Oliver Myers, Brandon Plastied, Messaoud Bahoura, Asha Hall, Jaret Riddick. Design and Fabrication of a Functionally Modified Bimorph Actuator, ASME 2014 Conference on Smart Materials, Adaptive Structures and Intelligent Systems. 08-SEP-14, Newport, Rhode Island, USA. : ,
08/23/2014	21.00	Wei-Hsin Liao, Doyle J. Baker, Casey Gonder, Frances Williams, Messaoud Bahoura, Oliver Myers. Design and simulation of PZT-based MEMS piezoelectric sensors, SPIE Smart Structures and Materials + Nondestructive Evaluation and Health Monitoring. , San Diego, California, USA. : ,

TOTAL: **2**

Number of Peer-Reviewed Conference Proceeding publications (other than abstracts):

(d) Manuscripts

Received		Paper
05/20/2012	1.00	Kevin Santiago, R.M. Mundle, C.B. Samantaray, M. Bahoura, A.K. Pradhan. Nanopatterning of Atomic Layer Deposited Al:ZnO FilmsUsing Electron Beam Lithography, Applied Physics Letters (05 2012)
05/20/2012	2.00	R.M. Mundle, H.S. Terry, K. Santiago, D. Shaw, K. Dasari, R. Palai, M. Bahoura, A.K. Pradhan. Atomic Layer Deposited Al-doped ZnO Films: Effects of Cycle Ratio on Electrical Conductivity and Photo-Resistance, Advaced Functional materials (05 2012)
06/06/2013	5.00	R.B. Konda, C. White, D. Thomas, Q. Yang, D. Sahu, A.K. Pradhan. Frequency dispersion and band alignments in ZrO2/n-GaAs MOS capacitor, Appl. Phys. Lett. (05 2013)
06/06/2013	6.00	R.B. Konda, C. White, J. Smak, R. Mundle, M. Bahoura, A.K. Pradhan. High-k ZrO2 Dielectric Thin Films on GaAs Semiconductor with Reduced Regrowth of Native Oxides by Atomic Layer Deposition, Chemical Physics Letters (05 2013)
07/24/2013	10.00	Curtis White, Thomas Donovan, Irving Cashwell, R.B. Konda, D.R. Sahu , Bo Xiao , M. Bahoura , A.K. Pradhan. Self-Cleaning and Electrical Characteristics of ZrO2 (HfO2)/GaAs MOS Capacitor Fabricated by Atomic Layer Deposition, Electrochemical Society Transation (07 2013)
08/20/2014	11.00	Johnson Fujamade, Frances Williams, Oliver Myers , Brandon Plastied, Messaoud Bahoura, Asha Hall, Jaret Riddick. Design and Fabrication of functionally modified biomorph actuator, Proceedings of the ASME 2014 Smart Materials, Adaptive Structures and Intelligent Systems (09 2014)
TOTAL:		**6**

Number of Manuscripts:

Books

Received		Book
TOTAL:		

Received	Book Chapter
07/13/2015	25.00 Jonathan Skuza. L10 Alloy Thin Films and Nanostructures, Pan Stanford, Boca Raton, FL : Taylor and Francis Group, (06 2015)

TOTAL: **1**

Patents Submitted

Patents Awarded

Awards

- Dr. Messaoud Bahoura:
  - Received the "Excellence Award for Outstanding Service in the Center for Materials Research", for the academic year 2013-2014, May 5th, 2014.
  - Received the "Excellence Award for Outstanding Service in the Engineering Department", for the academic year 2014-2015.
- Dr. Frances Williams:
  - Received the 2013 State Council of Higher Education for Virginia (SCHEV) Outstanding Faculty Award. The Outstanding Faculty Award is the Commonwealth's highest honor for faculty at Virginia's public and private colleges and universities and recognizes superior accomplishments in teaching, research and public service. Dr. Williams is one of 12 recognized statewide.
- Dr. Aswini Pradhan:
  - Received the 2015 State Council of Higher Education for Virginia (SCHEV) Outstanding Faculty Award.
  - Was elected as editorial board for Nature Journals, 2015.

Graduate Students

NAME	PERCENT_SUPPORTED	Discipline
Baker Doyle	1.00	
Carvajal Christian	0.33	
Cashwell Irving	0.33	
Falconer April	0.33	
Fletcher Sha'La	0.00	
Gonder Casey	1.00	
Konda Rajini	0.00	
Mundle Rajeh	0.33	
Rutherford Gugu	0.33	
Rylander Seth	0.00	
Santiago Kevin	0.00	
Walker Brandon	0.00	
Fujamade Johnson	1.00	
Chineyere Willis	0.33	
Cooper Camille	0.33	
FTE Equivalent:	**5.31**	
Total Number:	**15**	

Names of Post Doctorates

NAME	PERCENT_SUPPORTED
Xiao Bo	0.00
Skuza Jonathan	0.00
FTE Equivalent:	**0.00**
Total Number:	**2**

Names of Faculty Supported

NAME	PERCENT_SUPPORTED	National Academy Member
Messaoud J. Bahoura	0.13	
Aswini Pradhan	0.00	
Frances Williams	0.02	
Demetris Geddis	0.00	
FTE Equivalent:	**0.15**	
Total Number:	**4**	

Names of Under Graduate students supported

NAME	PERCENT_SUPPORTED	Discipline
Adnew Damtew	0.66	Electronics Engineering
Barry Abdul	0.66	Electronics Engineering
Bennet Franiece	0.66	Electronics Engineering
Floyd Robert	0.66	Electronics Engineering
Frazier Jared	0.66	Optical Engineering
George Kameron	0.66	Electronics Engineering
Goodman Christopher	0.66	Electronics Engineering
Gunawansa Taliya	0.66	Optical Engineer
Harris John	0.66	Optical Engineer
Hayes Dana	0.66	Optical Engineer
Heckstall Lester	0.66	Optical Engineer
Hill Joseph	0.00	Electronics Engineering
King Frank	0.66	Electronics Engineering
Knox Javon	0.66	Physics
Ribeiro Taylor	0.66	Biology
Roscoe Wilonte	0.66	Electronics Engineering
Shipman Nia	0.00	Biology
Skinner Tristan	0.66	Electronics Engineering
Walls Zachary	0.66	Electronics Engineering
Williams Thomas	0.66	Electronics Engineering
Green Fatima	0.66	Biology
FTE Equivalent:	**12.54**	
Total Number:	**21**	

Student Metrics

This section only applies to graduating undergraduates supported by this agreement in this reporting period

The number of undergraduates funded by this agreement who graduated during this period: 13.00

The number of undergraduates funded by this agreement who graduated during this period with a degree in science, mathematics, engineering, or technology fields:..... 13.00

The number of undergraduates funded by your agreement who graduated during this period and will continue to pursue a graduate or Ph.D. degree in science, mathematics, engineering, or technology fields:..... 11.00

Number of graduating undergraduates who achieved a 3.5 GPA to 4.0 (4.0 max scale):..... 5.00

Number of graduating undergraduates funded by a DoD funded Center of Excellence grant for Education, Research and Engineering:..... 0.00

The number of undergraduates funded by your agreement who graduated during this period and intend to work for the Department of Defense 10.00

The number of undergraduates funded by your agreement who graduated during this period and will receive scholarships or fellowships for further studies in science, mathematics, engineering or technology fields:..... 6.00

Names of Personnel receiving masters degrees

NAME
Cashwell Irving
Gonder Casey
Fujamade Johnson
Total Number: **3**

Names of personnel receiving PHDs

NAME
Total Number:

Names of other research staff

NAME	PERCENT_SUPPORTED
Wood Shirleigh	0.00
Powell Daphne	0.00
Springs Michelle	0.00
FTE Equivalent:	**0.00**
Total Number:	**3**

Sub Contractors (DD882)

Inventions (DD882)

Scientific Progress

"See Attachment" below

Technology Transfer

Final Report 2015:

Research and Education in Development of Multifunctional Sensors and MEMS Devices

ARO: W911NF-11-1-0133

Principle Investigator: Dr. M. J. Bahoura

Co-Principal Investigator: Dr. A. K. Pradhan

Co-Principal Investigator: Dr. F. Williams

Norfolk State University

Table of Contents

1. DEVELOPMENT AND CHARACTERIZATION OF PIEZOELECTRIC AND MAGNETIC MATERIALS FOR MEMS AND SENSOR APPLICATIONS 3

1.1. Growth and Characterization of Barium Strontium Titanate (BST) 3

1.2. Growth and Characterization of Barium Titanate (BTO) on GaN 6

1.3. Growth and Characterization of Aluminum-Doped ZnO Films by ALD 8

1.4. Nanopatterning of Atomic Layer Deposited Al:ZnO Films using Electron Beam Lithography for MEMS and Sensor Applications 16

1.5 Thin Film Growth of Epitaxial MGO on AL:ZNO 18

1.6 Low Thermal Budget Growth of Highly Crystalline PZT on Glass Substrates 28

1.7 Modeling and Simulation of ZnO and SiO2 Film Growth by Atomic Layer Deposition 30

1.8 Development And Characterization of $Pb(Zr,Ti)O_3$ On ZNO for MEMS and Sensors Applications 34

1.9 Development of Three-Dimensional Nanostructures for High Sensitivity Bio- and Chemical Detection 43

1.10 Development and Characterization of Tin Oxide Improved Gas Sensor 49

2. DEVELOPMENT, UNDERSTANDING AND INTEGRATION OF ACOUSTIC MICRO-SENSORS AND MEMS FOR SENSING CHEMICAL AND BIOLOGICAL AGENTS, AND FOR ACTUATION 53

2.1. The Design and Development of Acoustic Microsensors 54

2.2 Design and Fabrication of a Functionally Modified Bimorph Actuator 67

3. EDUCATION AND TRAINING OF STUDENTS FROM UNDERREPRESENTED MINORITY GROUPS IN MEMS AND SENSOR DEVELOPMENT AND FABRICATION 78

3.1 Education and Curricular Development 78

3.2 Students Training 78

3.3 Professional Development 79

3.4 Students' Achievements 84

3.5 Students' Graduations 86

3.6 Faculty Awards and Recognitions 87

3.7 Outreach Efforts 87

4. IMPACT OF INFRASTRUCTURE DEVELOPMENT 163

1. DEVELOPMENT AND CHARACTERIZATION OF PIEZOELECTRIC AND MAGNETIC MATERIALS FOR MEMS AND SENSOR APPLICATIONS

In this research we have grown, characterized and fabricated a family of PZT type piezoelectric materials, such as Barium Strontium Titanate (BST), Barium Titanate (BTO), Al doped ZnO (AZO) and PZT on ZnO for MEMS and sensors applications. We have demonstrated the nanopatterning of atomic layer deposited AZO films using electron beam lithography and we studied the growth of ZnO and SiO_2 by Atomic Laser Deposition for high sensitivity bio and chemical detection.

1.1. GROWTH AND CHARACTERIZATION OF BARIUM STRONTIUM TITANATE (BST)

Barium strontium titanate (BST) has been studied for many decades owing to its outstanding piezoelectric, dielectric, pyroelectric, and electro-optical properties offering great promise for various applications. In our recent work, we have been focusing on BST materials in the thin film form for micro-scale and nano-scale electromechanical sensors (MEMS and NEMS). We have been exploiting rf magnetron sputtering and pulsed laser deposition (PLD) for different BST multilayer structures and heterostructures on varieties of substrates (Si, Pt (100 nm)/Si and c-plane sapphire). Their related structural and dielectric properties have been studied to establish the physical foundation for device applications.

The BST films with the composition, Ba:Sr = 50:50, were grown by off-axis rf magnetron sputtering system on Si and Pt/Si using a 3 in. diameter target. During growth, Ar and O_2 gases were introduced into the growth chamber through mass flow controllers. Although the use of oxygen for growing oxide materials in rf sputtering enhances material oxidation and lowers the oxygen vacancies in the films, it causes resputtering of the growing films and dramatically deteriorates the thin film quality as seen in XRD scan of Figure 1.1(a). Therefore, the oxygen flow rate was set at a relatively low level of 5 SCCM (Cubic Centimeter per Minute) as compared to 30 SCCM of Ar gas. In addition, the off-axis sputtering geometry is intended to reduce resputtering. The total pressure of the Ar and O_2 mixture gas was kept at 3 mTorr. The rf power

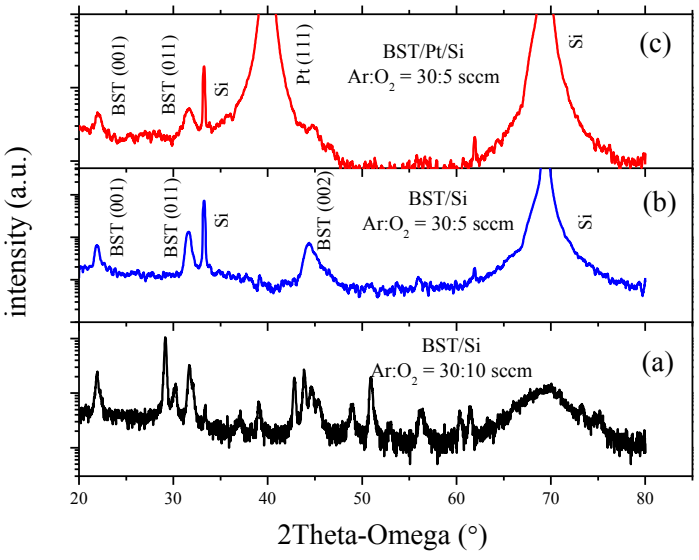

Figure 1.1 XRD patterns of BST thin films grown on Si and Pt/Si: (a) 2θ-ω scan of BST/Si with high oxygen to argon ration (b) 2θ-ω scan of BST/Si with 30:5 $Ar:O_2$ ratio, and (c) 2θ-ω scan of BST/Pt/Si with 30:5 $Ar:O_2$ ratio.

was set at 200 W. Reducing the oxygen ratio in the gas mixture, the BST thin films on Si and Pt (100nm) /Si showed the preferable (001) and (011) orientations.

BST thin films have been extensively studied on a variety of substrates such as MgO, $LaAlO_3$, $SiTiO_3$ and sapphire. Among these substrates, sapphire possesses advantages such as low cost, high chemical stability, and of particular importance, a low loss tangent which make sapphire an excellent substrate for bio- and chemical sensing. Despite this motivation to use sapphire for high performance devices, growth of BST thin films on sapphire has not been yet established as on other substrates due, in part, to the difficulty in achieving high quality BST thin films. Large lattice mismatch and different crystal structures between BST and sapphire apparently hamper the pace of this heterostructure growth. Polycrystalline BST films were generally reported on sapphire; therefore, it is imperative to utilize a bridge layer (nucleation or seed layer) between BST and sapphire, which can accommodate the lattice mismatch and promote the crystallization of BST films for high structural perfection.

We have established the growth of high-quality (001)-oriented BST films on *c*-plane sapphire using a double MgO/ZnO:Al bridge layer. The choice of MgO buffer layer was dictated by a well-established BST growth on (001)-oriented MgO single crystal substrates. However, usage of MgO substrates for our sensor and MEMS development is limited by its cost and compatibility of conventional semiconductor fabrication processes. Furthermore, it is difficult to grow highly oriented MgO directly on sapphire because of a large lattice mismatch and dissimilar crystal structures. We have that found introducing ZnO as an intermediate layer promotes the growth of (001)-oriented BST thin films. Additionally, Al doped ZnO layer is utilized as bottom electrode in our device application. Highly conductive epitaxial Al doped ZnO also have been successfully obtained in this work. Using 3% Al doped ZnO target, highly conductive ZnO have been obtained on *c*-plane sapphire. Four probe temperature measurements confirmed its metallic behavior, the resistance increases as the temperature rises. The temperature dependence of the Al:ZnO is shown in Figure 1.2.

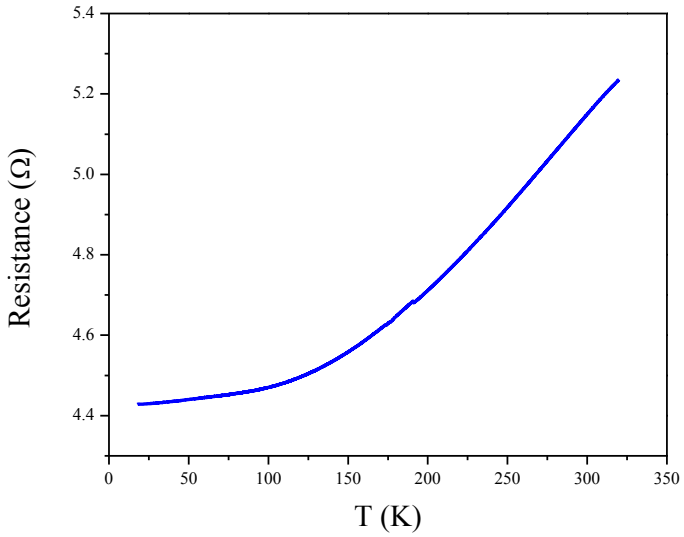

Figure 1.2. Temperature dependence of Al:ZnO on *c*-plane. sapphire

MgO/Al:ZnO bridge layers were grown epitaxially on c-plane sapphire by PLD. After the MgO/Al:ZnO buffer layer was prepared, the substrate was immediately transferred into the rf magnetron sputtering chamber for BST growth. The mixture of Ar and O_2 with the ratio 30:5 was used for the sputtering growth and the pressure was kept at 3 mTorr. The deposition rate was 350 Å/h at 200 W rf sputtering power and T_s was set at 700°C.

X-ray diffraction (XRD) was employed to determine the structural properties of the thin films. As seen in Figure 1.3, the 2θ-ω scan of XRD shows the reflections from the films of Al: ZnO and BST. The Al doped ZnO layer shows the (0002) reflection at 34.7°. Also the (00*l*) reflections of BST thin films are observed. The absence of other reflections indicates that the [001] axes of BST films are well aligned with [0001] ZnO.

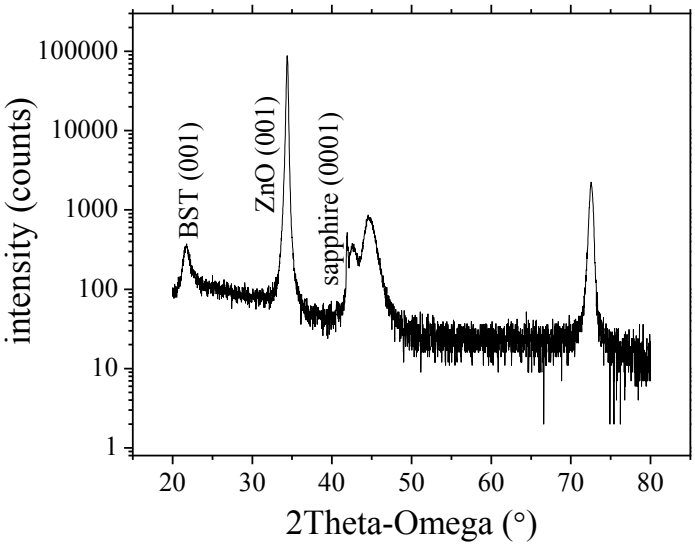

Figure 1.3. 2θ-ω XRD scan of BST on MgO/ZnO/c-plane.

Measurements of the dielectric properties for BST films grown on MgO/Al:ZnO/sapphire substrates were performed by a LCR meter. Using conductive Al:ZnO as the bottom electrode provides a simple and direct way to examine electrical properties. Au/Ti (50 nm/10 nm in thickness) circular top electrodes were patterned on the surface of BST films using photolithography and lift-off process. The diameter of the top electrode is 400 μm. In the C-V measurement, the applied DC bias voltage was swept from -6 to 6 V. In Figure 1.4, the BST thin film on *c*-plane sapphire exhibits the maximum capacitance of 3.99 nF around -2.8 V instead of zero bias. This shift of the maximum capacitance is most likely caused by the contribution of the bottom contact on Al:ZnO (Schottky contact with the Au/Ti) and the semiconducting

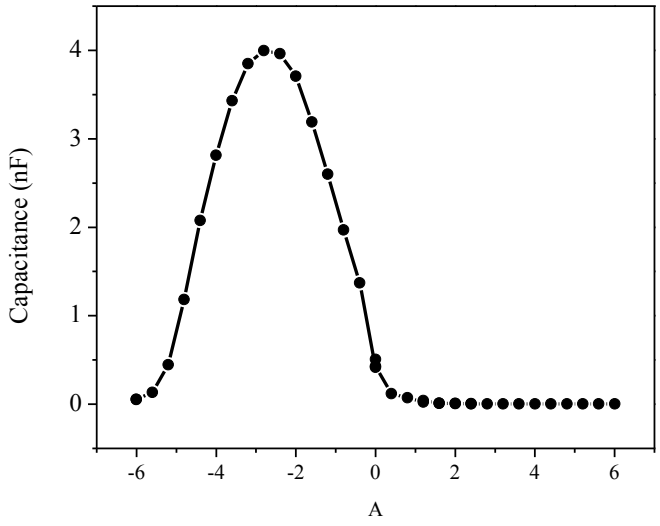

Figure 1.4. C-V measurement of BST/MgO/Al:ZnO/c-sapphire capacitor structure.

behavior of Al:ZnO. Further investigation is on-going to lower the contact resistance and increase Al:ZnO conductivity.

1.2. GROWTH AND CHARACTERIZATION OF BARIUM TITANATE (BTO) ON GAN

We have grown series of $BaTiO_3$ (BTO) thin films on GaN by PLD using a one-inch stoichiometric $BaTiO_3$ target. In oxygen environment the background pressure was maintained at 10mT, and the substrate temperature was set at 700°C. A laser power of 220 mJ was used to grow the films. At these growth conditions, the growth resulted in the formation of reproducible step-terrace patterns indicating a 2D growth mode as displayed by Atomic Force Microscopy (AFM) picture in Figure 1.5.

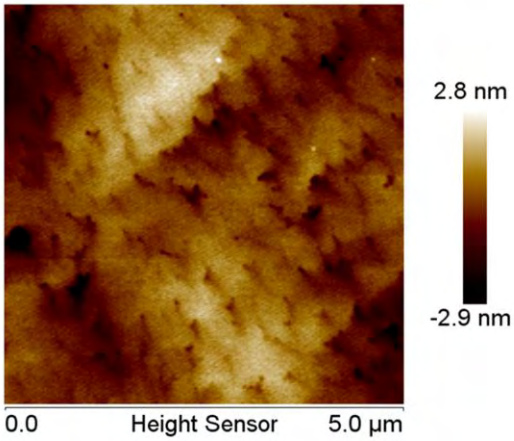

Figure 1.5. AFM image of BTO thin films grown on GaN by PLD.

The XRD pattern showed (004) reflection in the as-grown BTO thin films without annealing treatment, Figure 1.6. This confirmed the formation of highly oriented BTO thin films on GaN. However, the intensity of the (004) reflection in BTO was weak. This suggests that the crystal of BTO thin films suffers dislocations or oxygen vacancies that exist in heterostructure perovskite oxide/GaN due to large lattice mismatch and oxide deficiency. Further investigation using high-resolution transmission electron microscopy (HRTEM) and X-ray photoemission spectroscopy (XPS) is necessary to clarify this issue.

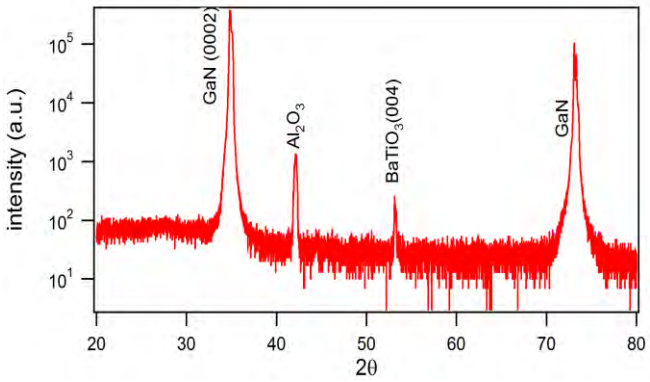

Figure 1.6. XRD 2θ scan of BTO grown on GaN by PLD.

Because of the electron leakage over the barrier height created between the BTO and GaN, there is a need to use a buffer layer between BTO and GaN. We used Sc_2O_3 (band gap of 6.3 eV) as a buffer layer to which also serves in reducing the lattice mismatch between BTO and GaN. Figure 1.7 shows almost a linear dependency of the

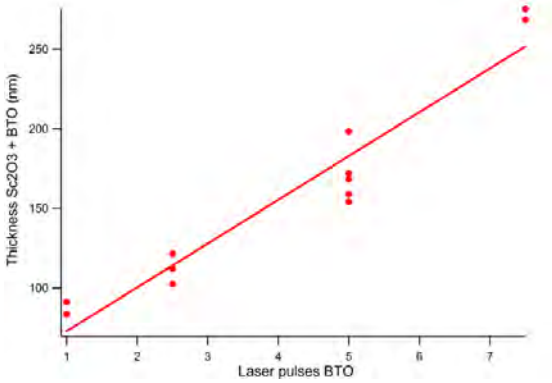

Figure 1.7. Thickness of BTO on Sc_2O_3/GaN versus the laser pulses of BTO.

growth thickness of BTO on Sc_2O_3 with laser pulses of BTO.

The morphology of the grown films was investigated using AFM shown in Figure 1.8. The grain structure if BTO is very clear in Figure 1.8(b).

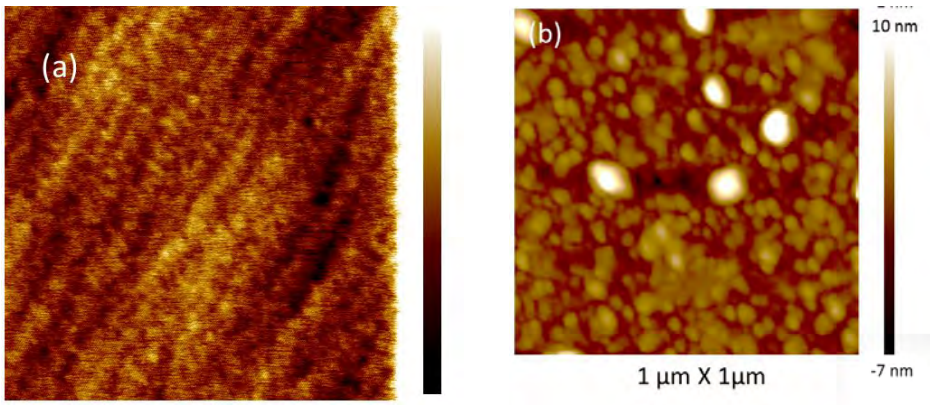

Figure 1.8. Atomic Force Microscopy images of (a) Sc2O3/GaN and (b) BTO/Sc2O3/GaN films.

The preliminary electrical behavior of BTO/Sc_2O_3/GaN is shown in Figure 1.9. The leakage current is very small as seen in the inset. The C-V shows the asymmetric behavior. Detail characterization is in progress.

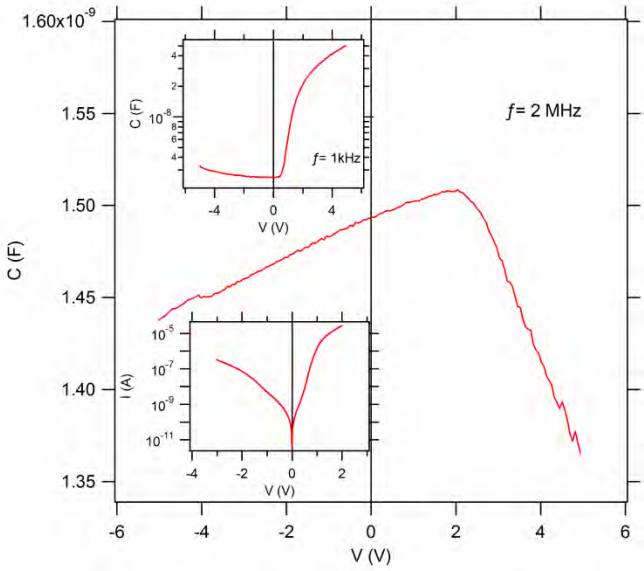

Figure 1.9. The capacitance – voltage (C-V) characteristics of the grown BTO/Sc2O3/GaN films at f=2 MHz. Top inset shows C-V measurement at f =1 kHz and bottom inset shows the I-V characteristics of the same structure.

To study the multiferroic properties of our films, we have grown BTO (Ferroelectric material) on LSMO (Ferromagnetic material) using the PLD technique. The microscopic polarization is of great use for MEMS functionalities. We have chosen a small region of the sample 1µm×1µm and applied a local 9 V electric field to the tip of the AFM cantilever in contact with the BTO/LaSrMnO/STO film. We reduced the voltage to below 1V and zoomed out of the region and used electric force microscopy (EFM) mode to scan the same area. We found that the film was polarized, as shown in Figure 1.10. This ferroelectric property allows the manipulation and control of the local polarization of the film by the application of the electric field.

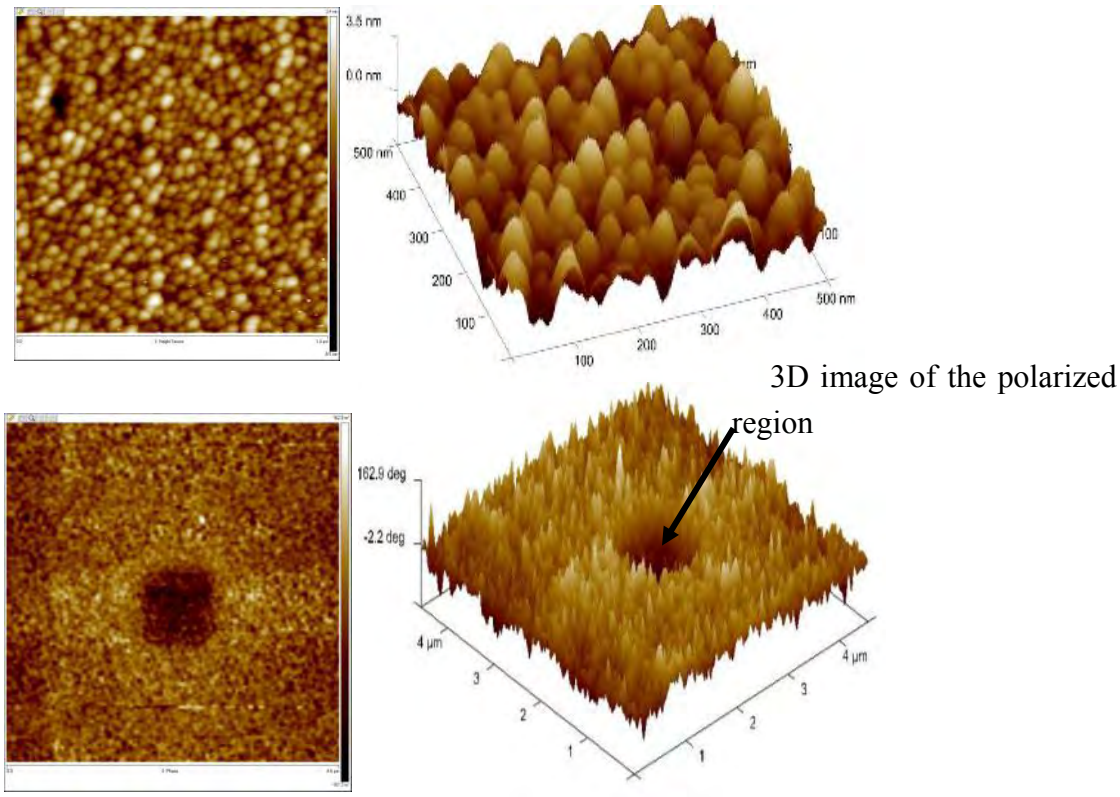

Figure 1.10. 2D and 3D AFM images of BTO/LaSrMnO/STO showing local polarization obtained after the application of an electric field.

1.3. GROWTH AND CHARACTERIZATION OF ALUMINUM-DOPED ZNO FILMS BY ALD

Atomic layer deposition (ALD) is recently used to attain conformal films with a high degree of thickness control. The sequential exposure of reactants used in ALD adjusts the composition of multicomponent materials by changing the number of cycles used for each precursor materials and deposits pinhole-free films on a variety of surfaces. Taking into account the combination of conformality due to the surface-saturated and self-limiting reaction mechanism with atomic precision, among many ultrathin films Al-doped ZnO (AZO) films have been fabricated via ALD, using trimethylaluminum (TMA), diethylzinc (DEZ), and water as precursors.

We deposited AZO films using the ALD on both glass and sapphire (0001) substrates. The Al content in the films was varied by controlling the Zn:Al pulse cycle ratios. We carried out electrical and optical properties measurements of the ALD grown AZO films, including resistivity and photo-resistance, varying Al doping concentrations. In addition, the films were characterized by XRD and AFM. The concentrations of Al dopant were investigated using X-ray photoelectron spectroscopy (XPS). Specifically, we focused on the correlation between these properties and the extrinsic doping behavior of ALD-AZO films, as well as on the remarkable dependence of photo-resistance on electrical conductivity, which varies with the cycle ratios.

We measured the films resistivity as a function of Zn:Al cycle ratios as well as temperature for films grown at various substrate temperature used for ALD deposition. We found that the resistivity of the AZO grown films decreases significantly as the cycle ratio increases, leading to an increase in the carrier concentration.

Experimental Results

We have grown AZO films via alternate deposition of diethyl Zinc (DEZ, $Zn(C_2H_5)_2$), H_2O and trimethylamine (TMA, $Al(CH_3)_3$) through ALD cycles, Figure 1.11(a). We found that the ALD-AZO film has a growth rate of ≈0.2 nm per cycle. The knowledge of the average numbers of hydroxyl groups reacting with each DEZ or TMA molecule during AZO growth by ALD is important for analyzing the surface chemistry during ZnO/Al_2O_3 alloy growth. We noticed that the measured thicknesses for many of the AZO films are significantly below the thicknesses predicted using the "rule of mixtures". This is due to the fact that alloy film thicknesses require a finite number of cycles both for ZnO and Al_2O_3 to nucleate and diffuse to form AZO. However, the ALD growth rate gradually increases as nucleation precedes, and finally reaches the

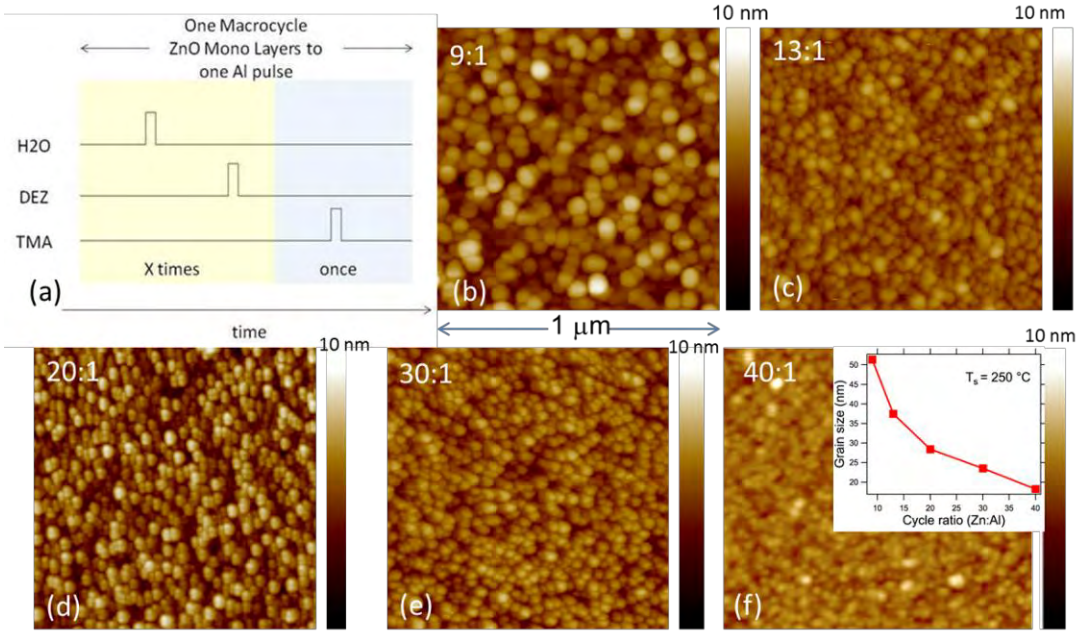

Figure 1.11. (a) Diagram of the growth cycle sequences of Al:ZnO films on sapphire (0001) substrates. The AFM images of AZO films grown at 250°C for different cycle ratios of DEZ/TMA, (b) 9:1, (c) 13:1, (d) 20:1, (e) 30:1, and (f) 40:1.

estimated value.

The surface roughness of AZO films, as shown by the AFM images in Figure 1.11 (b)-(f), drastically decreases as the cycle ratios increase from 9:1 to 40:1 for films grown at the substrate temperature of T_s=250 °C. Homogeneous distribution of grains was observed on the surface of

all films. For films grown at T_s=250 °C, the root-mean-square (rms) surface roughness of the AZO films varies from 1 nm to 0.3 nm as the cycle ratios increase from Zn:Al=9:1 to 40:1. The grain size varies from about 50 to 18 nm with the variation ratio from 9:1 to 40:1. The reduced rms can be explained by the growth of more oriented grains on the surface, compared to more randomly oriented grains for lower cycle ratios.

XPS analysis was performed with a dual source VG Microtech XPS microprobe system using an Al X-ray (λ = 1486.8 eV) source at 8×10^{-10} torr with pass energy of 100 eV. The XRD spectra were measured using a Rigaku D-Max diffractometer. Film thicknesses were measured using Bruker Icon AFM, and the same AFM is used for imaging the surface of the films. The optical absorption measurements were performed on a Perkin-Elmer 950 UV-vis-IR spectrophotometer. The temperature dependent resistivity and photocurrent were measured in an optical cryostat with the temperature down to 15K using 4-probe configuration.

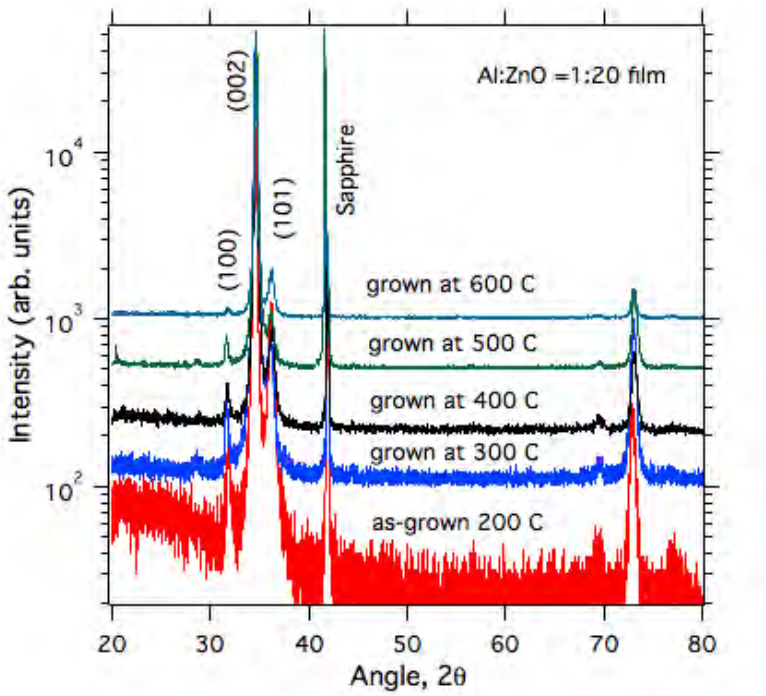

Figure 1.12. XRD patterns of as-grown AZO films (200°C), and subsequently annealed at 300, 400, 500 and 600°C of ALD grown AZO films.

The AZO grown films showed polycrystalline nature even after the films are post-annealed up to 600°C, as shown in the XRD patterns in Figure 1.12. However the diffraction peak (002) observed at 2θ=34° for (002) orientation sharply increased with increasing annealing temperature demonstrating the enhanced crystallinity. The XRD graph shows the (002) peak along with (100) at 2θ ~32° and (101) orientations at 2θ ~37°. We did not observe any additional peaks upon annealing the films up to 600°C.

To study the composition of the ALD grown AZO films in details, we have grown Al:ZnO (1:20) films via alternate deposition of diethyl Zinc (DEZ) of ALD cycles, H_2O and ALD cycle of trimethylamine (TMA) at 200°C on either pre-cleaned sapphire or glass substrates as shown in

Figure 1.13 (a). The films are optically very smooth without any microscopic defects. AZO films of thickness 80-100 nm show atomically flat surfaces with rms value of surface roughness around 1 nm for as grown as well as for annealed films at 600°C (Figure 1.13 (c)). However, the field emission scanning electron microscopic (FE-SEM) images show a clear coalescence of grains with annealing temperature as shown in Figure 1.13 (c), and (e) at 600°C. All AZO films deposited in this study showed wurtzite structure analyzed by XRD (Cu *Kα* radiation, wavelength: 0.154 nm).

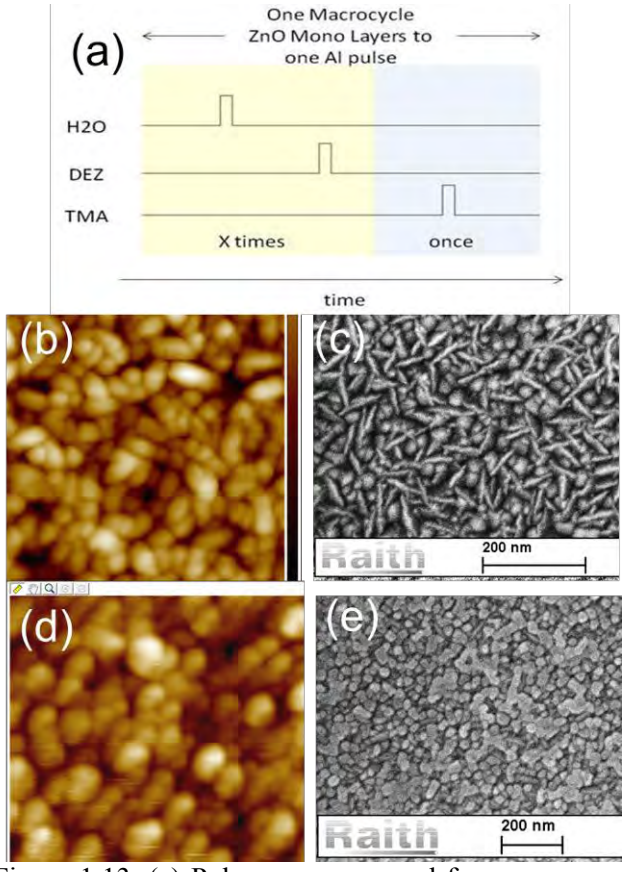

Figure 1.13. (a) Pulse sequence used for one macro-cycle of Al:ZnO films by the ALD technique, (b) AFM, and (c) SEM images of as grown films at 200°C, (d) AFM and (e) FE-SEM images of films annealed at 600°C. The scale for the AFM images is 1 μm × 1μm.

We performed XPS studies on all AZO films varying the Zn:Al cycle ratios with ZnO terminated surface. Figure 1.14 shows the typical XPS analysis of Zn and oxygen peaks for AZO films grown at 250°C at various Zn:Al cycle ratios. We found that the composition of Al varies from about 5% to 1% almost linearly for Al and about 45±1 % Zn, and 50±3% O as Zn:Al cycle ratios vary from 5:1 to 30:1. The absence of carbon contamination suggests the complete removal of ligands from the metal-organic precursors during the reaction process. The influence of T_s on Al 2s of Zn:Al=20:1 ratio in XPS spectra is seen around 120 eV, suggesting different degree of oxidation state in AZO.

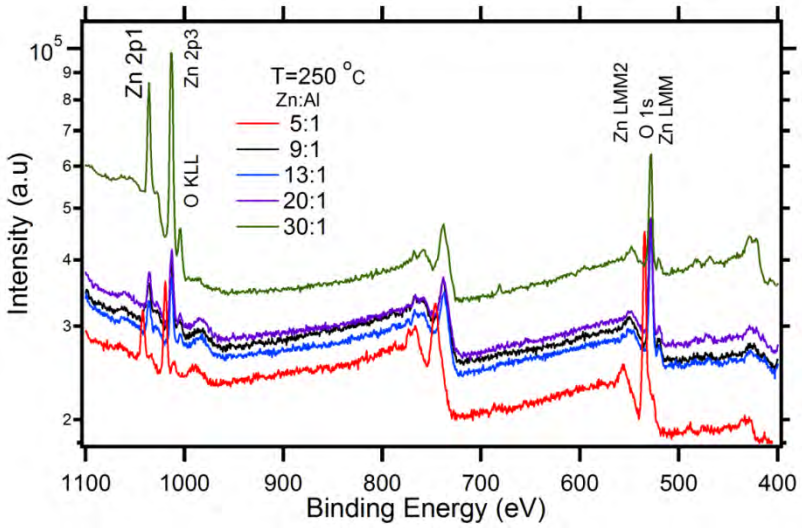

Figure 1.14. XPS analysis of AZO films Zn:Al cycle ratio of 5:1 to 30:1. Zn and oxygen peaks for AZO films grown at 250°C at various Zn:Al cycle ratios.

The XPS analysis of the Al

2p peak for Al-O bonding state, shown in Figure 1.15, indicates higher Al–O bonding state for AZO films with various Zn:Al ratios. It is predicted that higher Al–O bonding (as evidenced by movement of the Al 2p peak to higher binding energy), in AZO films, might induce a metastable $(ZnO)_3$ (Al_2O_3) phase during the ALD process, especially for higher concentration of Al. This region was predicted to be amorphous supersaturated ZnO–AlO phase rather than Al_2O_3 segregation region. However, the most preferred and stable phase is Al_2O_3, may be present in the form of micro or nano- size clusters.

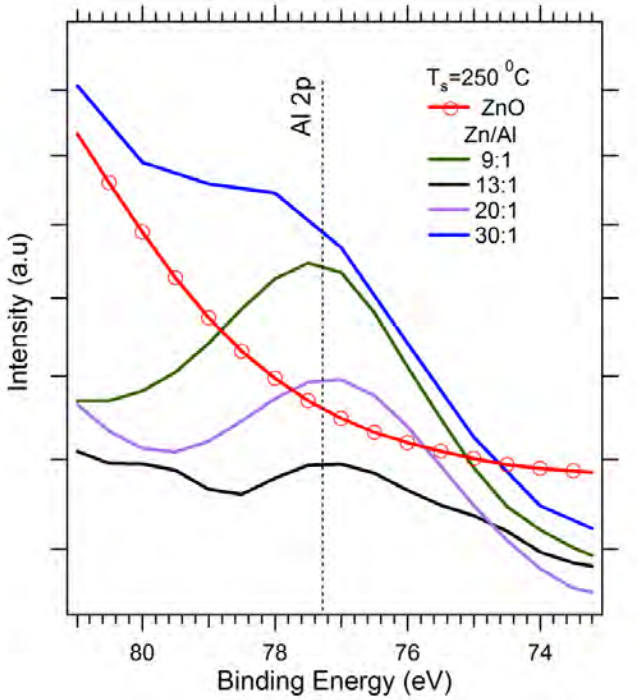

Figure 1.15. XPS analysis for Al 2p peaks of AZO films for different cycle ratios. For comparison, the XPS results for Al 2p peaks of pure ZnO film (500 cycles) are shown.

We performed structural characterization consisting of phase analysis on the films using XRD for all samples with cycle ratios of Zn:Al=5:1 to 40:1 for AZO films grown at T_s=250°C. The presence of (100), (002), (101), and (200) peaks of ZnO confirms the hexagonal wurtzite phase. The crystalline Al_2O_3 (except at (0002) due to substrate peak) or $ZnAl_2O_4$ peaks were not found. Similar peaks (except at $2\theta \sim 42°$) were observed for AZO films grown on glass substrates. This suggests that there is no major phase segregation; however, any presence of nanophases of Al_2O_3 could not be detected. On the other hand, a slight increase in the diffraction angle to higher values suggest the substitution of Al into Zn site with decreasing cycle ratios, in agreement with the XPS results.

The systematic measurements of temperature dependence of the resistivity of the films at various cycle ratios clearly demonstrate the crossover of the metal-semiconductor-insulator phase. The average transmission of all films is greater than 85% and the optical absorption increases significantly in the visible region as the cycle ratio increases. We observed a remarkable dependence of photo-resistance on electrical conductivity for ALD-grown films with varying cycle ratios, which control the Al content in the film. Our results suggest that Al^{3+} ions are incorporated as substitutional or interstitial sites in the ZnO matrix. However, an addition of an excessive amount of Al content causes the formation of Al_2O_3 and related clusters as carrier traps opposed to electron donors, resulting in an increase in the resistivity and other associated phenomena.

Literature report shows that the resistivity of AZO film exhibited a minimum value of $\approx 2.2 \times 10^{-3}$ Ω cm when 2 at% of Zn atoms were replaced by Al atoms, when the films were grown with modulating an ALD cycle ratio of ZnO and Al_2O_3. There are several reports available proving valuable information, however a cross-over from highly resistive (insulating) state to metallic state via a semiconducting state and their correlation to the optical and opto-electronic properties are not reported yet in ALD-AZO films. This information is essential to understanding the extrinsic doping and remarkable transition in electron conduction behavior of these films.

The resistivity dependence on the cycle ratios growth temperature, for Ts= 250 °C is shown in Figure 1.16. The resistivity decreases sharply as the cycle ratio increases up to 20:1, then nearly levels off. The lowest resistivity we measured is 1.4×10-3 Ω-cm for Zn:Al ratio of 40:1. However, the resistivity becomes orders of magnitude higher, ~ 2 Ω-cm for Zn:Al ratio of 5:1. We found that the resistivity also depends on Ts as shown in the inset of Figure 1.16 for Zn:Al ratio of 20:1. We found that, for every cycle ratio, there exists an optimum Ts for which to achieve lower resistivity. For example, Ts= 200°C for Zn:Al ratio of 20:1. However, this statement may be true only for the higher cycle ratios.

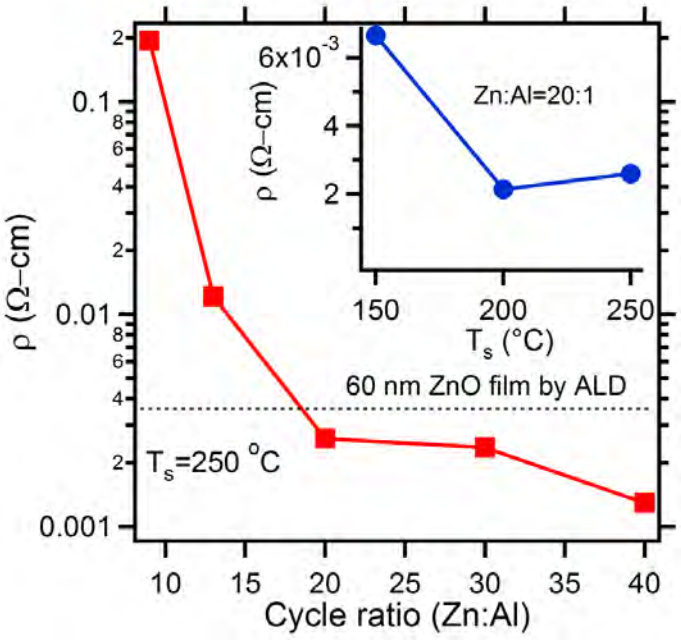

Figure 1.16. AZO resistivity dependence on cycle ratios (Zn:Al) for growth temperature, T_s= 250 °C. Dotted line: resistivity for film with 60 nm thickness of pure ZnO. The inset: dependence of resistivity on T_s for Zn:Al ratio of 20:1.

The resistivity dependence on temperature for grown films is shown in Figure 1.17. The films with Zn:Al ratio of 9:1 and 13:1 showed usual semiconducting behavior over the whole temperature range, with an exception that the resistivity is slightly high. On the other hand, the film with Zn:Al ratio of 20:1 demonstrated a semiconductor to metallic behavior with an optimum T_s= 200°C, Figure 1.17(a) and (b). Film with Zn:Al ratio of 30:1 and 40:1 showed a metal-semiconductor transition (MST) behavior with an optimum T_s= 250°C, Figure 1.17 (a) and (d). Similar behavior was observed for the pulsed-laser deposited AZO film. However, the hierarchical observation of resistivity dependence on the temperature transport properties using

the ALD technique for the growth of AZO films is very interesting and to our knowledge not reported in literature.

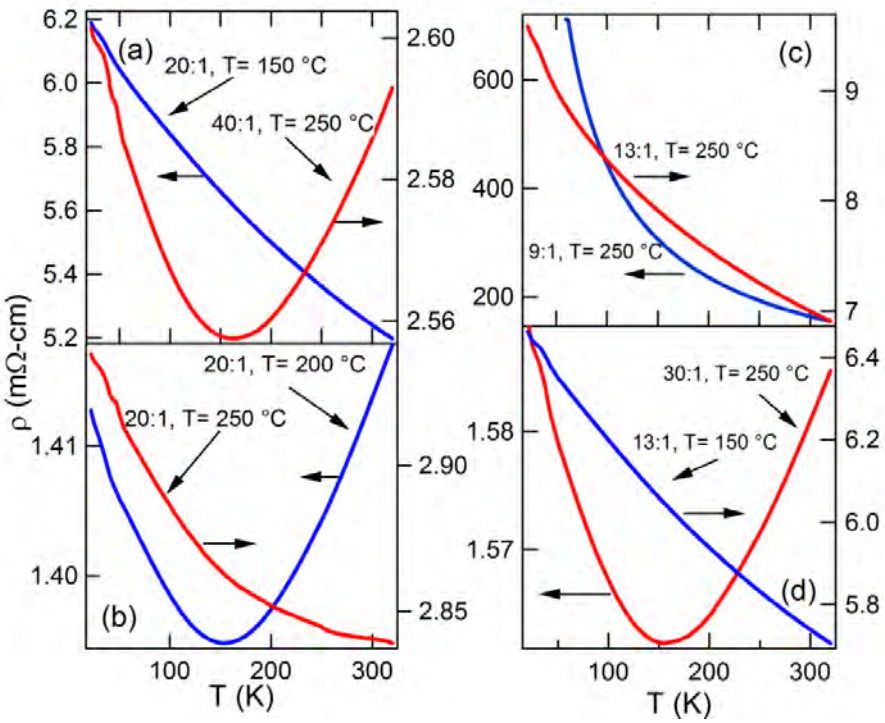

Figure 1.17. Resistivity temperature dependence for films with Zn:Al=9:1, 13:1, 20:1, 30:1 and 40:1.

While a small amount of Al doping is used, for example Zn:Al=20:1 to 40:1, it seems the Al^{3+} ions are incorporated as substitutional or interstitial sites of the ZnO matrix. However, a higher level of Al incorporation causes the formation of Al_2O_3 clusters as carrier traps opposed to electron donors, resulting in an increase in the resistivity. The Al dopants in the films can also produce ionized impurity scattering centers and conduction electrons. It is worth noting that the electron scattering plays a role in the resistivity behavior, especially the electron grain-boundary scattering, which is related to the grain size rather than ionized impurity scattering. However, the grain size variation from about 50 to 18 nm with change in rms value from 1 to 0.3 nm does not explain the order of magnitude decrease in resistivity taking into account the scattering phenomena of electron.

Using a 4 Tesla applied magnetic field, we determined the carrier concentration n to be 2×10^{20} cm^{-3} at room temperature for AZO (20:1) films, and almost remains constant up to films with Zn:Al ratio of 40:1 ratio. However, the carrier concentration significantly decreases to 2×10^{18} cm^{-3} for Zn:Al ratio of 9:1. The lower carrier concentration is attributed to a higher probability of dopant clustering. Considering the number of Al atoms deposited using TMA during one ALD cycle on ZnO terminated surface is $\sim3 \times10^{14}$ cm^{-2}, we determined that the average spacing between Al atoms is ~0.55 nm. In contrast, the spacing of Al atoms in AZO films deposited by other techniques using bulk target, such as pulsed laser deposition or sputtering, that spacing is about 1 nm with a doping concentration of the order of 10^{21} cm^{-3}. Hence, it is expected that the ALD grown AZO films would be energetically favorable to form Al_2O_3 clusters as well as segregated nano-islands, which are most probably stoichiometric to

Al_2O_3 compound. The defects are the trapping centers for electrons for excessive dopant concentration. This clustering, or segregation of dopants, results in decrease in the carrier concentration, hence higher resistivity in AZO films, in agreement with previous observation on clusters in ZnO.

The light illumination influence on electrical properties of ALD grown AZO films is shown in Figure 1.18. We performed photo-resistance versus time measurements for a particular radiation dose, recorded in real time (interval of 1 s) using high resolution and automated transport measurement system. Sharp decrease in resistance was observed when the AZO film (Zn:Al=9:1) was illuminated with 1W/cm^2 white light, Figure 1.18 (a). The change in the electrical resistance is reproducible and reversible between on and off (*on* ↔ *off*) conditions.

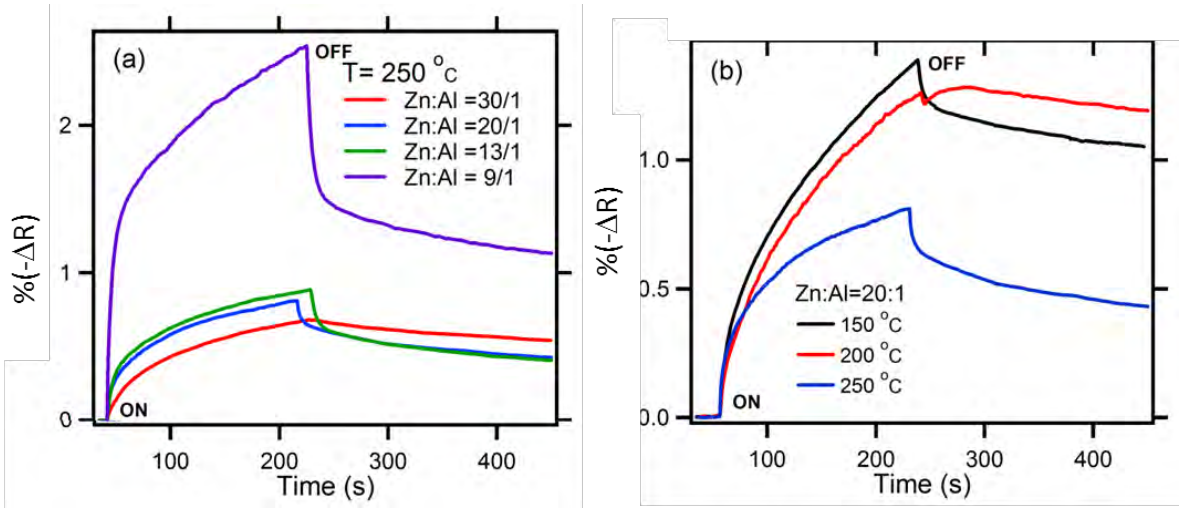

Figure 1.18. Time dependence of photo-resistance of (a) AZO films with different cycle ratios at T_s=250°C, and (b) at different T_s values for Zn:Al=20:1. The %ΔR observed is the decrease in resistance on illumination.

The rise and fall times (responsivity) of the films strongly depend on the Zn:Al ratios. However, slow resistance change (both rise and fall times) under white light illumination may be attributed to the charge trapping which caused current transient in the former case. We noticed a significant difference in electrical resistance when Zn:Al ratio was increased, mainly the resistivity decreased significantly with increasing Zn:Al cycle ratio. This clearly suggests that the photo-generated carriers in low Zn:Al ratio films are directly related to intrinsic carriers trapped at the defect site. The smallest rise and fall times of this on-off transient observed in the highest conducting films suggest significant reduction of such defect centers, hence higher carrier concentration as described earlier. Similarly, taking into account the photo-response on the films grown at different T_s values, Figure 1.18 (b), brings out again the fact that the transient is very weakly dependent on time for films with the lowest electrical resistivity (see Figure 1.17).

As summary, Al-doped ZnO films were deposited by the ALD by controlling the Zn:Al pulse cycle ratios. The films were characterized by XRD, AFM, XPS and optical measurements. We found that the resistivity of the ALD grown AZO films decreases significantly, and so an increase in the carrier concentration, as the cycle ratio of Zn:Al increases. The systematic measurements of resistivity dependence on temperature of films at various cycle ratios clearly demonstrate the crossover of the metal-semiconductor-insulator phase with the function of temperature as well as the cycle ratios. The average transmission of all films is greater than 85% and the optical absorption increases significantly in the visible region as the cycle ratio increases. We have demonstrated a remarkable dependence of photo-resistance on electrical conductivity for ALD-grown films with varying cycle ratios, which control the Al content in the film. Our results suggest that Al^{3+} ions are incorporated as substitutional or interstitial sites of the ZnO matrix. However, an addition of an excessive amount of Al content causes the formation of Al_2O_3 and related clusters as carrier traps opposed to electron donors, resulting in an increase in the resistivity and other associated phenomena.

1.4. Nanopatterning of Atomic Layer Deposited Al:ZnO Films using Electron Beam Lithography for MEMS and Sensor Applications

We have demonstrated the nanopatterning of atomic layer deposited (ALD) AZO films using electron beam lithography (EBL). We have annealed the ALD grown samples at several temperatures to control the grains in order to study their influence on planar nanostructures with a repeatable nanolithography process. Our results demonstrate that the nanopatterning of AZO by the EBL technique is limited and controlled by the granularity of ALD grown AZO films, and could be improved by post annealing. In contrast, the films lose their conductivity upon annealing.

AZO films were grown via alternate deposition through ALD cycles of diethyl Zinc (DEZ), H_2O and trimethylaluminum (TMA). Al:ZnO (1:20) 100 nm was deposited on sapphire substrates using ALD (Cambridge Savannah S100). The growth temperature was kept at 200°C, with a flow rate of 20 ccm of N_2 gas. All samples were annealed in ambient atmospheric at different temperatures, 300°C, 400°C, 500°C, and 600°C. The Hall effect measurements were performed using a four-probe technique under a 4T magnetic field.

After annealing and cooling at room temperature, each sample was spin-coated with 2% 996K PMMA diluted in chlorobenzene for 40 seconds at 6000 rpm. This resulted in a resist thickness around 50 nm. High-resolution lines, gratings, and Fresnel lens structures were exposed on the spin coated AZO (using EBL, Raith Pioneer). The Beam energy was 10 kV and the working distance was kept at 10 mm. The aperture was set to 20 μm and the beam current was measured to be 0.126 nA. The base dose for lines, areas and curves elements were 700 pC/cm^2,

300 μC/cm^2 and 300 pC/cm^2, respectively. All exposures were developed in MIBK: isopropyl alcohol (IPA) (1:3) for 1 minute, and dipped in IPA for 30 seconds and dried in N_2.

ALD is recently used to attain conformal films with a high degree of thickness control. The sequential exposure of reactants used in ALD adjusts the composition of multicomponent materials by changing the number of cycles used for each precursor materials and deposits pinhole-free films on a variety of surfaces. There is a need to control the grain structure and crystal orientations in order to fabricate low loss optical waveguide devices. This can be achieved using the ALD technique for films growth.

The EBL patterns of periodic gratings for as-grown films and annealed films at different temperatures are shown in Figure 1.19. It is anticipated that the surface roughness as well as line edge roughness (LER) of AZO films will be reduced after post annealing. Both surface and line roughness of the patterns are crucial for maintaining the device % of efficiency, which is directly related to the scattering. It is interesting to note that the surface roughness remains around 1 nm as shown in the inset of Figure 1.19, regardless of annealing up to 600^{o}C. The gratings are well separated with pitch 200 nm and line width of 100 nm as shown it the inset.

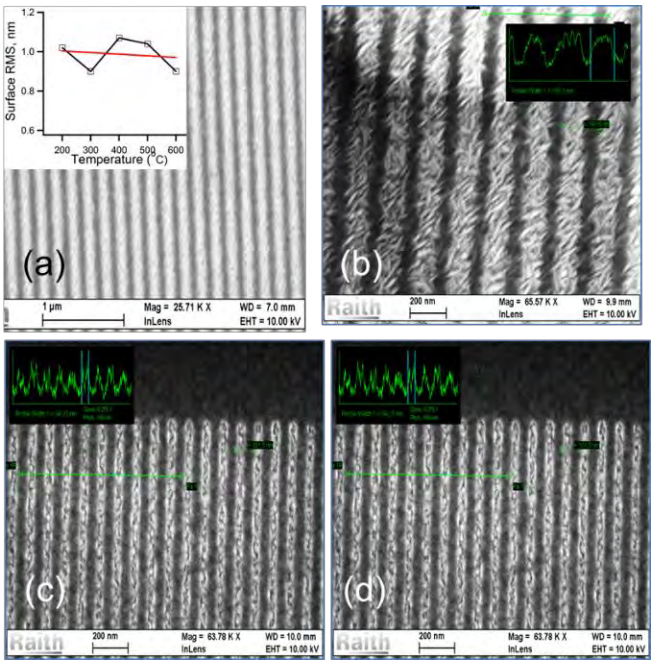

Figure 1.19. EBL patterns of periodic gratings in (a) as-grown films (200^{o}C), and subsequently annealed at (b) 400, (c) 500 and (d) 600^{o}C of ALD grown AZO films. The inset (a) shows the surface roughness of the film as a function of annealing temperature.

The crucial challenge of the current research is the line roughness of the gratings, which is limited by the grain size of the films. The grain size increases from about 30 nm for as-grown AZO film at 200^{o}C to about 50 nm upon annealing at 600^{o}C. The LER was measured from the SEM images. The LER is slightly decreased as films were annealed until 500^{o}C as shown in the inset in Figure 1.20 (b). This is due to the improved crystallinity of the film and coalescence of grains. Because there are fewer grain boundaries, and because the surface roughness of the annealed AZO films is less, the probability of backscattering due to inelastic collisions is reduced. Backscattering may result in exposures in neighboring regions, which will distort features and produce roughness along the boundaries of the exposures. The roughness on the surface of the film increases significantly for film annealed at 600 =°C. Annealing the films

at high temperature resulted in a large increase in resistivity, orders of magnitude higher than that of as grown sample. Because the sample became very insulating, charge accumulation took place during exposures. Charging of the substrate results in repulsive forces between the film surface and electron beam. Subsequently, the roughness of the edges of the exposures increased for AZO films annealed at 600°C. The edges of the Fresnel rings show irregularity and distinct granularity, which can drastically reduce the efficiency in device applications.

The resistivity increases as annealing temperature increases for AZO films. The resistivity remains the lowest at 7.9×10^{-4} Ω-cm for the as-grown AZO films. However, the resistivity exponentially increases up to 0.82 Ω-cm after annealing at 500 ºC. This value is orders of magnitude higher than that of the as-grown films grown at 200 ºC.

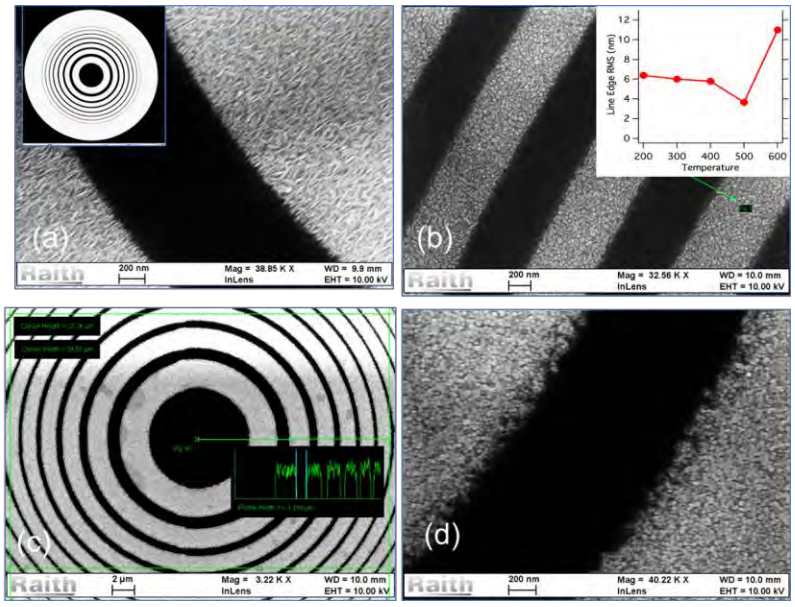

Figure 1.20. EBL patterns of Fresnel rings (a) as-grown films at 200ºC, and annealed at (b) 400, (c) 500 and (d) 600ºC of ALD grown AZO films.

In conclusion, we have demonstrated the nanopatterning of atomic layer deposited Al:ZnO films using electron beam lithography. The influence of grains on repeatable planar nanostructures by nanolithography process was studied for annealed films in order to avoid effects of granularity, which is one of the major reasons of the limiting factors in device applications. Our results demonstrate that the nanopatterning of AZO by the EBL technique is limited due to granularity of ALD grown AZO films. This finding suggests the limitations of ALD grown samples for optical applications where nanopatterns are fabricated by the EBL technique. Furthermore, the ALD grown films lose conductivity orders of magnitude upon annealing.

1.5 Thin Film Growth of Epitaxial MGO on AL:ZNO

We have studied the epitaxial growth of MgO thin films on (0001) Al-doped ZnO (Al:ZnO) underlayers, by oxygen plasma assisted PLD technique. We systematically investigated the MgO thin films using X-ray diffraction and atomic force microscopy, as well as along current-voltage characteristics. As the growth temperature increases, we observed a distinguishable behavior that the preferred MgO orientation changes from (111) to (001) in the films. Two completely different in-plane epitaxial relationships were also determined from X-ray diffraction as:

[110]MgO//[11$\bar{2}$0] Al:ZnO and [110]MgO//[1$\bar{1}$00] Al: ZnO for (001) MgO with 60° rotated triplet domains, and [110]MgO//[11$\bar{2}$0] Al: ZnO for (111) MgO with 180° rotated twin. The noticeable temperature dependence indicates a reconciliation of the nucleation driving forces among surface, interfacial and strain energy for heteroepitaxy of cubic MgO on hexagonal Al:ZnO. The related interfacial atomic registry is considered to be important in the formation of unusual (001) MgO on hexagonal crystals. Furthermore, the electrical characterization revealed a dramatic reduction of the leakage current in (001) MgO thin films, however the large leakage current is attributed mainly to the small grain size of (111) MgO as identified by atomic force microscopy.

Recently, oxide thin films, such as oxide semiconductors and perovskite oxides, have attracted much attention for their use in a wide range of device applications. Among these oxide semiconductors, wide bandgap ZnO (3.37 eV) has been of great interest today, owing to its large exciton binding energy (60 meV), pursuing reliable p-type conductivity and investigating transition metal doped ferromagnetic behaviors. In addition, conductive ZnO thin films have interesting applications such as transparent electrodes for solar cells and light emitting diodes, transparent thin film transistors and MEMS applications.

The integration of complex perovskite oxides on wide bandgap semiconductors potentially forms the basis for multifunctional microelectronic and electro-optic devices. However, high performance materials used in such multifunctional multilayers, heterostructures and nanostructures not only stay at the core of the development but also create major challenges to combine two dissimilar materials. Hence, it is crucial to incorporate a bridge layer as a nucleation or seed layer, which can promote the thin film crystallization.

Rocksalt MgO, a high transparent and large dielectric constant material, showed its compatibility with hexagonal ZnO as well as GaN and SiC. MgO provides close lattice match with extensively researched perovskite thin films such as lead Zirconate Titanate (PZT), Barium Strontium Titanate (BTO), and Yttrium Barium Copper Oxide (YBCO). The combination of MgO and the high conductivity Al-doped ZnO appears to be a promising multitude material system to achieve miniaturization of functional thin film components.

The growth of high quality epitaxial (Ba, Sr)TiO_3 on an MgO/ZnO bridge layer and MgO gated ZnO transistors have demonstrated the capability of integration of MgO and ZnO.

In our previous work, we found that the introduction of ZnO as intermediate layer enables the growth of (001)-oriented MgO on *a*-plane sapphire. A cursory investigation of similar substrates occurred with respect to the cost and flexibility of *c*-plane sapphire revealed the changes of the MgO orientations or textures at different growth temperatures. We accrued out a detailed investigation and confirmed the temperature dependence of the orientation preference and

heteroepitaxy of MgO thin films on Al-doped ZnO by X-ray diffraction, and determined their inplane epitaxial relationships. We also studied surface morphology and electrical performance to characterize their properties.

We used pulse laser deposition (PLD) equipped with a radio-frequency (rf) oxygen plasma source to deposit MgO and Al-doped ZnO thin films. For the ablation of Al-doped ZnO and Mg targets, we used a KrF excimer laser (wavelength = 248 nm, pulsed width = 25 ns, repetition rate = 1 - 5 Hz) , and the laser beam is aligned with the target at an angle of 45° with a pulse energy density of 2-3 J/cm^2 and a spot size around 1mm -3mm). The use of the rf oxygen plasma source provides a stable and high flux of reactive oxygen and thus enable us to utilize magnesium metal target for either the deposition of MgO thin films or the magnesium doping at relative low growth pressure. For low complexity and high efficiency deposition of for Al: ZnO, we synthesized a ceramic Al:ZnO target by mixing an amount of ZnO and 3% (weight) aluminum powders, followed by isostatic pressing at 500 MPa, and then sintering at 1000°C for 12 hours. In this work, the thin films were grown on *c*-plane sapphire substrates. After pumping the growth chamber and gas lines to the base pressure less than 5x10^{-8} Torr, we loaded the cleaned and heated substrates. The laser repetition rate was set to 5 Hz and growth rate of Al: ZnO films were about 130 -140 nm/hr (2 - 3 nm/min). We deposited a 150 nm Al:ZnO film as an underlayer or template, to serve as a bottom electrode in the electrical measurement. By setting its growth temperature at 450°C, we achieved high conductivity of Al:ZnO. We deposited a series of MgO thin films at the substrate temperatures ranging from 450 to 700 °C with an oxygen plasma pressure of 6x10^{-5} Torr and a plasma power of 250 W.

At the laser repetition rate of 3 Hz, the MgO growth rate was about 2 Å/min. To examine the structural properties of as-deposited films, we used X-ray diffraction (XRD) and to inspect the morphology of the films we used a Bruker Icon atomic force microscopy (AFM).

Experimental Results

We used a Rigaku X-ray diffractometer with Cu $K\alpha$ radiation to characterize the crystal structures of MgO/Al: ZnO thin films. The XRD 2θ patterns of MgO/Al: ZnO thin films deposited at the substrate temperatures of 450, 500 and 700 °C, is shown in Figure 1.21.

Highly crystalline Al:ZnO films have been regularly attained at a wide temperature range, which set a good starting point for following MgO growth. (0001)-oriented Al:ZnO films can be identified with the 2θ angle of 34.3° in all the films where the *c*-plane sapphire substrates exhibit the typical (0006) reflections at 41.7°. High quality ZnO epitaxy has been widely achieved, in spite of the large misfit (16%) between sapphire and ZnO, and the epitaxy results from the domain matching were reported elsewhere.

The data of 2θ scans show only an MgO reflection at 36.8°, corresponding to its (111) planes for MgO grown at 450°C. For MgO films grown at the temperature of 700°C, exclusive (002) reflections observed at 42.7° (Figure 1.21(c)) and indicates the formation of (001) MgO films. We found the coexistence of (001) and (111) MgO textures for temperature between 500 and 600°C. The trend of this orientation change in MgO films provides a reliable representation that the growth temperature has a pronounced effect on the nucleation of MgO films on Al:ZnO. The absence of other reflections, such as (011), demonstrates that (001) and (111) MgO are preferred orientations, and [001] or [111] axes of MgO films can be well aligned with Al: ZnO [0001] direction.

We found that for ~25 nm-thick films, the full-width at half-maximum (FWHM) of the MgO (002) at 700 °C is around 0.9 ° in the ω scan, whereas the one of (111) MgO grown at 450 °C is 1.5°. Since the growth temperature is one of the most critical factors in the oxide film growth, it is not surprising to see this discrepancy produced by the growth temperature. It is believed that high growth temperature as well as low oxygen partial pressure promotes high crystal quality of oxide films. We found that the peak positions of the MgO films, obtained by high resolution XRD, were referred to the (0006) reflections of the *c*-plane sapphire, and are converted to the *d*-spacing values as $d = 2.11$ Å for (002) and $d = 2.44$ Å for (111) MgO plane.

Using $a_0 = d\sqrt{h^2 + k^2 + l^2}$, h, k and l are miller indices, it translates a lattice parameter a_0 of MgO in both cases as 4.20 Å, which is close to the one of the bulk MgO crystal, $a_0 = 4.21$ Å.

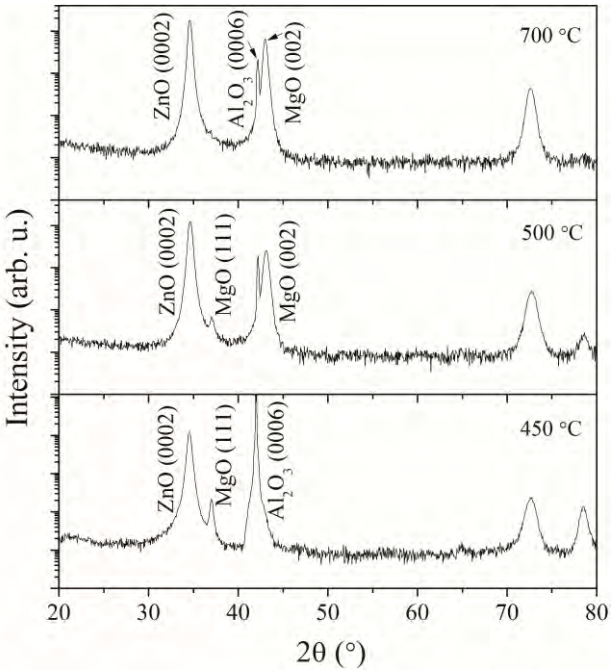

Figure 1.21 XRD 2θ patterns of MgO thin films grown on Al: ZnO at 450, 500 and 700 °C. However, the rocking curve scans showed better crystallinity of (001) MgO films than (111) films.

It is worth noting that the lattice parameter from the XRD scans is used as a method to prove that the formation of the well-aligned (001) and (111) MgO films quantitatively instead to confirm that MgO films are strain-relaxed.

In order to inspect the epitaxial growth relationships, we used a PANalytical X'Pert diffractometer to collect the data corresponding to the azimuthal scans as shown in Figure 1.22. In Figure 1.22(a) the Φ scan data shows the (022) reflections of (111) MgO as compared to Al: ZnO $(10\bar{1}1)$ reflections. It is worth noting that the six-fold reflections separated by 60° indicate the existence of 180° rotated twin MgO domains, which match the XRD positions of Al: ZnO $(10\bar{1}1)$ reflections. Hence the (111) MgO growth follows the in-plane relation as $[110]MgO//[11\bar{2}0]$ Al: ZnO as shown in Figure 1.22(a). Identical epitaxial relationship has been found in similar cubic MgO on hexagonal GaN.

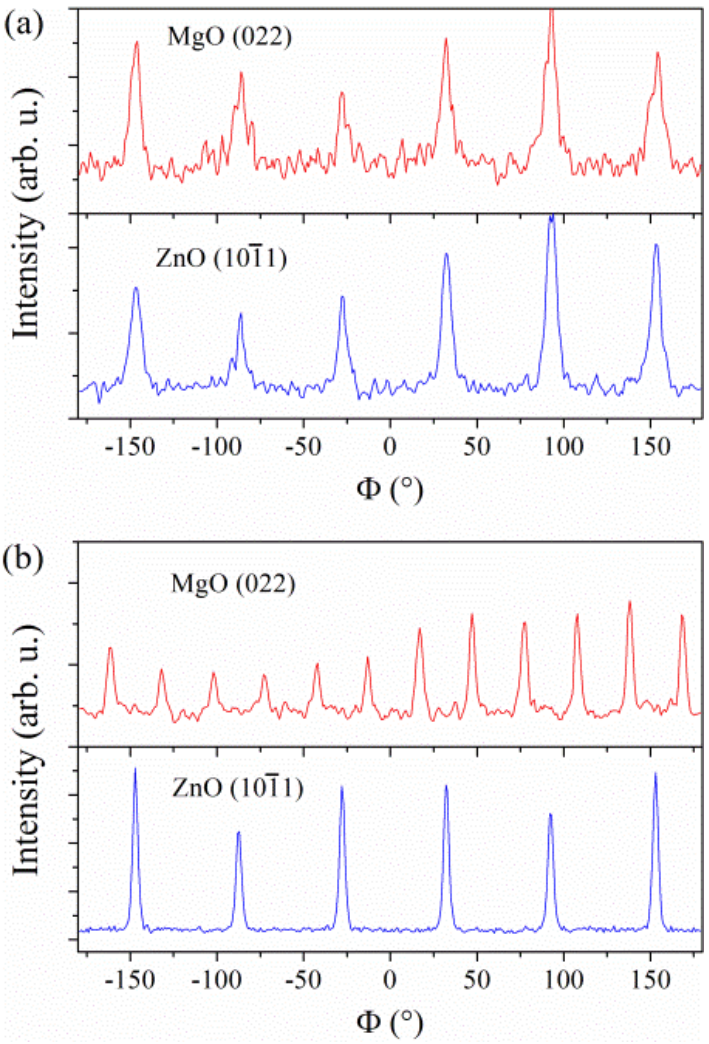

Figure 1.22 XRD Φ scans of (a) (022) planes from (111) MgO and $(10\bar{1}1)$ planes from (0001) Al: ZnO and (b) (022) planes from (001) MgO and $(10\bar{1}1)$ planes from (0001) Al:ZnO.

In contrast, we found out that the films grown at 450 °C, when MgO forms on Al:ZnO at elevated temperature, the in-plane epitaxial relationship was developed differently than the out-of-plane. MgO (022) planes display twelve reflection peaks rotated by 30º with respect to each other, as shown in Figure 1.22(b). This suggests three sets of (001) MgO domains with 60º rotation, and the in-plane epitaxial arrangement of (001) MgO on Al:ZnO to be $[110]MgO//[11\bar{2}0]$ Al:ZnO and $[110]MgO//[1\bar{1}00]$ Al: ZnO. This epitaxial relationship is consistent with previous reports.

The epitaxial arrangements of (001) and (111) MgO lattices on (0001) Al:ZnO is illustrated in Figure 1.23. The in-plane projections of the Al:ZnO unit cells are represented by the dashed lines connected hexagons, and the projections of MgO are the squares or triangles represented by solid lines.

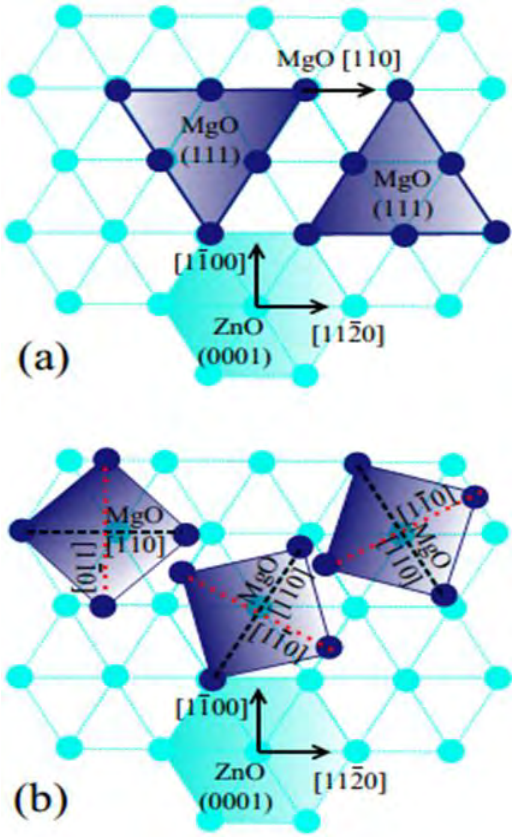

Figure 1.23 Schematic diagram showing the in-plane epitaxial relationship between (a) (111)-oriented and (b) (001)-oriented MgO thin films on (0001) Al: ZnO.

The epitaxial relationships can be evaluated quantitatively on the basis of lattice fitting arguments. An essential quantity is the lattice mismatch m, which is defined as $m = (a_f - a_s)/a_s$ where a_f and a_s refer to the unstrained lattice parameters of film and substrate, respectively. Since there are two dissimilar lattice structures between cubic MgO on hexagonal Al:ZnO, the formula is modified as $m = (\sqrt{2}a_{MgO} - 2a_{AZO})/2a_{AZO}$ to calculate the misfit along the MgO [110] direction. For the cases of (001) and (111) MgO, the MgO [110] directions lie along the GaN $[1\bar{1}00]$ and the resulting misfit is around -7% where a_{MgO} = 4.2 Å and $a_{AlZnO} \approx$ 3.25 Å (ZnO lattice constant, a = 3.25 Å). Additionally, the negative sign of the misfit indicates that the both (001) and (111) MgO films would be contracted in compression of the initial layers. The argument above is based on a simple geometry model and limited the stress only along the direction of MgO [110]. It is evident that the epitaxy of face-centered cubic films on hexagonal structures is much complicated in respect with their epitaxial relationship and film nucleation. To gain comprehensive understanding of this combination, numerous other issues must be taken into account, such as surface, interfacial, and strain energy in addition to the geometric matching.

We studied the morphological properties of the grown films using Atomic Force Microscopy (AFM).The AFM images of the 25 nm MgO films over a 2×2 μm^2 area is shown in Figure 1.24. Root mean square (RMS) roughness for (111) films is 0.5 nm and (001) is about 0.9 nm. We estimated the average grain size of (001) to be ~25 nm and (111) to be ~70 nm. It is believed that, in general, surface recrystallization and large grain growth occur at the high temperatures with large activation energy.

Owing to twin and triplet domains in the MgO epilayers on Al:ZnO, dislocations, and the defects between the grain boundaries, this factors provide a direct leakage path, especially when the film thickness is 25 nm which is less than their grain sizes.

It is worth noting that (111) MgO is susceptible to hydroxylation and easier to interact with water due to the compensation of the polar dipole. In addition, due to (111) MgO films small grain sizes and relatively low crystal quality, it is not surprising to see the large leakage current density in (111) MgO films. In contrast, (001) MgO is less reactive due to a neutral charge surface. Therefore it is possible that (111) MgO might suffer the degradation of the electrical performance in air.

We have further investigated the quality of the epitaxy MgO films with respect to their electrical properties. We deposited Pt/Ti circular top electrodes of 30/10 nm in thickness and 100 - 300 µm on ~20 nm (001) and (111) MgO films by successive use of photolithography, e-beam evaporation, and liftoff. The underneath Al:ZnO layers were used as bottom conductive electrodes.

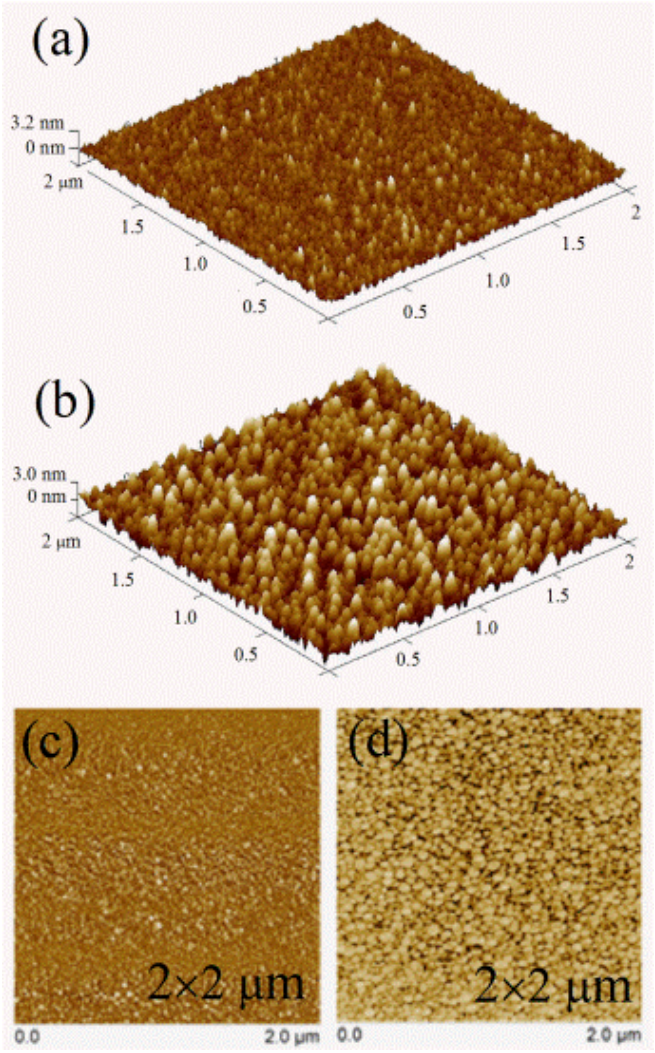

Figure 1.24 AFM 3D height images of (a) (111) and (b) (001) MgO thin films, and phase images of (c) (111) and (d) (001) MgO thin films.

The leakage current density of (001) MgO is shown in Figure 1.25. At a bias voltage of 10 V, corresponding to an electric field of 5000 kV/cm, we found the leakage current density of (001) MgO to be ~5×10^{-6} A/cm^2. However, (111) MgO shows poor insulation quality and at the bias of 2 V the leakage current density reaches as high as 0.5 A/cm^2.

In the comparison experiment of the MgO electrical property, the Al:ZnO underlayers were used as the bottom electrodes and presumably their conductivity was not affected at elevated growth temperate of (001) MgO. We used a standard four-probe technique to measure the electrical resistivity of Al: ZnO films. The temperature dependence curves of the Al:ZnO resistivity is shown in Figure 1.26. Although all Al: ZnO films were deposited at 450°C, we noticed that the followed high temperature growth of MgO had a small impact on Al: ZnO resistivity.

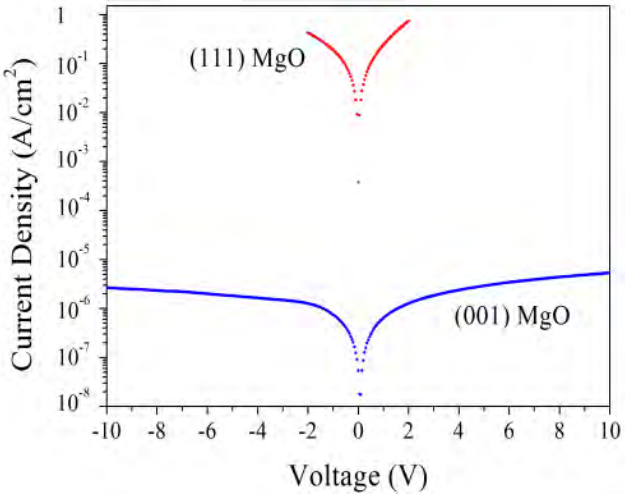

Figure 1.25 Leakage current-voltage characteristics of Pt/(001) MgO/Al: ZnO and Pt/(111) MgO/Al: ZnO structures.

We found that as the growth temperature of MgO was raised from 450 to 700°C, the room temperature resistivity of the Al:ZnO underlayer increased from 0.26×10^{-3} to 0.80×10^{-3} ohm-cm, and the metallic behavior of the temperature dependence has a slight change as the measurement temperature drops below 100 K.

In addition, Al doping produced several effects in the ZnO electrical conductivity. Mainly, Al acts as an effective donor due to the contribution from the Al ions at the substitutional sites of Zn ions as well as Al interstitial atoms that change the oxygen vacancy characteristic. It is interesting to note that the following high temperature MgO growth, which acts as a post-annealing for the Al:ZnO underlayer, can affect this contribution and causes the change of the conductivity. As seen in Figure 1.26, the resulted increase in the resistivity would not be large enough to cause any remarkable difference in the MgO electrical properties. Therefore, one can reasonably neglect this effect.

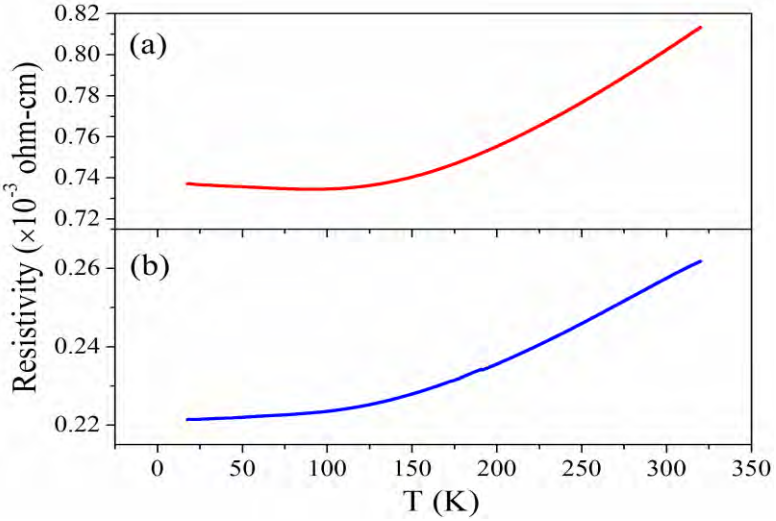

Figure 1.26 Resistivity temperature dependence of the Al: ZnO thin films. The top MgO thin films were grown at (a) 700°C, and (b) 450°C.

We found that, depending on the substrate temperature, the growth of MgO on the Al:ZnO (001) surface was controlled by two different regimes, which can exist exclusively and mainly differ in the symmetry of the MgO lattice arrangement. It is known that γ_f, the energy of the film, γ_s the energy of the underly, and γ_i the interfacial energy play a critical role in the formation of the heterogeneous nucleation and grain structure. The (001) planes are the natural cleavage planes of MgO, which are charge neutral and have a low cleavage surface energy 2.39 J/m^2 compared to a higher cleavage energy of 3.08 J/m^2 in (111) MgO surfaces.

It is known that, in thermodynamic equilibrium state the (111) surfaces of MgO system will be unstable with respect to (001), and the formation of (001) facets is favored in a discrete MgO system. As the films are thin (~25 nm), if the interfacial energy, γ_i, is neglected and the chemical bonding related interfacial energy is treated as the same for the (111) and (001) MgO films on Al:ZnO, the strain energy must be taken into account.

For simplicity, we consider only the effect of biaxial situation and assume the same strain for (001) and (111) MgO films. A quantity of interest, the strain energy per unit volume (W_s) has a magnitude:

$$W_s = M_{hkl}\varepsilon_1^2 \tag{1}$$

where ε_1 is the strain and M_{hkl} is an orientation dependent biaxial modulus and can be calculated from the equations (2) and (3) below.

The stiffness matrix has the following components c_{11} = 289 GPa, c_{12} = 88 GPa, and c_{44} = 155 GPa and the elastic anisotropy factor $A = 2c_{44}/(c_{11}-c_{12}) = 1.54$. The biaxial elastic modulus $M_{(001)}$ and $M_{(111)}$ are isotropic in the MgO (001) and (111) planes and are given by:

$$M_{(001)} = c_{11} + c_{12} - \frac{2(c_{12})^2}{c_{11}} = 323\ GPa \tag{2}$$

$$M_{(111)} = \frac{6c_{44}(c_{11}+2c_{12})}{c_{11}+2c_{12}+4c_{44}} = 399\ GPa \tag{3}$$

The result implies that for MgO, (001)-oriented grains, when subjected to a biaxial strain and under plane stress, have the low elastic strain energy density of all orientations in the film, and that (111) grains have the high elastic strain energy density of all orientations. Consequently, under these conditions, the formation of the (001) oriented MgO is definitely preferred. Nevertheless, interestingly, regarding the growth behavior on GaN and SiC where (001) plane was not found, (111) MgO was observed and its formation dominates the growth.

Similar temperature dependence of MgO on (111) Si substrates was reported elsewhere using atomic layer deposition (ALD) growth but opposite temperature dependence trend on (001) Si

substrate. The main factor of the orientation growth is attributed to the variances of the surface diffusion of Mg and O species. The large diffusion coefficient promotes the populated planes.

It is important to note that considering MgO alone is not a conducive to understanding the competition between (001) and (111) MgO growth. (111) MgO shows good interfacial atomic registry, where all interfacial Mg species can be accommodated with the underlying ZnO lattice atoms, as seen in the diagram of atomic arrangement in Figure 1.23. However, the atomic arrangement of (001) MgO is not possible to be fully satisfied with the atoms along $[1\,\bar{1}0]$ directions.

Dislocations, formed at the interface or relaxed epitaxy, would occur on the initial stage of nucleation. This suggests that (001) MgO suffers large lattice dislocation and has large strain energy anisotropy. Due to this $[1\,\bar{1}0]$ lattice mismatch, strain energy accumulates in the growing film, and when this strain energy is released; the high energy at the interface of the intermediate-layer changes the total energy site. Therefore, at low growth temperatures, the (001) nucleation become unfavorable and because of the low diffusion mobility, bulk grain growth and surface recrystallization are suppressed. As seen in the AFM images, .the (001) nucleation may trigger island formation and cause a rougher surface formation.

It is worth mentioning that, at the low growth temperatures, good interfacial registry is realized in (111) MgO even when large surface energy may be necessary in the thin layer with large surface to volume ratio. However, as the temperature increases the Mg ions, with high diffusion mobility, are gradually pulled out their preferred locations to satisfy the minimization of surface energy. Consequently, as the growth temperature increases, the growth of (001) MgO becomes dominant.

In several different growth techniques, it is not uncommon that MgO molecules are formed before landing on the growth surface, particularly under high growth pressure. In this case the thermal energy would not be high enough to allow MgO molecules to adjust the locations to favor the good atomic registry where the densely populated (001) MgO is dominant. Nevertheless, in our experiments, we used a magnesium metal target and a highly active oxygen plasma source, and the MgO molecular formation is suppressed mainly due to the low growth pressure, $6x10^{-5}$ Torr. At this pressure range, we estimated the mean free path λ to be roughly 100 cm which is in turn much longer than the distance of the Mg target to the substrate which is d = 10 cm. Therefore, the majority of Mg ions are transferred to the substrate prior to the formation of MgO molecules. This provides Mg ions a good chance to locate their preferred lattice registry and lead to the (111) MgO nucleation. In addition, high quality PZT thin films have been deposited on ZnO/glass substrates. The use of an MgO buffer layer grown by PLD

prior PZT deposition paved the way to achieve highly (111)-oriented PZT films at relatively low growth temperature.

1.6 Low Thermal Budget Growth of Highly Crystalline PZT on Glass Substrates

Several processing challenges were imposed onto the deposition of high quality PZT thin films. Although deposition of PZT thin films has been widely studied, high growth temperature, typical 600 -700 ºC for crystalline PZT still hurdles the development of PZT thin film devices on varieties of substrates. In this research we have being studying high quality PZT thin film growth on glass substrates, which have a low transition temperature and are not suitable for high temperature thin film deposition.

In order to avoid the structural deformation of the glass substrates, the MgO/ZnO templates grown on Corning 1737 glass were prepared at 450ºC using the similar process as aforementioned growth on sapphire substrates. The templates were then transferred into the sputtering growth chamber for PZT deposition. In addition, the templates with MgO buffer was kept at 6 mTorr pressure of oxygen during ramping up the temperature. For the growth of PZT films on glass, the growth condition was calibrated. The pressure of the 2:1 Ar/O_2 gas mixture was set as 2 mTorr.

The crystalline structure and orientation of the as-deposited PZT films were determined by Rigaku X-ray diffractometer with Cu $K\alpha$ radiation. A single perovskite phase was observed in the sputtered PZT thin films with the MgO buffer layer as shown in Figure 1.27 , corresponding to the PZT (011) orientation. The 2θ angle of PZT (011) reflection located at 31.0º, which was close to the Bragg angle for the PZT from the international center for diffraction data. One additional peak at 42.8º is associated with MgO (002). Although the coexistence of MgO (002) and MgO (111) was found in the integration of MgO and ZnO on sapphire substrate, where the growth temperature is below 500 ºC, the XRD patterns didn't show noticeable MgO (111) reflections for ZnO grown on glass even at 450 ºC of the growth temperature.

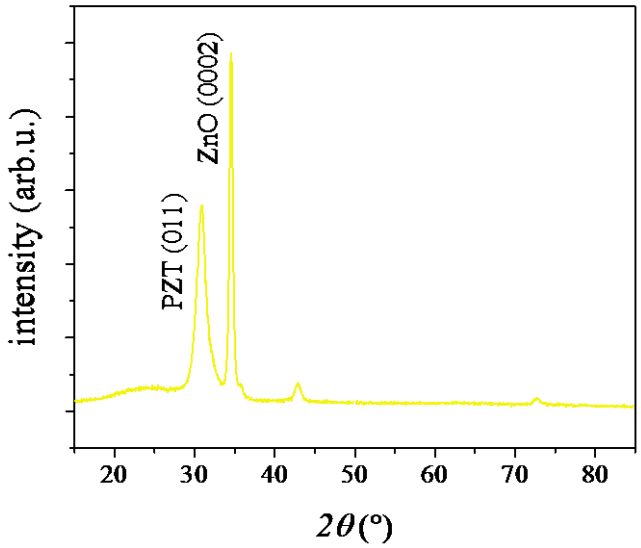

Figure 1.27 XRD pattern of PZT deposited on MgO buffered Al-doped ZnO glass template.

As discussed, surface, interfacial, and strain energy are critical factors to influence the nucleation of MgO thin films. It suggests that these energies would not be identical as ZnO grown on amorphous glass substrates. Furthermore, crystallinity of ZnO on glass is much lower than ones on sapphire that induces the complexity of the nucleation.

In contrast, PZT films directly grown on ZnO without the MgO buffer layer did not show any perovskite phase reflect. Only a peak at 29.3º Degree corresponding to the reflection of the pyrochlore phase was observed in the XRD patterns see Figure 1.28. Therefore, the XRD data strongly suggest that the MgO buffer layer influences the orientation and crystal nucleation of perovskite PZT films and promotes heterogeneous PZT formation with ZnO on glass substrates.

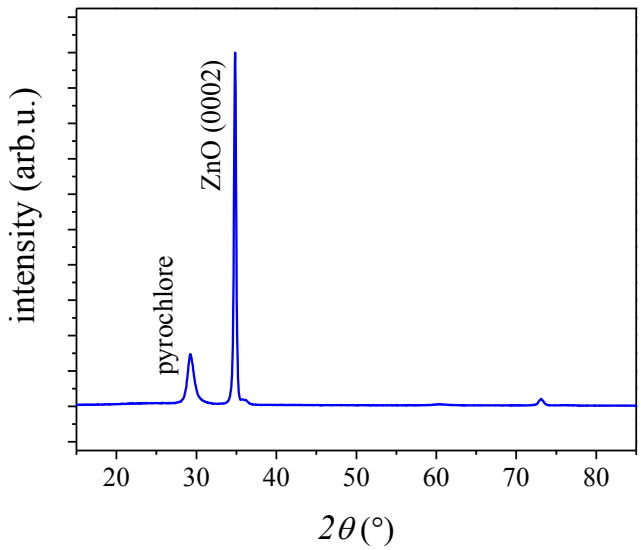

Figure 1.28 XRD pattern of PZT deposited on Al-doped ZnO glass template

Considerable insight related to PZT nucleation with or without MgO buffer layers has come from AFM analysis, Figures 1.29 and 1.30. The grain size can be measured by means of AFM, where grains can be resolved on the surface. Figure 1.29 shows AFM images of the PZT thin films over a 2×2 μm^2 area. Root mean square roughness for (011) PZT films is 0.9 nm and the pyrochlore PZT is around 1.2 nm. The average grain size of single phase PZT (011) is 25 nm. However

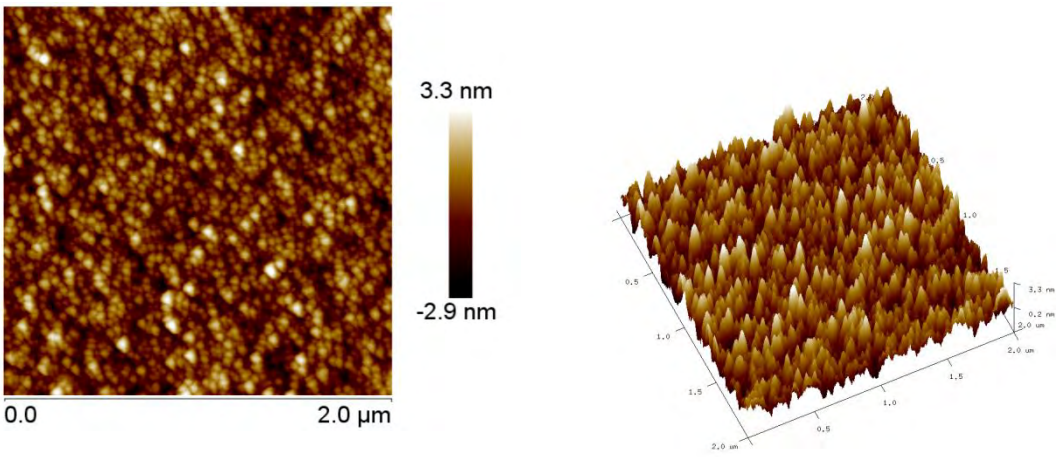

Figure 1.29. AFM images of PZT on MgO buffered Al-doped ZnO glass template.

the pyrochlore phase PZT has two different grain sizes around 25 and 70 nm. In general the different grain size indicates the abnormal nucleation of PZT directly grown on ZnO. The mechanism of this kind nucleation is under investigation. Most likely it would be caused by the large lattice mismatch between perovskite PZT and wurtzite ZnO crystal structures.

In this study, we have established the epitaxy growth of (111) and (001) MgO films on (0001) Al: ZnO. We found a notable behavior in the change of orientation, from (111) to (001). This change depends on the growth temperature under low plasma pressure. From X-ray diffraction, we observed two completely different in-plane epitaxial relationships, [110]MgO//$[11\bar{2}0]$ Al:ZnO and [110]MgO//$[1\bar{1}00]$ Al:ZnO for (001) MgO with 60° rotated triplet domains, and [110]MgO//$[11\bar{2}0]$ Al:ZnO for (111) MgO with 180° rotated twin.

The noticeable temperature dependence indicates a reconciliation of the nucleation driving forces on the surface, interfacial and strain energy. These factors are affected by the atomic registry of cubic MgO on hexagonal Al:ZnO.

While the electrical characterization revealed a poor electrical property in (111) MgO films compared to (001) MgO, the MgO surfaces with different orientations provide a good template to realize the complex oxide integration on ZnO.

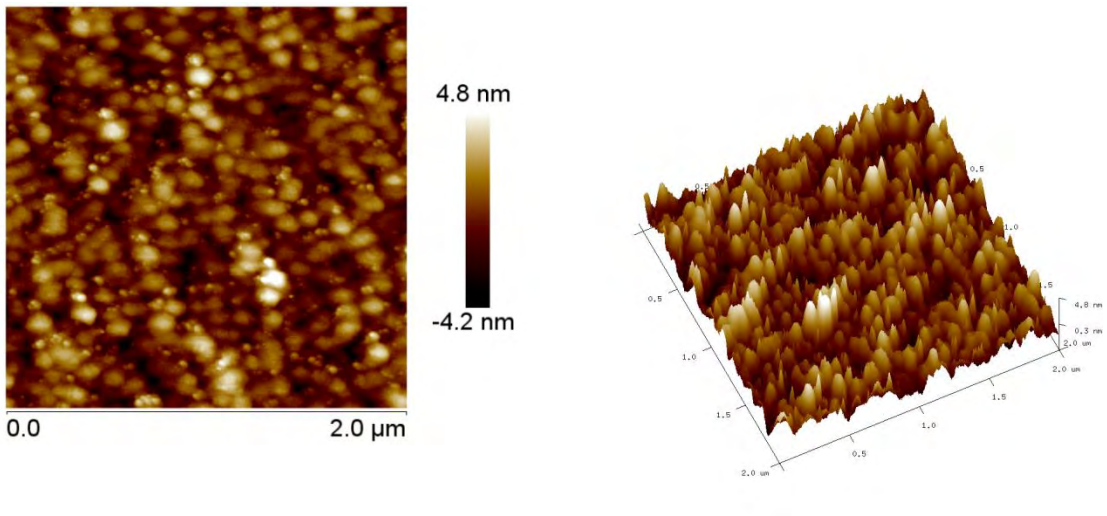

Figure 1.30 AFM images of PZT on Al-doped ZnO glass template.

1.7 Modeling and Simulation of ZnO and SiO2 Film Growth by Atomic Layer Deposition

ALD is a promising fabrication technique for metallic and dielectric materials due to its low deposition temperature and high quality of the deposited films. In order to understand film

deposition mechanism and to compare it to other deposition techniques in terms of film quality, we performed modeling and simulation of chemical deposition reaction on film surfaces and simulated the film macroscopic properties comparing with experimental results.

Modeling of the ZnO Atomic Layer Deposition Process

In this section we present results of the modeling and simulation of ZnO film deposition reaction used in ALD process. The ZnO films are grown at low temperature by decomposition of diethyl-zinc molecule in vacuum chamber. The diethyl-zinc $(C_2H_5)_2Zn$, or DEZn, is a highly pyrophoric organo-zinc liquid compound consisting of molecules with the zinc center atom bound to two ethyl groups as shown in Figure 1.31. This colorless liquid is an important reagent in organic chemistry and available commercially as a solution in hexanes, heptane, or toluene.

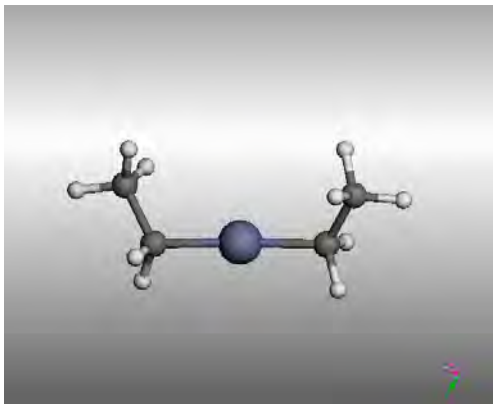

Figure 1.31 Atomic structure of diethyl-zinc molecule.

We use the first principles density functional theory (DFT) to study mechanisms of thin film growth focusing on the processes used in ALD film deposition technology. The ZnO surface has been modeled by a Zn-terminated slab saturated with hydroxyl groups as shown in Figure 1.32. The deposition starts by adding the DEZn molecule to the hydroxyl terminated ZnO surface (Figure 1.32a) and ended by creation of next Zn-atom monolayer on the surface accompanied by ethanol molecules that will be removed (see Figure 1.32b)

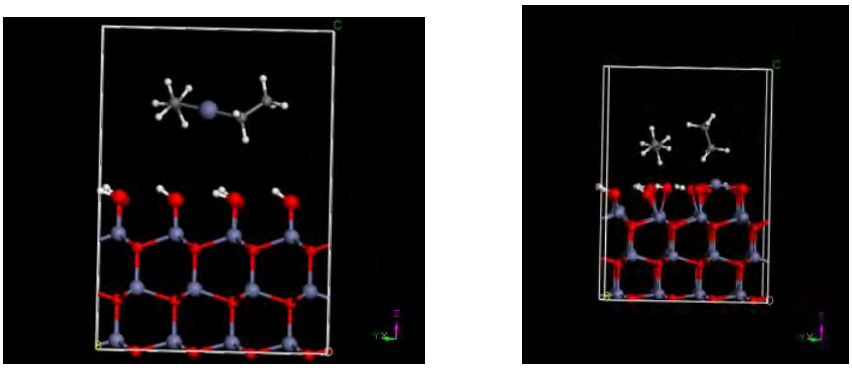

a b

Figure 1.32. Initial and final steps of the DEZn reaction on ZnO surface in ALD process.

Figure 1.33 shows atom configurations corresponding to initial and final step of the DEZn molecular decomposition and creation of thedrahedrally coordinated new Zn-layer on top of the O-layer of the ZnO surface. Study of the reaction energy characteristics was based on the calculation of the total energy variations accompanied the molecular decomposition and new

bond creation on ZnO surface. According to the analysis the entire reaction contains at least the seven well-distiguishable steps labeled by numbers in Figures. 1.32 and 1.33.

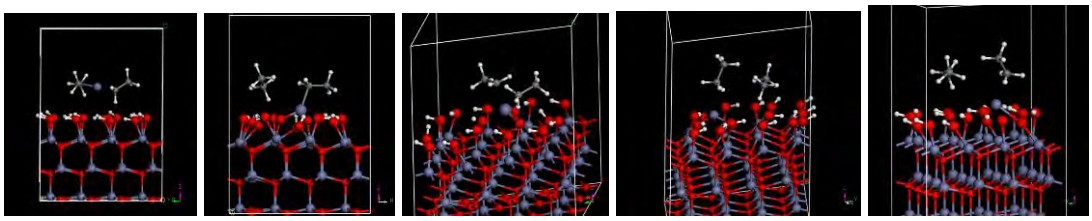

2 3 4 5 6

Figure 1.33 Atomic configurations of the major ZnO-growth reaction steps.

In order to understand mechanisms of the reaction, total energies, related to every reaction step, are calculated. In Figure 1.34 we show total energies per atom for every reaction step. The analysis clearly reveals several transition states of the reaction labeled by configurations 2, 4, and 6. Note that intermediate configuration 3 and 5 are separated by a quite low energy barrier corresponding to the transition state 4. The low energy reaction path is reversible.

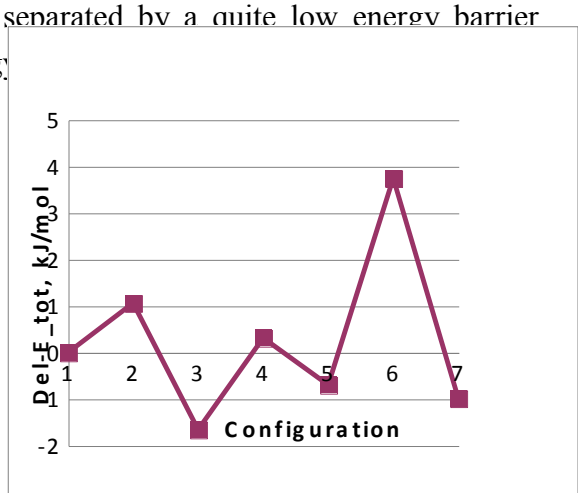

Figure 1.34 Calculated energy reaction path that simulates ALD ZnO film growth.

Another important component of the ALD process is water that is normally added into the chamber. Water is an important component of the reaction helping activation of the DEZn molecule. We found that adding water to the system remarkably increases the barrier 4 thus making the reaction not reversible.

In this work, we studied the reactions of three Zn-containing species – $Zn(C_2H_5)_2$, $HZnC_2H_5$, and $(ZnC_2H_5)_2$ – and water. By the DFT calculations the optimized molecular structures are determined and the reaction transition states are obtained. Our study demonstrates that by varying water concentration in the system one can affect internal reaction energy barriers and in such a way control the deposition reaction. This finding opens a possibility of the optimization for the ALD ZnO-film deposition technology.

Vibrational Spectroscopy of the ALD Grown SiO2 Films

Silicon dioxide (SiO_2) is a basic element of modern electronic devices. Growth of SiO_2 high-quality films at lower temperatures is essential for modern applications, e.g. in nano-scaled semiconductor devices and/or opto-electronic devices that use organic thin films or organic-

inorganic nano-composites. In this work, we study the ALD grown SiO_2 by Raman spectroscopy comparing with the Raman spectrum calculated for the model system.

In order to study the mechanisms that govern Raman optical excitation in ALD grown films at the atomic level, we calculated the Raman spectrum of the SiO_2 modeled system using a first principles quantum mechanical method implemented in DMoL3 simulation package (Material Studio). The alpha-quartz basic cluster structure has been chosen for the Raman spectrum calculation. The atomic model is shown in Figure 1.35.

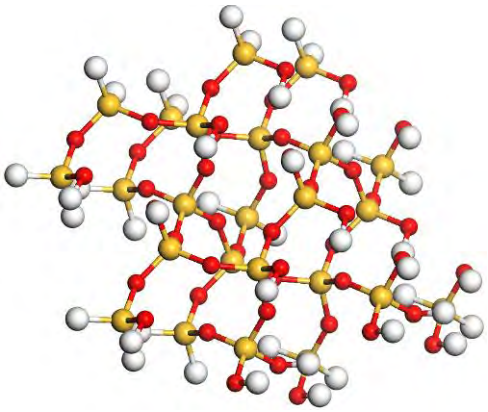

Figure 1.35. SiO_2 basic atomic cluster unit of alpha quartz used for Raman spectrum calculation.

We used the SiO_2 model built (as the H-terminated atomic fragment of alpha quartz). The result is compared to the Raman spectrum obtained experimentally on bulk amorphous SiO_2 film. Analysis of the vibrational spectra in a system is a very powerful tool to study specific atomic configurations presented in the film. The reason for this is that optical response caused by vibrational excitations is mostly sensitive to the nearest atomic order. Therefore a basic idea of present study is to calculate Raman spectra for different molecular atomic formations and compare the results to experimental Raman spectrum of the ALD SiO_2 samples. The analysis should indicate which atomic configurations are reproduced by ALD comparing to CVD processes.

Alpha quartz is chosen in this work as a basic model system for theoretical study. Ground state and electronic structure are obtained from first principle DFT calculations. Atomic force characteristics of the bonds are obtained from the self-consistently calculated potential energy functional. These results are used to calculate the Raman spectrum of the system. Figure 1.36 presents the theoretical Raman spectrum corresponding to the atomic model of the SiO_2 film given in Figure 1.35.

In Figure 1.36 the Raman spectrum with yellow squares corresponds to the theoretical results while the graph with the brown circular markers corresponds to the bulk SiO_2 ALD film. The band labelled as region I corresponds to the acoustic phonons with a well-known peak location near 60 cm^{-1}. This peak was reported only in the bulk SiO_2 film. The band II (located from 200 cm^{-1} to 550 cm^{-1}) is composed of several peaks. In literature, the leading Raman bands are identified. The line at 295 cm^{-1} corresponds to the scissor-like vibrations of the extended tetrahedron [SiO4/2]-[Si4/4]. The peak at 380cm^{-1} (and 465 cm^{-1}) corresponds to the bending vibrations in 5 (or more) - membered rings. Another peak (490 cm^{-1}) corresponds to four membered ring defect vibrations in the structure of bulk silica. These vibrations correspond well

to the narrow peak at ~488 cm^{-1} observed on our ALD grown SiO_2 film. The 600/601 cm^{-1} (region III) of Raman response corresponds to the vibrations in three membered rings and corresponds to the D_2 line. The Raman peak at 800 cm^{-1} corresponds to the 792 cm^{-1} or 800 cm^{-1} bands (region IV) observed before.

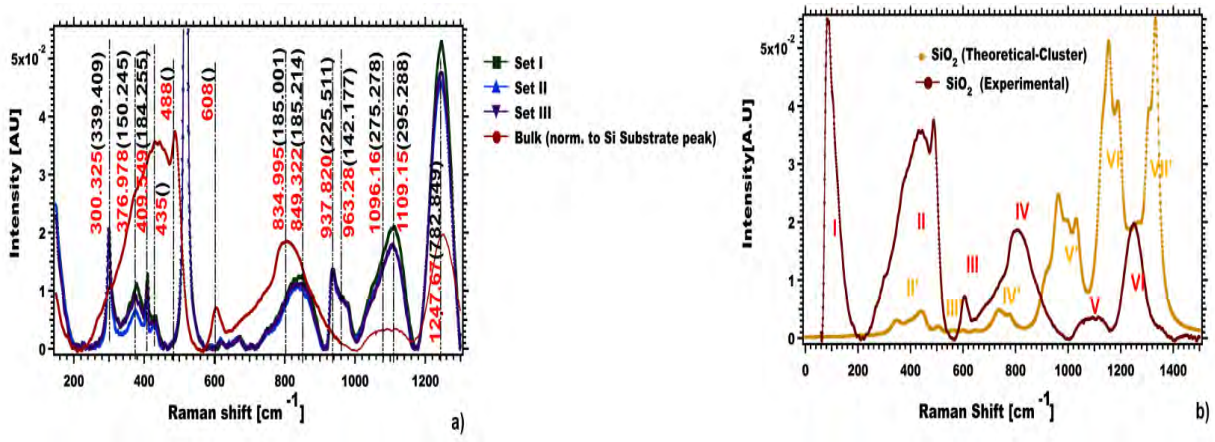

Figure 1.36 Raman spectra of the SiO_2 calculated (b) for the alpha quartz model system in comparison with the spectrum measured (a) on the ALD SiO_2 films. Most prominent Raman bands are labeled by roman numerals and discussed in text (b).

Our theoretical spectrum agrees very well with the aforementioned bands. We state a red shift of the theoretical spectrum compared to the experimental one measured on bulk ALD SiO_2 with much lower peak intensities. The red shift of the predicted vibration frequencies is due to the underestimation of the interatomic forces as a result of the generalized gradient approximation method used in DMol3 package to describe the exchange and correlation interaction. Therefore, a comparison between calculated and measured Raman spectra of the SiO_2 films indicates that the theoretical model used in this work reproduces all major optical singularities observed experimentally. This confirms that the cluster model presented in Figure 1.34 correctly represents most dominant atomic configurations in the nearest order region of the ALD grown SiO_2 film. Comparison of the calculated and measured Raman spectra indicates the presence of tetrahedral pseudo-crystalline phases of SiO_2 like cristobalite and alpha quartz. This gives a clear indication of some short range order in the films grown by this technique.

1.8 Development And Characterization of $Pb(Zr,Ti)O_3$ On ZNO for MEMS and Sensors Applications

One of the most interesting and active research topics in oxide semiconductors and perovskite oxides is oxide thin films. Due to its excellent ferroelectric, piezoelectric, pyroelectric, electro-optical properties and its potential applications in broad range of applications, especially multifunctional devices and MEMs, Lead Zirconate Titanate (PZT)- $Pb(Zr,Ti)O_3$ has proven to

be a promising material in the class of perovskite oxides. The development of thin-film-based multifunctional materials with semiconductors integration is the consequence of the need for the miniaturization of the electronic systems. Due to their chemical compatibility, there has been a growing interest in integrating PZT perovskite oxides with ZnO. In addition, Aluminum doped Zinc Oxide (AZO), due its large exciton binding energy, has been investigated for dependable p-type conductivity and transition metal doped ferromagnetic behavior studies.

It is worth noting that, because of the large lattice mismatch and dissimilar crystal structures between PZT and ZnO, it has been very difficult to achieve high quality thin films. To promote the formation of high quality ferroelectric-semiconductor heterostructures and to mitigate the problem of integrating dissimilar crystal materials, a considerable research has been done with the introduction of a buffer or seed layer between the two structures.

The growth of PZT thin films have been investigated on a variety of substrates such as $SrTiO_3$, MgO, silicon, sapphire, glass, quartz and so on. In particular, glass substrates are widely used in the display, imaging and optical applications due to the mass production scaling and low cost. In addition, the integration of PZT material with glass provides a new platform to exploit the transparent electronic and optical devices. MgO, a highly transparent and large dielectric constant material, showed a promising compatibility as an interfacial layer to accommodate the PZT nucleation. For high quality thin film materials growth, studies showed that MgO can be used as substrate for materials such as lead zirconate titanate, barium strontium titanate, yttrium barium copper oxide.

In this research, we have deposited high quality PZT thin films on glass substrates by rf sputtering using Al-doped ZnO as the bottom electrode with an MgO interfacial seed layer. We carried out systematic investigation of the heterostructures by X-ray diffraction, atomic force microscopy, along with the experimental and mathematical simulation of the electrical characteristics. X-ray diffraction revealed the formation of highly (011)-oriented perovskite phase in $Pb(Zr,Ti)O_3$ thin films with the MgO layer, whereas only the pyrochlore phase was observed in the films deposited directly on ZnO/glass. It is worth noting that surface morphology revealed by atomic force microscopy indicates that the nucleation of perovskite $Pb(Zr,Ti)O_3$ thin films are promoted to form uniform grain structures and improved smoothness as the introduction of MgO interfacial seed layer. A systematic investigation of the PZT on conductive Al-doped ZnO with an MgO seed layer revealed the formation of the highly orientated or textured structure at different growth temperatures. The investigation has confirmed the dependence of the orientation preference and surface morphology of PZT thin films on Al-doped ZnO by X-ray diffraction and atomic force microscopy.

To characterize the electrical properties and performance of the grown films, we carried out different experimental characterizations, including CV (capacitance-voltage) and PE

(polarization versus electric field) measurements. The CV measurements displayed a butterfly shape of the capacitance curves which resembles to the typical metal-ferroelectric-metal structures. To understand the unsaturated hysteresis loops, we experimentally investigated the behavior of the PE curves.

Experimental Studies

We used a PLD equipped with a radio-frequency (rf) oxygen plasma source. This rf oxygen plasma source provides a stable and high flux of reactive oxygen and consequently enables the use of magnesium metal target for either the deposition of MgO thin films or the magnesium doping at relative low growth pressure. The PLD uses a KrF excimer laser (wavelength = 248 nm, pulsed width = 25 ns, repetition rate = 1 - 5 Hz) used for the ablation of Al-doped ZnO and Mg targets. The laser beam is aligned with the target at an angle of 45° with a pulse energy density of 2-3 J/cm^2 and a spot size around 1mm × 3mm). The used a ceramic Al:ZnO target was synthesized by mixing an amount of ZnO and 3% (weight) aluminum powders, followed by isostatic pressing at 500 MPa, and then sintering at 1000 °C for 12 hours. After pumping the growth chamber and gas lines to the base pressure less than 5x10^{-8} Torr, the cleaned glass substrates were loaded into the chamber and heated. We used a growth rate of Al: ZnO films was 130 -140 nm/hr (2 - 3 nm/min), laser repetition rate of 5 Hz and growth temperature of 500 °C. We deposited a 200 nm Al: ZnO film as an underlayer or template, serving as a conductive electrode in the electrical measurement.

We deposited a series of PZT thin films by an off-axis rf magnetron sputtering using a 3 inch diameter PZT target. This target has the morphotropic phase boundary (MPB) composition, Zr:Ti = 52:48 containing 10 mol% excess PbO to prevent lead deficiency due to the high Pb volatility. We injected a mixture of Ar and O_2 gases into the growth chamber and maintained the pressure at 2 mTorr. At the sputtering rf power of 100 W, the PZT growth rate was about 5 Å/min. We investigated the structural properties of as-deposited films by X-ray diffraction (XRD) and the morphology of the films by Bruker Icon atomic force microscopy (AFM).

Results and Discussion

Using Rigaku X-ray diffractometer with Cu $K\alpha$ radiation, the structural properties of the thin films have been investigated. The 2θ patterns of as-deposited thin films with an MgO interfacial seed layer as compared to the PZT film grown directly on ZnO/glass is shown in Figure 1.37.

One can notice that Al:ZnO layers have the (0002) reflections at 34.5° and also that there is only a weak diffraction at 43.0° due to the fact that MgO layer is thin and its thickness is only 10 - 15 nm. This is consistent with the (002) MgO reflection. Contrarily, (111) MgO orientation was dominant at the growth temperature of 500 °C in the MgO/ZnO/c-plane sapphire multilayer structures using exactly same growth techniques. This indicates that the substrates play a critical role here which affects the MgO nucleation on Al:ZnO. Due to the high crystallinity of sapphire substrates compared to amorphous glass substrates, the quality of the ZnO films deposited on glass substrates is much lower. It might suggest that the interfacial Mg species cannot achieve well-arranged atomic registry during the initial nucleation owing to the lack of the surface perfection of those ZnO films.

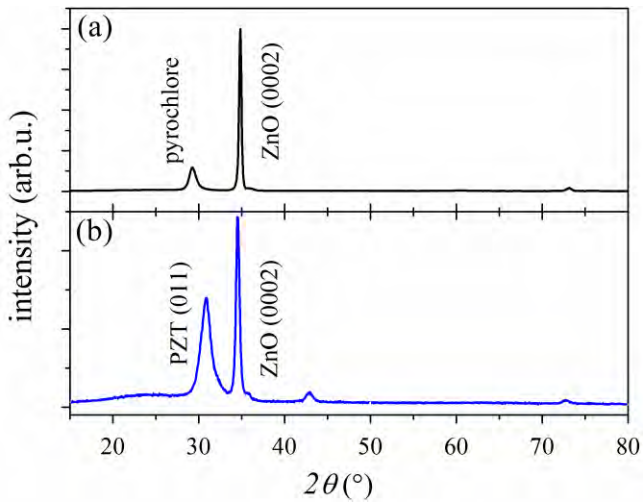

Figure 1.37. XRD 2θ patterns of the PZT thin films grown on (a) ZnO and (b) MgO/ZnO.

The nucleation process is dominated by the minimization of the total energy factor making the (001) nucleation more favorable. As shown in the XRD patterns, using the MgO seed layer, the (011) perovskite PZT phase appeared and there is no indication of any other perovskite reflections. The absence of other phases indicates that the (011)-oriented PZT are preferable and well aligned with [0001] ZnO axes. In contrast, as-grown PZT films grown directly on ZnO at the same condition show only one peak at peak at 29.1° corresponding to the reflection of the pyrochlore phase and not any perovskite reflections. The XRD data demonstrate that the MgO seed layer influences the nucleation and the resulted orientation of PZT films. In addition, the MgO seed layer promotes the highly (011)-oriented PZT on ZnO/glass, even at relatively low processing temperature.

We investigated the structural quality of the grown PZT films with respect to the surface morphology by AFM, Figure 1.38. The data obtained provided a significant insight into the grain structures and film formation. Significant nucleation change of the top PZT thin films were observed as shown by the distinctive of the film topography. We found that the root mean square (RMS) surface roughness for MgO buffered PZT is around 0.9 nm and the one without MgO is 1.3nm. As seen in Figure 1.38, one can notice, from AFM height and phase images, more uniform grain structures (average grain size 30~60 nm) for PZT thin films with an MgO layer, Figures 9.2(b) and 9 (c).

In contrast, the PZT thin films grown directly on ZnO at the same condition as a batch exhibit different morphological structures (large variation in size ranging from 20~200 nm), Figures 1.38(a) and (d). Interfacial energy minimization is critical at the initial atomic layer nucleation and the morphology in the thin films commensurate with the energy minimization. This is evident in high contrast in color of the phase images also shows rough surface topography.

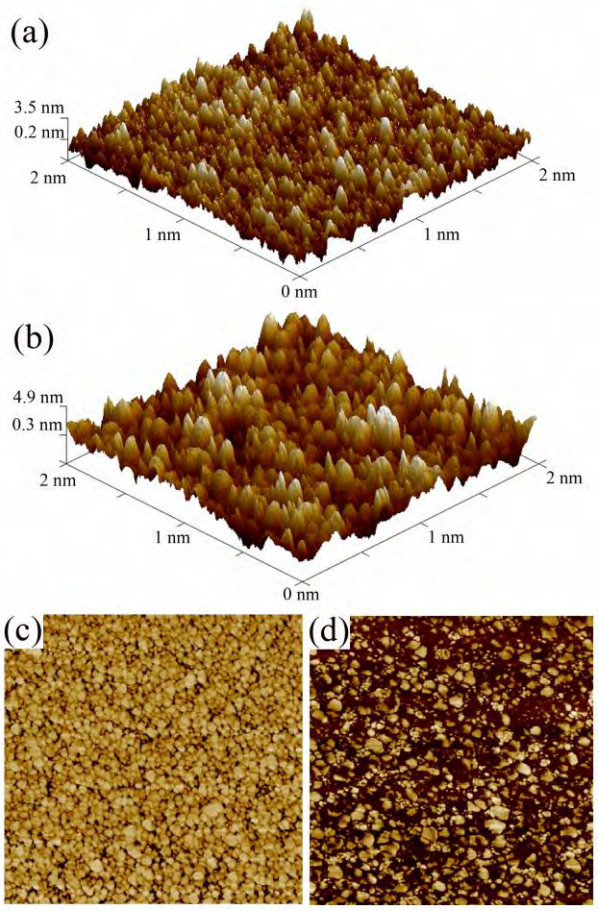

Figure 1.38. AFM 3D height images of (a) PZT on MgO/ZnO and (b) PZT on ZnO, and phase images of (c) PZT on MgO/ZnO and (d) PZT on ZnO.

Due to the large lattice misfit, the density of the misfit dislocations is high between the incoherent interface of PZT and ZnO where the island growth mode is dominant. As seen, in the AFM data, the introduction of MgO seed layer alleviate the interfacial incoherence to some extent. The uniform grain structure and smooth topography show that the incorporation of MgO in this ferroelectric/semiconductor system provides a favorable platform to ease the perovskite PZT nucleation. The results displayed the flexibility of MgO layers which can easily accommodate with ZnO and achieve preferable atomic registry.

Good optical transmission is one of the prerequisites for optoelectronic devices in light modulation. We also studied the effects films morphology via optical transmission spectra, Figure 1.39. This Figure shows the transmission spectra of the films on the glass substrates as a function of wavelength ranging from 200 to 1200 nm.

The thicknesses of PZT, MgO and Al: ZnO are 120 nm, 10nm and 400 nm, respectively. The optical spectra of the film on MgO seed layer shows the absorption edge at the wavelength around 450 nm and a relatively high degree of optical transmission through all measured visible and infrared region. The transmission spectra show an improved transparency of the PZT film even with the extra MgO layer, compared to the MgO/ZnO structure. This is an indication that the transparency strongly depends on the top PZT thin films.

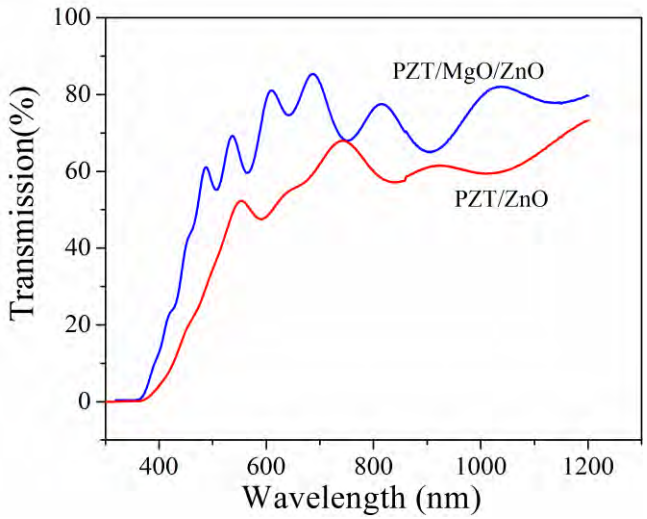

Figure 1.39. Transmission spectroscopy measurements of PZT thin films grown on MgO/ZnO and ZnO structures.

It would be difficult to analyze the optical properties of the single thin film layer separately since we have heterostructures with multiply layers. But it is evident, from the spectra, that the absorption edge of the MgO/ZnO shows a red shift. Nevertheless, the big difference showed in the optical spectra further suggests the high degree of the crystallinity in the MgO seeded PZT thin films is directly related to the microstructural defects. It is worth noting that the reduction of defects structures plays a significant part in reducing light scattering and absorption in the grains, and grain boundaries. In addition, thanks to films surface smoothness, the optical transmission of the MgO buffered PZT thin films is further improved. For the comparison of the PZT electrical properties, we used Al-doped ZnO underlayers as conductive electrodes. We used the top-top electrode configuration in the electrical measurements and 50 nm Cr metal contacts patterned on the PZT thin films to avoid the Schottky junction and interface effects from the metal-semiconductor contact.

The CV measurements, for the as-deposited PZT/MgO/ZnO heterostructure based on top-top electrode configuration, were recorded for different frequencies with a dc bias sweep from -8 to 8 V, Figure 1.40. One can notice that the CV measurement exhibits butterfly shape curves which resembles typical metal-ferroelectric-metal CV behavior. Nonetheless, there is a variation in the behavior of metal-ferroelectric-semiconductor which significantly depends on the capacitance contribution of the semiconductor.

Low carrier concentration or conductivity in the semiconductor may cause the domination of the semiconductor capacitance and mask the ferroelectric behavior in the PZT film. Partially this is the reason that the conductive Al-doped ZnO was used to examine the properties in this material combination. In addition, using MgO as interfacial seed layer also introduced an insulator between the ferroelectric and semiconductor. The flat capacitance response at low bias voltage might be due to the effect of the low dielectric constant of the MgO, compared to the PZT, on the electric field distribution.

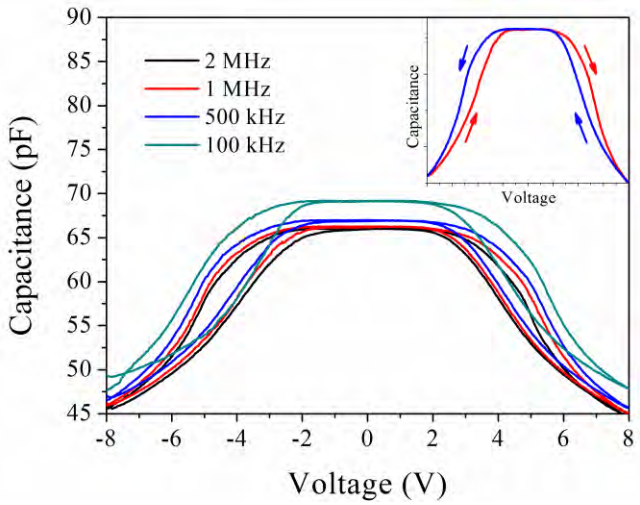

Figure 140. Capacitance-voltage measurement of PZT/MgO/ZnO heterostructure based on top-top electrode configuration. The inset shows the capacitance change as sweeping bias voltage.

Figure 1.41 shows the polarizations versus electric field (P-E) measurements used to characterize the ferroelectric properties of the grown structures. As shown from this Figure, the polarization curves of the heterostructure displays hysteresis loops but not the typical ferroelectric hysteresis as in the metal-ferroelectric-metal. These hysteresis loops alone are not a satisfactory indication of the ferroelectricity. Such hysteresis curves might be caused by back-to-back junction configuration from the interfaces between layers or contacts. Consequently, the explanation of the ferroelectric hysteresis need to be further explored.

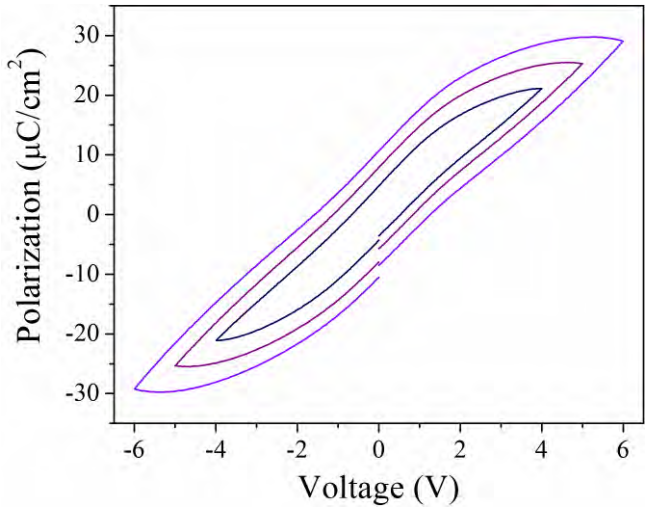

Figure 1.41. Polarization-Electric field hysteresis loops of PZT/MgO/ZnO heterostructure.

To help us understand the hysteresis property of ferroelectric-semiconductor heterostructures we used the physical model to characterize the ferroelectric behavior qualitatively. This basic model, related to field-dependent ferroelectric polarization, simulate the ferroelectric hysteresis on complex ferroelectric-dielectric or ferroelectric-semiconductor heterostructures. Associated with a Sawyer-Tower simulation circuit, the model is capable to demonstrate the *P-E* characterization analytically. In the case of the ferroelectric-semiconductor capacitor structures, the conductive Al-doped ZnO is simplified as a dielectric capacitor where the negative bias applied to the top

electrode forms a depletion layer in the n-type Al-doped ZnO. The electric field distributed in the depletion region has to be considered accordingly.

Due to the difficulty in extracting the related parameters of Al-doped ZnO, a simplified ferroelectric capacitor model is used to characterize its ferroelectric behavior as illustrated in the inset of Figure 1.42. In this model, the dielectric constant of the ferroelectric and semiconductor layers are ε_1 and ε_2, respectively and the thickness of the ferroelectric and semiconductor layers are d_1 and d_2, respectively.

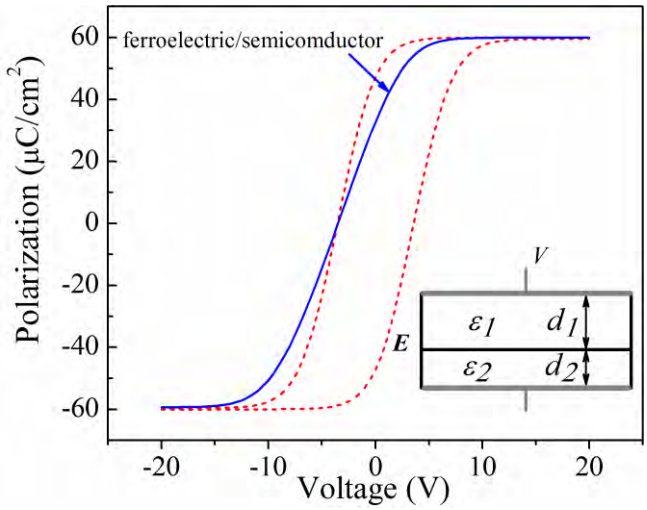

Figure 1.42 Simulated P-E hysteresis curves of a ferroelectric capacitor including the effect of a non-switching dielectric layer.

The electric displacement vectors $\boldsymbol{D}$ in the ferroelectric and dielectric layers are both perpendicular to the plane of the electrode and are defined as $\boldsymbol{D}_1 = \varepsilon_1\varepsilon_0\boldsymbol{E}_1 + \boldsymbol{P}_1$ and $\boldsymbol{D}_2 = \varepsilon_2\varepsilon_0\boldsymbol{E}_2 + \boldsymbol{P}_2$, where $\boldsymbol{P}_1$ is the electric polarization of the ferroelectric material which depends on the electric field $\boldsymbol{E}_1$, and P_2 is the polarization of semiconductor, which can be neglected owing to the relatively small polarization in the polar ZnO. Utilizing charge conservation law, the voltage applied to the whole ferroelectric capacitor structure can be expressed as:

$$V = E_1(d_1 + \frac{\varepsilon_1}{\varepsilon_2}d_2) + \frac{1}{\varepsilon_2\varepsilon_0}(P_1 - P_2 + \sigma_i)d_2 \tag{4}$$

In accordance with the Sawyer-Tower circuit model, the electric field dependence of the ferroelectric polarization P_d is calculated. In order to obtain the behavior of the polarization, a hyperbolic tangent function is used as follows

$$P_d(E) = P_{sat}\tanh[\frac{E - Ec}{2\delta}] \tag{5}$$

where δ is given by

$$\delta = E_c[\log(\frac{1 + P_r / P_{sat}}{1 - P_r / P_{sat}})]^{-1} \tag{6}$$

In equation (6), P_r, P_{sat} and E_c refer to remanent polarization, saturation polarization and coercive field, respectively.

The ideal symmetric hysteresis loop, without the dielectric layer and interface charges, is shown in as the red dashed curve in Figure 1.42. The solid blue line curve, Figure 1.42, is simulated with non-switching dielectric layer model. The dielectric layer underneath the ferroelectric material affects the polarization switching of the structure. To characterize the contribution of the dielectric layer, as the applied voltage sweeps from positive to negative, the hysteresis behavior is simulated. We neglect the influence of the trapped interface charges, because they could not alone dramatically change the ferroelectric hysteresis behavior. However, the collective contribution of both the dielectric layer and the trapped interface charges could cause a considerable rise of the coercive field. The simulated results represent the noticeable features of the measured data shown in Figure 1.41.

It is worth noting that the incorporation of the MgO buffer layer in heterostructure, integrating PZT and ZnO, could have a stronger effect on the gradient of the hysteresis change. This gradient will steadily decrease as the capacitance contribution of the semiconductor increases. In addition, this also causes the non-saturation of the hysteresis due to the semiconductor layer as compared to the simple metal/ferroelectric/metal structures. Nevertheless, the used simplified model has the merit to help us understand the shape deformation in Tower-Sawyer based polarization versus electric field measurement, and it demonstrates the slope change in ferroelectric-semiconductor structures. The incorporation of the MgO seed layer has to be considered as an insulator between the ferroelectric and semiconductor layer, which forms a ferroelectric/insulator/semiconductor (FIS) structures. A detailed simulation has been discussed in literature to investigate the influence of the insulator in FIS structures where the ferroelectric polarization becomes unsaturated. Consequently, it is not useful to use typical P-E measurement alone to characterize the ferroelectric behavior.

Conclusion

In this research, we have successfully demonstrated the growth of high quality (011) PZT films on ZnO/glass substrates with an MgO buffer seed layer. We found that the MgO buffer seed layer influences the change of orientation in the top PZT thin films from pyrochlore to (011). The incorporation of the MgO buffer seed layer resulted in uniform grain structures and improved smoothness of the nucleation of perovskite $Pb(Zr,Ti)O_3$ thin films, as surface morphology revealed using atomic force microscopy. A butterfly shape of the capacitance curves, resembling that of typical metal-ferroelectric-metal structures, were exhibited in the capacitance-voltage measurements. We experimentally quantitatively investigated the behavior of the polarization versus electric field to investigate the unsaturated hysteresis curves caused by the insulating MgO layer.

1.9 Development of Three-Dimensional Nanostructures for High Sensitivity Bio- and Chemical Detection

Advances in nanoscience and instrumentation have brought significant innovations to nanostructure synthesis and fabrication. Artificial and engineered nanoscopic structures which interact with the electromagnetic field at optical frequencies extend the radio frequency and microwave concepts into the optical wavelength. Conversion of propagating light into confined or enhanced fields exploits another revolutionary field in electronics and photonics for optical characterization, manipulation and quantum information processing at nanoscale. The recent advances in optical nanostructures have brought new understanding of its physics and show its enormous potential in the applications of imaging, energy harvesting and sensing. As the dimension is being pushed down to the nanometer scale, the applications of nanostructures raise theoretical and experimental challenges to design and fabricate those artificial nanoscale structures.

In our research work, we dedicated our effort to the top-down manufacturing nanostructures with sufficient precision and high density to understand optical effects for chemical and bio-sensing applications. Top-down techniques seek to modify large structures into small features commonly through many technologies that descended from the conventional Si-based microchip fabrication such as film deposition, lithography, milling, etching and so on. In particular, electron beam lithography (EBL) provides a high degree of freedom in nanostructure fabrication with flexible control of shapes and sizes.

A great amount of developments and findings have been conducted and achieved on nano-optics. Our concept to construct novel nanostructures for chemical and bio-sensing has been explored gradually. Unlike the traditional nanofabrication methods, our approach is focused on three-dimensional nanostructure stacking with ultrathin film deposition to achieve high degree of freedom in fabrication and high sensitivity detection. Our research has demonstrated several flexible ways to produce nanostructures, deepened the understanding of material properties in optical nanostructures, and contributed to the education of the nanotechnology.

Developments of Metal Nanodots and Nanowires

Norfolk State University (NSU) acquired Raith PIONEER electron beam lithography (EBL) system to support the education and research on nanoscience and nanotechnology. Since then a lot of work has been done to explore the nanotechnology and the achievements have been published and presented in several peer-reviewed journals and conferences. After setting the routine process on the submicron level, a great effort has been exerted to explore the capabilities of the system. So far the process for sub-100 nm and ~20 nm features has been established successfully that can create a wide variety of metal nanostructures. Figure 1.43a and 1c show the Au arrays of nanodots with ~40 nm of diameter and nanowires with ~50 nm of width. The EBL

recipe developed at NSU is based on single or bilayer resist process using MMA 8.5, PMMA 495 and 950. Metal layers were deposited by electron beam evaporation and patterned by the lift-off process. Clean depth profile has been obtained in the pitch lower than 100 nm. Figure 1.43b shows the AFM image of the Au nanowire array and the depth profile. Moreover, metal assisted Si nanostructures has been developed using bi-layer liftoff Cr (thickness ~20 nm) as hard mask to create ~150 nm Si nanopillars by dry etching as seen in Figure 1.43d.

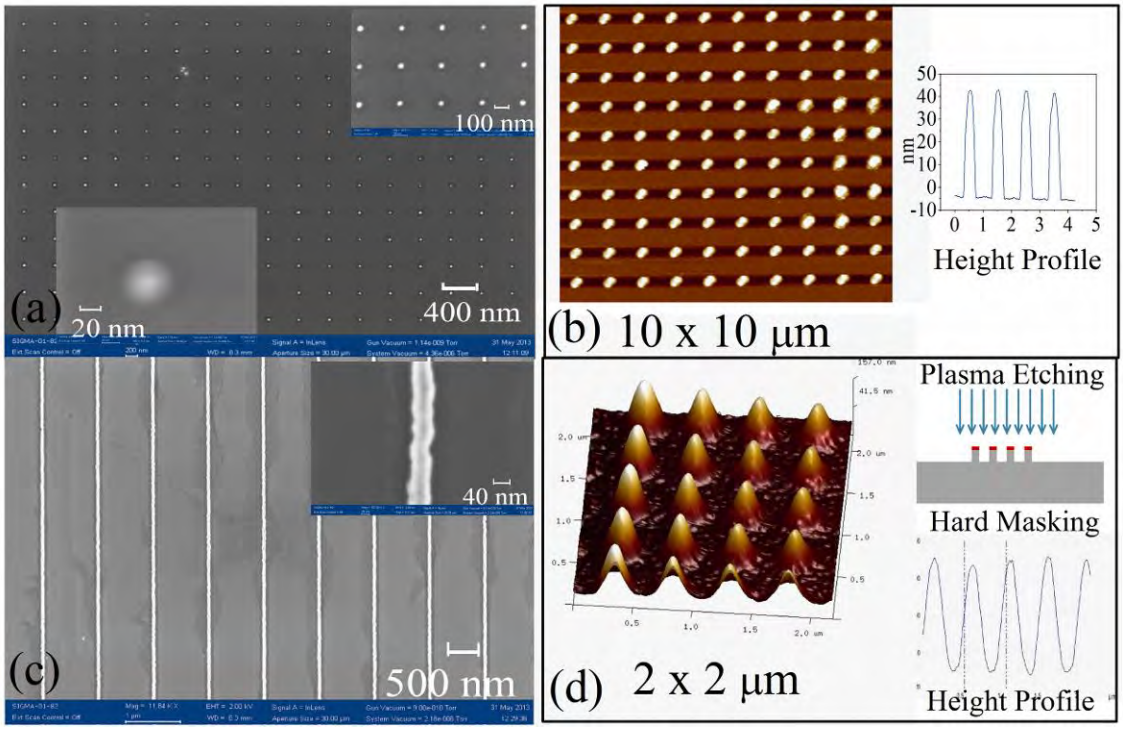

Figure 1.43 Metal nanodots and nanowires. (a) SEM image of Au nanodot array, (b) AFM image and height profile of Au nanodot array, (c) SEM image of Au nanowires, and (d) AFM image, height profile and process diagram of Si nanopillars.

Three-dimensional Nanostructures for High Sensitivity Bio- and Chemical Detection

The establishment of EBL process as demonstrated above allowed us to further develop novel nanostructures for chemical and bio-detection application. Recently, we have put a lot of effort into surface plasmon enhanced nanostructure detection. Noble metal nanostructures are able to confine electromagnetic field into small volumes where the localized field can greatly enhance molecule vibration and amplify weak scattering or emission signals from “hot spot” such as nano-tip and nano-gap. Currently, investigations were focused to build nanostructures onto 2D thin film through lithography or focused ion beam etching. However, such processes suffer from limitations of electron or ion beam proximity effects, as the size of hot spots shrinks to sub-10nm range. Therefore, we proposed a novel method to construct nanostructures to make three-

dimensional nanostructure stacking with dielectric thin films grown by ALD. Using chemical precursors alternatively in thin film growth, ALD shows advantages of high uniformity, accuracy of atomic level thickness control, and high conformity. In addition, high quality thin films can be obtained at relatively low growth temperatures 100 °C – 300 °C. Our method is designed to coat the first layer nanostructures with dielectric thin films by ALD and then fabricate top layer nanostructure accordingly to realize the functionalities. Because of the high accuracy in atomic level thickness control of ALD, we can achieve nano-gaps or nano-cavities at the distance below ~10 nm.

The method provides a simple way to develop nano-gaps and nano-cavities. But it requires precisely matching of the first and second nanostructures. So we developed several matching processes to control the positioning of the second nanostructures. Our ongoing research on nanoring resonators demonstrates the precision of the process as shown in Figure 1.44. The nanoring is considered as a resonator which can be excited by specific electromagnetic wave. The position, size and gap to the nanorings of the patches on the resonator can modulate its resonance frequency or phase. 200x 200 nm patches were placed on 100 nm width nanorings. Shift error of the patches on the nanorings is less than 50 nm.

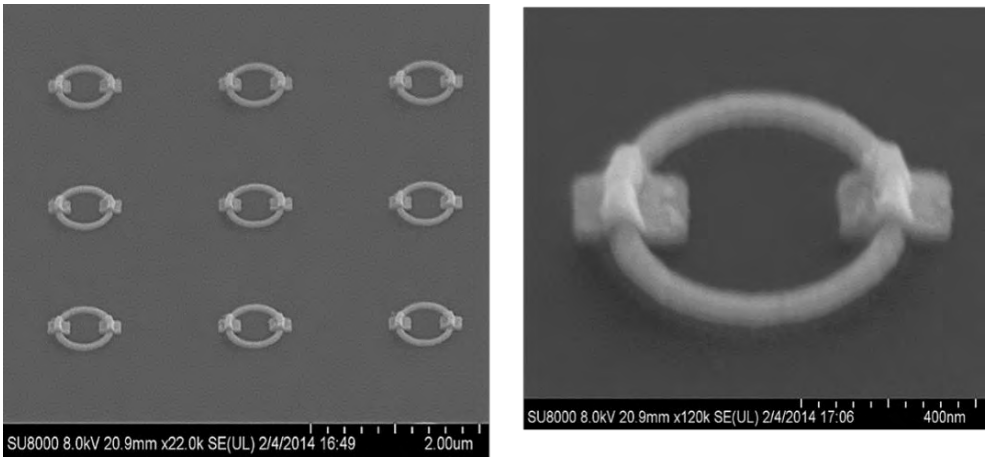

Figure 1.44 SEM images of nanoring structures with 200x200 nm patches

In order to study surface enhanced Raman scattering (SERS), we designed a simple 3-D mesh nanostructure which comprises two layers of gold nano-gratings. Figure 1.45 presents scanning electron microscope (SEM) images of the nano-meshes with the period of 400 nm. The nanostructure, showed in Figure 1.45(a), used the nano-gap process, which deposited a 5 nm oxide dielectric following the first nano-grating fabrication and then was etched to form the nano-gaps after completing the second nano-grating. The nano-gaps are not visible through the SEM imaging due the limited resolution. Experiments are obviously desirable to verify the validity of the SERS. Raman spectra are presented in Figure 1.46, where the structures were covered with rhodamine 6G (R6G) dye.

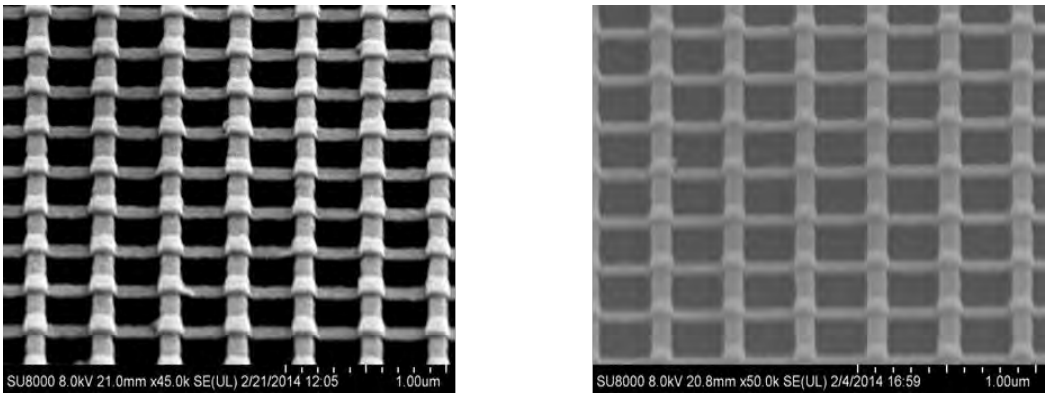

Figure 1.45 nano-mesh structures fabricated on silicon substrates (a) with ALD deposited oxide dielectric layer between two nano-gratings, which has been etched to form the nano-gaps after fabricating the second nano-grating, (b) without nano-gaps.

For the case of nano-mesh without gaps, the concentration of 0.1 Molar R6G water solution was used to measure the Raman scattering on gold thin film and gold nano-mesh in Figure 1.46(a). At such high R6G concentration, both thin film and nano-mesh showed the typical Raman peaks, centered at Raman shifts of 1185, 1311, 1361 and 1575 cm^{-1}. Although nano-mesh indicated higher peak intensity, the enhancement of the Raman scattering is not significant. On the other hand, the introduction of a ~5 nm gap between the two nano-gratings, the enhancement of the Raman scattering was dramatically increased as showed in Figure 1.46 (b), where we used much lower concentration R6G dye solution, 10^{-4} M. Raman shifts were hardly detected on bare silicon or gold thin film at the concentration. But the nano-mesh with the gap structures exhibits pronounced R6G Raman shift peaks at the positions of 1185, 1310, 1363, 1510, 1595 and 1650 cm^{-1}.

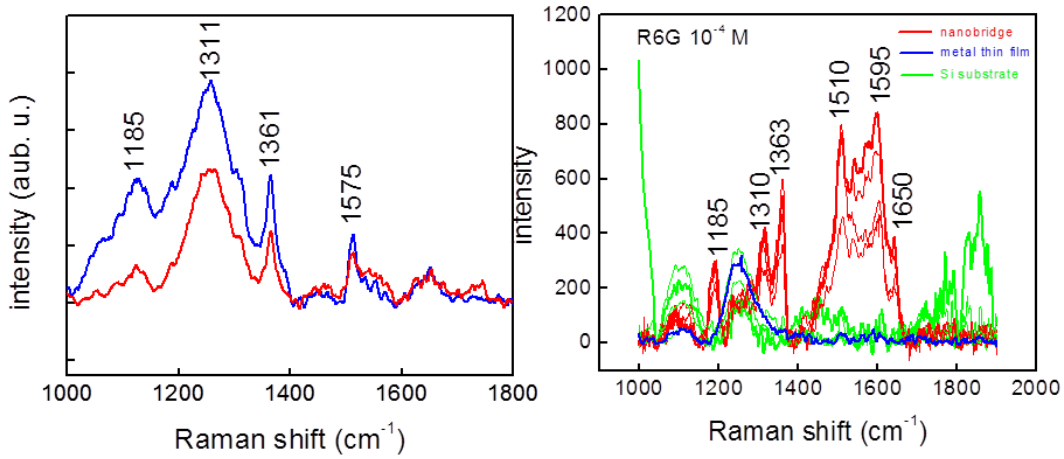

Figure 1.46 Raman spectra of (a) 0.1 M R6G on Au thin film (red line) and nano-mesh (blue line), (b) 10-4 M R6G on nano-mesh with gaps.

To understand the relationship between observed Raman scattering enhancement and the geometrical dimensions of the nanostructures, the electromagnetic wave responses of the nanostructures were simulated by using commercial software COMSOL Multiphysics. In order to simplify the modeling, the shape of the nano-mesh was approximately modeled in 2D cross-section as periodic nanowire and thin film slab. Figure 1.47 indicates the profile of the electromagnetic field intensity. The "hot-spot" region is located around the nanostructures. Consequently, the enhanced Raman scattering can be attributed to the nanocavity volume between the two nano-grating structures.

Raman Scattering is a measurement technique that analyzes the signature of vibrational modes of many materials. It is especially useful when analyzing biological specimen such as proteins, bacteria, antigens, etc. This is due to the fact that chemical and structural changes in most biological materials can be identified by changes in the Raman mode signature. The main drawback of this technique is measuring biological specimen at low concentrations. At low concentrations, the Raman scattering cross-section can be very small, and Raman modes of the materials in question can become increasing difficult to detect. Many optical techniques have been employed to compensate for the low signal, but they can only be used to detect concentrations on the mM scale; detecting signals with concentrations below that by enhanced optical means is impractical.

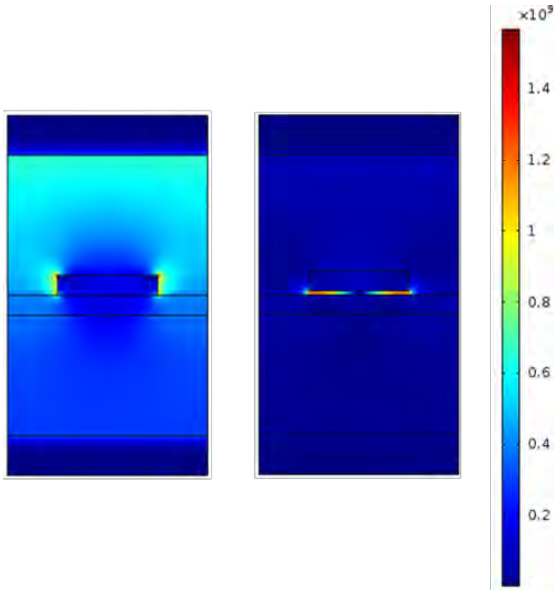

Figure 1.47 Simulated cross-sectional electric-field intensity enhancement distributions.

To combat this drawback, researchers have implanted the use of Surface Enhanced substrates. Noble metals nanostructures have the capability to create very dense local electric fields; these electric fields can increase the Raman scattering intensity of any material under study. For biological materials in solution, this will result in an enhanced Raman signal that can be detected for even nM level concentrations. Over the past few years, plasmonic metals such as Au and Ag have been heavily researched in terms of their optical and plasmonic properties. It has been shown by many research groups that the shape, size, proximity, as well as fabrication technique all affect the localized surface Plasmon resonances. Plasmonic nanostructures have a wide variety of uses, from superlensing, direct fiber sensing, metamaterials, to the more popular SERS application. In our current research, the latter is what we are focused on.

These types of plasmonic nanostructures have a wide variety of shapes and sizes. In our lab,

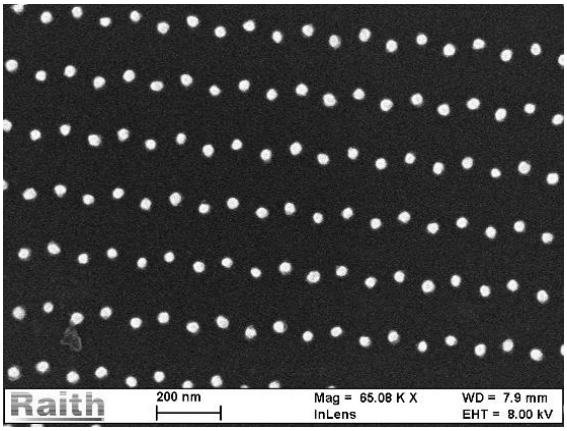

Figure 1.48 shows a Dimer Array with an offset geometry. Different geometries result in different structural proximities. This will result in different local surface plasmonic resonances.

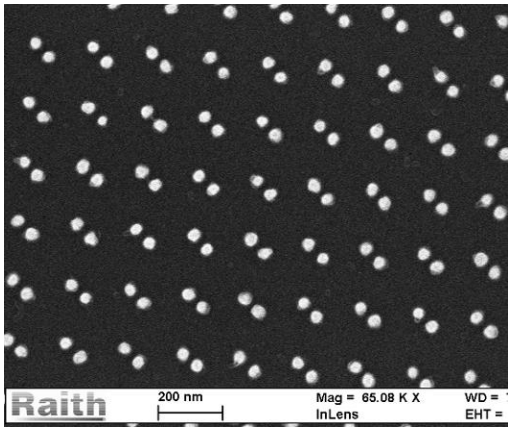

Figure 1.49 shows a dimer structure where the dots were places as close as possible to one another. The closer they are, the more intense the electric field is between them. Some gap spaces are as small as 15 nm.

We have fabricated these types of nano structures out of Au and Ag, by way of a top down technique. We use EBL, in conjunction with E-Beam Evaporation, and liftoff of the E-beam resist. This results in nanostructures left on a conductive substrate (in our case Si was used). Plasmonic nanostructures were also fabricated on glass substrates, but additional processing steps were needed in order to properly pattern the E-beam resist.

Figures 1.48, 1.49 show SEM images of some of the gold and silver nanostructures structures created on Silicon and cover glass substrates. Figure 1.50 shows different achieved geometries on glass substrate. This was especially difficult to achieve due to the fact that it is a non-conductive sample. Still, we were able to achieve a pitch distance around 150 nm (Figure 1.50 (c), (e)). There are some discontinuities, we attribute them to contaminants on the surface.

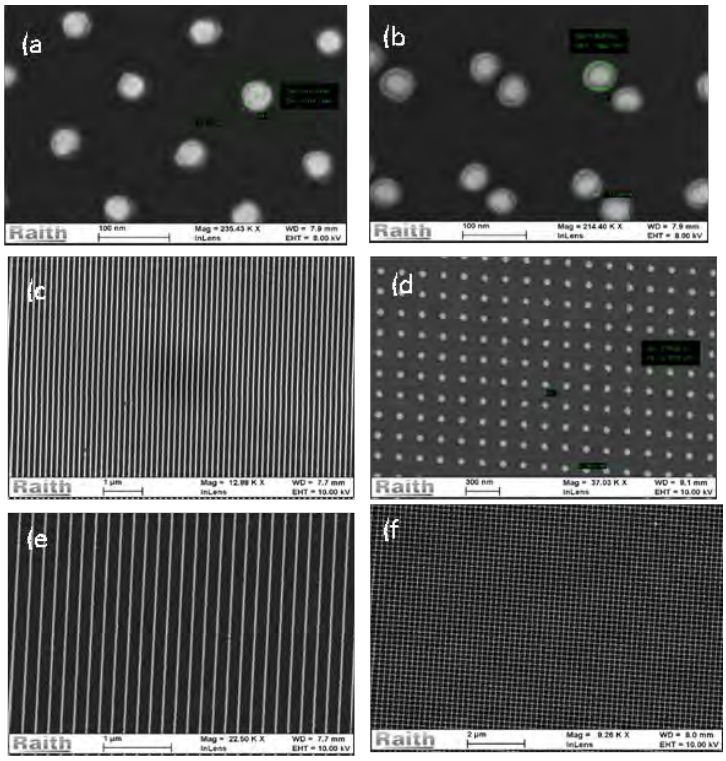

Figure 1.50 Shows a similar grating structure on a glass substrate.

1.10 Development and Characterization of Tin Oxide Improved Gas Sensor

In the recent years, several semiconducting metal-oxides have been used to fabricating nanorod gas sensors, like that of Zinc Oxide (ZnO) and Tin Oxides (SnO_2). The surface of these materials is electrically and chemically active due to their rich oxygen vacancy surface. SnO_2 interaction with oxygen lead to a decrease in the electrical conductivity, similar effects have been also observed with ZnO.

These 1D nanoarray offer key advantages, some of them being easy to fabricate, low cost material, enhanced surface properties due to the increased surface to volume ratio. Zinc Oxide (ZnO) based nanorod arrays have been used to make chemical sensors. ZnO is commonly used due to its excellent semiconducting features. This type of semiconducting material has several structures like that of the flower-like nanorods that increase the charge carrier movement rate creating a faster response time. By adding the ZnO to the SnO_2 sensor, the surface area increases dramatically and is well known that the rise in surface area is a factor that leads to the improvement of the sensing performance. In this research we report a method for developing a large surface coverage with SnO_2–ZnO hybrid layer. This hybrid nano-micro composite is suitable for vapor/gas sensing and has promising features to explore the hybrid layers chemistry to improve selectivity as an electronic nose approach.

Growth of SnO_2 layer was achieved and its properties were tested as a suitable transducer for gas sensing measurements of Ethanol and Acetone vapors. The vapor–liquid–solid method (VLS) has proved to be a cheap, easy, and fast way to fabricate high surface nanostructured films. Tin oxide nanorods have an average size in between 50–100 nm in diameter and 2μm in length. Adsorption of Au Nanoparticles to SnO_2 nanorod films promotes surface chemistry enhancements resulting on increased sensitivity of the transduction device due to its extraordinary high catalytic activity of partial oxidation of, acetone, ethanol, and other gases and vapors. These properties are attributed to Au nanoparticle size and surface to volume ratio.

VLS Growth of SnO2 Nanorods and Au Nanoparticle Decoration

For the growth of tin oxide nanorods the VLS technique was used and carried out by evaporation of a 4:1 ratio mixture of zinc dichloride powder ($ZnCl_2$) and tin dichloride anhydrous powder ($SnCl_2$), Figure 1.51.

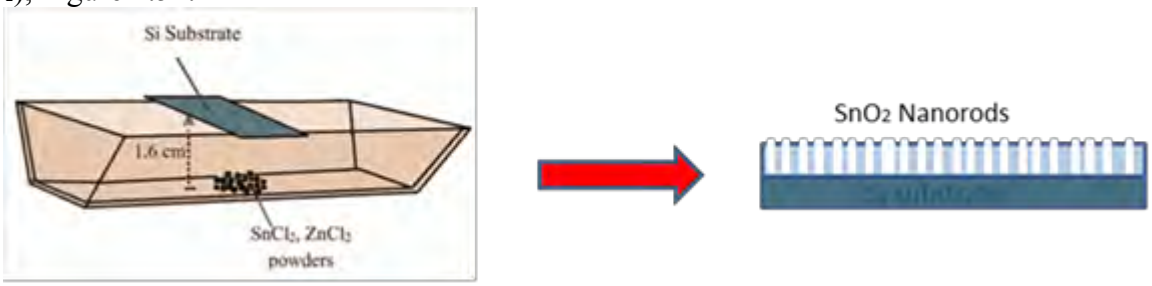

Figure 1.51. Schematic representation of the experimental setup.

Au nanoparticle decoration on the SnO_2 nanorods surface was achieved by UV irradiation in presence of a solution of $AuCl_4$ $3H_20$ in Ethanol at a 1:2000 volume ratio respectively as shown in the Figure 1.52. Exposure time can be changed from 1 minute to 4 minutes to achieve the decoration density desired for the sample. Au nanoparticles attach to the metal-oxide nanorods and grow dispersedly across the sample surface.

The sample is then heated to 650°C in constant argon flow to evaporate organic traces during 1h. The sample is rinsed in DI water and sonicated during 2 minutes dried with N_2 and stored for characterization.

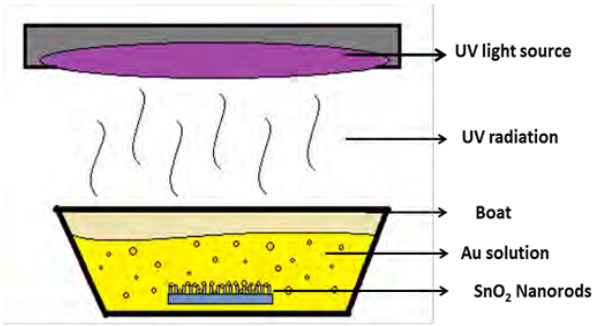

Figure 1.52. Au nanoparticle decoration experimental setup.

SEM Characterization

SnO_2 Nanorods were characterized using a Field Emission Scanning Electron Microscope (FESEM), images of Au decorated and non-decorated samples are compared in the following Figures 1.53.a and 1.53.b:

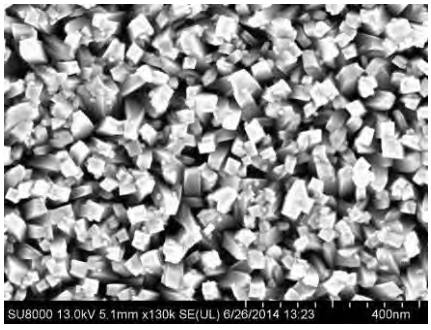

Figure 1.53.a. SnO_2 nanorods with Au decoration.

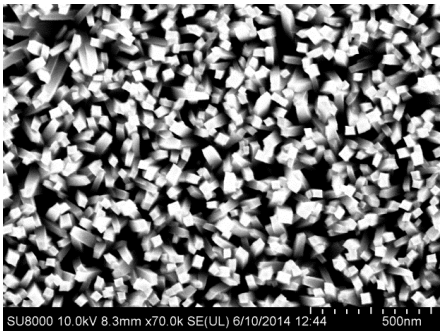

Figure 1.53.b. SnO_2 nanorods with no Au decoration.

Also, a closer investigation with high magnification reveals that Au nanoparticles attach very uniformly onto ZnO surfaces as shown in Figure 1.54.

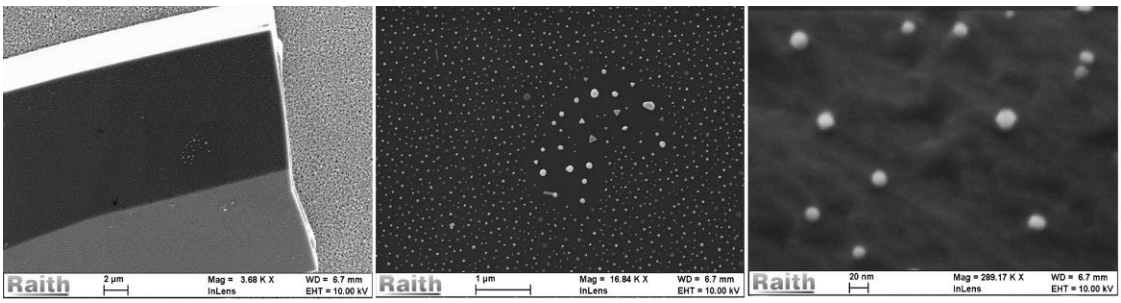

Figure 1.54. ZnO Microstucture decorated with Au.

Gas Sensing Measurements

To measure the sensitivity from SnO_2 nanorod layers to reducing gases, Argon (Ar) is used as carrier gas. Two electrodes are deposited on the nanorods surface using silver paint keeping a distance of 0.5 mm from each other. Copper wires are attached to the electrodes and the whole sensor is inserted in a tube furnace to keep the sensor at the working temperature (250°C) during vapor exposure, LabView software recorded change in resistance over time. Ethanol and Acetone were used as the analytic vapors, as shown in Figure 1.55.

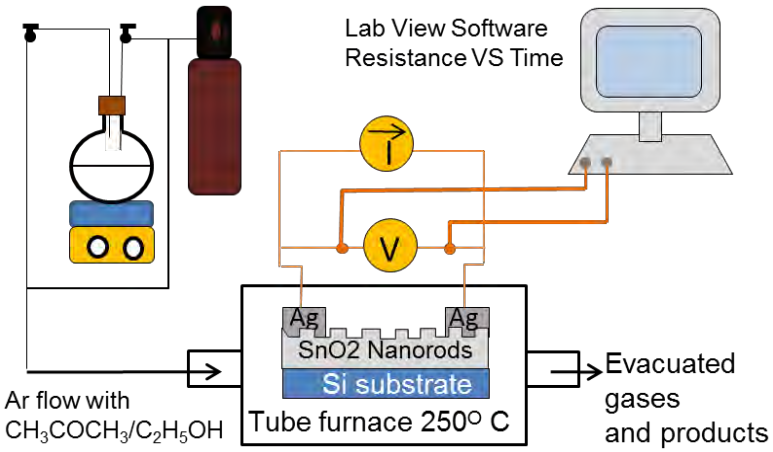

Figure 1.55. Schematic representation of the gas sensor fabrication process.

A SnO_2 Nanorods layer without Au decoration was used as the base sensor, resistance versus time testing was performed at 250°C under exposure to ethanol and acetone vapors 50°C and 35°C, respectively. The response versus time curve was also recorded and reported in Figures

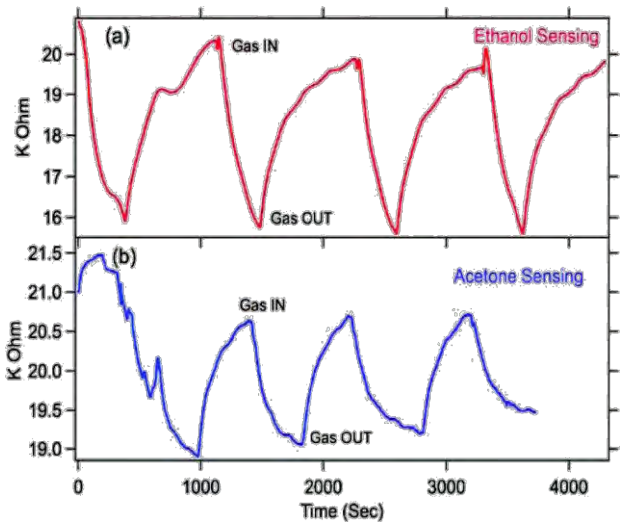

Figure 1.56. Resistance vs time curves; sensing measurements for ethanol vapors (a), sensing measurements for acetone vapors (b).

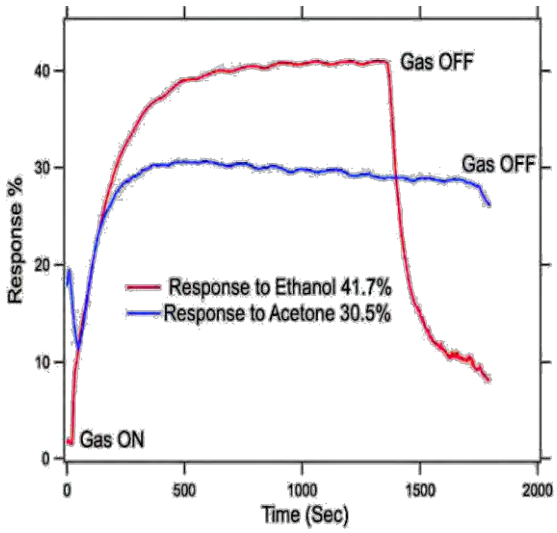

Figure 1.57. Sensor response percentage graph for acetone and ethanol.

1.56 and 1.57.

To calculate the response percentage of the base sensor, Figure 1.58, the resistivity of the sensor both in air (Ra) and in the presence of the vapor species (Rb) are recorded. We calculated the percent by using the equation [((Ra−Rb)/Ra) × 100%]. Table 1.1 describes the sensor response in percentage to each analyte.

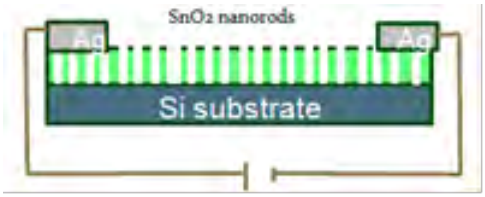

Figure 1.58. Base sensor schematic diagram.

Carrier Gas	Analyte	Analyte T°	Sensor T°	Δ kΩ	Response%
Argon	Ethanol	50°C	250°C	−11 kΩ	41.70%
Argon	Acetone	35°C	250°C	−7 kΩ	30.50%

Table 1.1. Data summary of the SnO_2-ZnO sensor conditions and performance.

Sensor Performance Summary

The SnO_2 sensor with Au decoration was created by UV exposure during 3 minutes. Silver paint was deposited on the Au decorated nanorods to make two electrodes. Copper wires are attached to the electrodes and the whole sensor is inserted in a tube furnace to keep the sensor at the working temperature (250°C) during vapor exposure, Figure 1.59. LabView software recorded the change in resistance over time. Ethanol and Acetone were used as the analytic vapors.

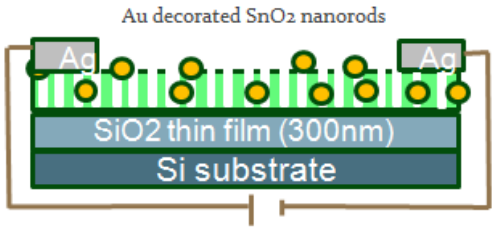

Figure 1.59. SnO2 sensor with Au decoration sensor schematic diagram.

Resistance versus time testing was performed at 250°C under exposure to ethanol and acetone vapors (50°C and 35°C respectively). Interestingly, the sensor using Au decorated nanorods works under oxygen conditions. The response versus time curve was also recorded and reported in Figures 1.60 and 1.61. The Au decorated SnO_2 sensor showed a faster response and flexibility to work using oxygen as carrier gas. The Response was three times higher for acetone in comparison to the base sensor.

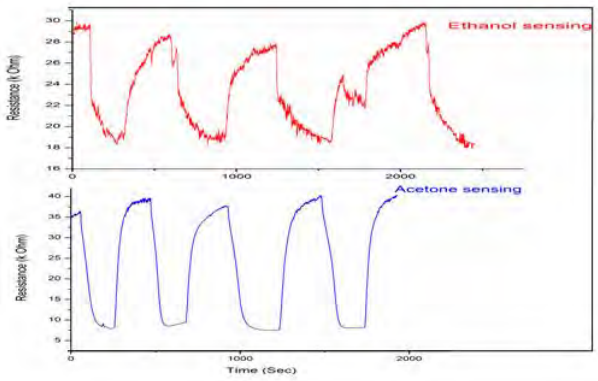

Figure 1.60. Resistance vs time curves; sensing measurements for ethanol vapors (a), sensing measurements for acetone vapors (b).

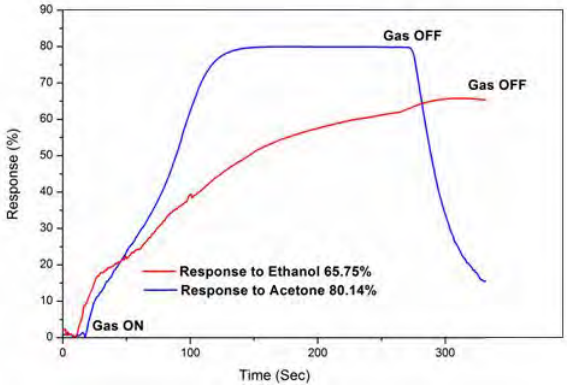

Figure 1.61. Sensor response percentage graph for acetone and ethanol.

The sensor performance comparison is summarized in the table 1.2, showing the increased features showed by the Au decorated sensor.

Au attachment	Carrier Gas	Analyte	Analyte T°	Sensor T°	Δ kΩ	Response %
No	Argon	Ethanol	50°C	250°C	-11kΩ	41.70%
No	Argon	Acetone	35°C	250°C	-7kΩ	30.50%
Yes	Ar & O_2	Ethanol	50°C	250°C	-11kΩ	65.75%
Yes	Ar & O_2	Acetone	35°C	250°C	-33kΩ	80.14%

Table 1.2. Data table with sensor performance comparison.

We conclude that Au nanoparticles contributed to the increased rate of sensitivity thanks to the catalytic activity of partial oxidation of Acetone and Ethanol vapors. Also the high electron density cloud from Au nanoparticles facilitates the charge transfer from oxidation reactions to the conduction band of the SnO_2 nanorods. Ethanol, Acetone, and dangerous gases such as Carbon Monoxide can be sensed using Au decorated SnO_2 nanorods in open air environment. Improvement sensitivity of the sensor translated into a twice increase in efficiency for Ethanol and approximately ten times higher efficiency for Acetone compared to base SnO_2 sensor with no Au nanoparticles decoration.

2. DEVELOPMENT, UNDERSTANDING AND INTEGRATION OF ACOUSTIC MICRO-SENSORS AND MEMS FOR SENSING CHEMICAL AND BIOLOGICAL AGENTS, AND FOR ACTUATION

In this research acoustic microsensors and MEMS devices were developed and fabricated for bio-sensing and actuation applications. The tasks for this project included characterization and identification of device materials for optimum device performance, device design using theory and finite element software, and fabrication of the devices based on characterization and modeling results.

2.1. THE DESIGN AND DEVELOPMENT OF ACOUSTIC MICROSENSORS

Flexural Plate Wave Bio-sensors

The goal of this project is to design and develop microelectromechanical systems (MEMS) sensors and sensor arrays integrated on Si-CMOS circuits. Bio-sensor and related device research has greatly increased in recent years due to a rise in demand for reliable, smaller sensors to monitor physical, chemical, and biological quantities for the defense, health, nuclear, and environmental industries. In this research, the sensors developed employ flexural plate waves (FPWs). FPW devices are highly sensitive to surface perturbations and indirectly sense analytes by detecting mass changes on the sensing plate surface. FPW devices are advantageous for bio-chemical applications because of their high sensitivity and ability to sense in both liquids and gases.

The FPW sensor was designed, developed, and fabricated and has a sensitivity of 0.0424 m^2/g. It was modeled using tools such as ANSYS finite element analysis software as shown in Figure 2.1. It was fabricated using common integrated circuit (IC) and micromachining techniques. Its structure consists of a silicon substrate, titanium/gold inter-digital transducers (IDTs), a piezoelectric layer (ZnO), silicon nitride, and silicon dioxide. The total thickness of the device membrane is 1.5µm and the area is 1×1.71 mm^2. Figure 2.2 shows the top view of the fabricated sensor. The fabrication process employed a new technique that allows for the separation of the sensors from their native substrates and the heterogeneous integration of the sensors onto supporting electronics circuitry, thus enhancing the customizing of each sensor in the future and leading to sensor arrays. The device is fabricated to have (bio) chemical sensitivities using a selective surface coating that interacts with the analyte under investigation. Thus, this device can be used to sense various analytes by detecting changes in mass of the sensing plate/surface.

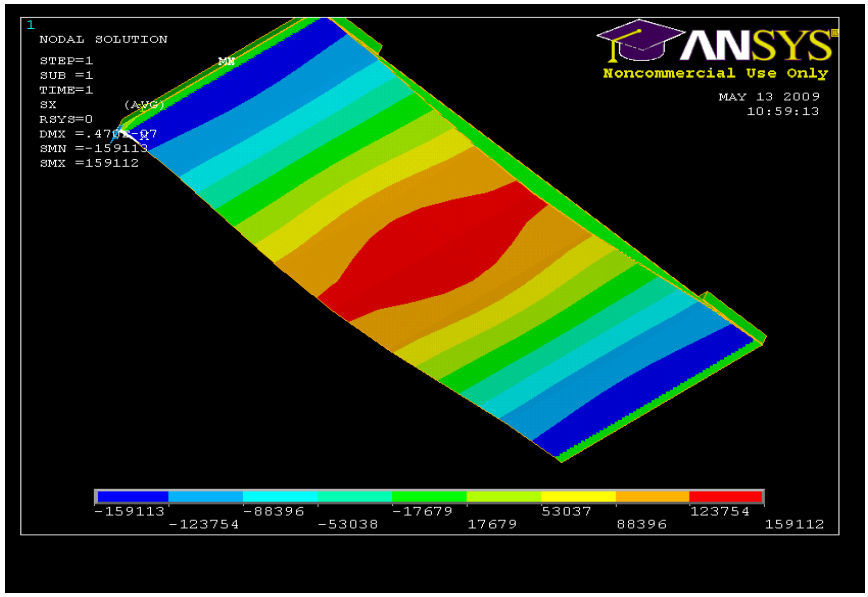

Figure 2.1. ANSYS Simulation of FPW Sensor.

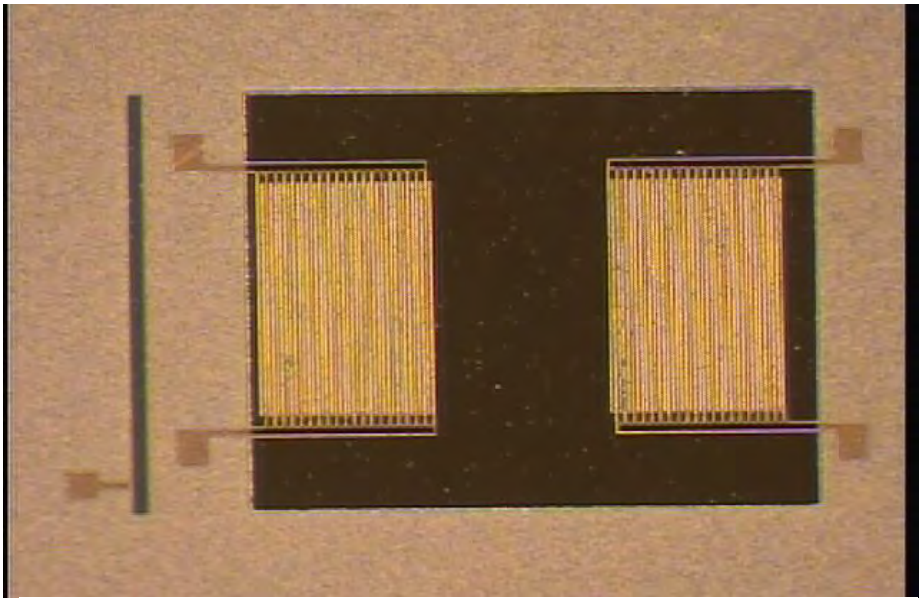

Figure 2.2. Top view of the fabricated FPW Sensor.

Thin-Film Bulk Acoustic Resonators

The goal of this project is to design and develop a bio-chemical film bulk acoustic resonator (FBAR) to detect an analyte in liquid. The thin-film bulk acoustic resonator (TFBAR) is being investigated to operate as a mass-sensing device whereas it can be functionalized and used to detect various bio-chemical species. The design of the TFBAR device includes a piezoelectric material sandwiched between electrodes and is used to sense a change in mass by measuring a change in resonant frequency. The device consists of aluminum, lead zirconate titanate (PZT/piezoelectric layer), platinum, titanium, silicon dioxide, and a silicon handle layer.

COMSOL Modeling

Modeling of the TFBAR sensor, using finite element analysis (FEA) software COMSOL, was performed to examine optimal device design parameters. COMSOL finite element analysis software was used to model the device structure and operation via 2D and 3D modeling. COMSOL was used to vary device parameters and dimensions for greatest device sensitivity. The FBAR consists of a membrane that can be modeled as a thin plate with clamped edges. Figure 2.3 below from COMSOL simulation shows the areas of the diaphragm that will experience the greatest bending stress. Segmented electrodes placed in these regions will be used

to collect the charges generated by the sensor. Figures 2.4 and 2.5 show the simulations of the deformation of the device membrane for 2D and 3D models, respectively.

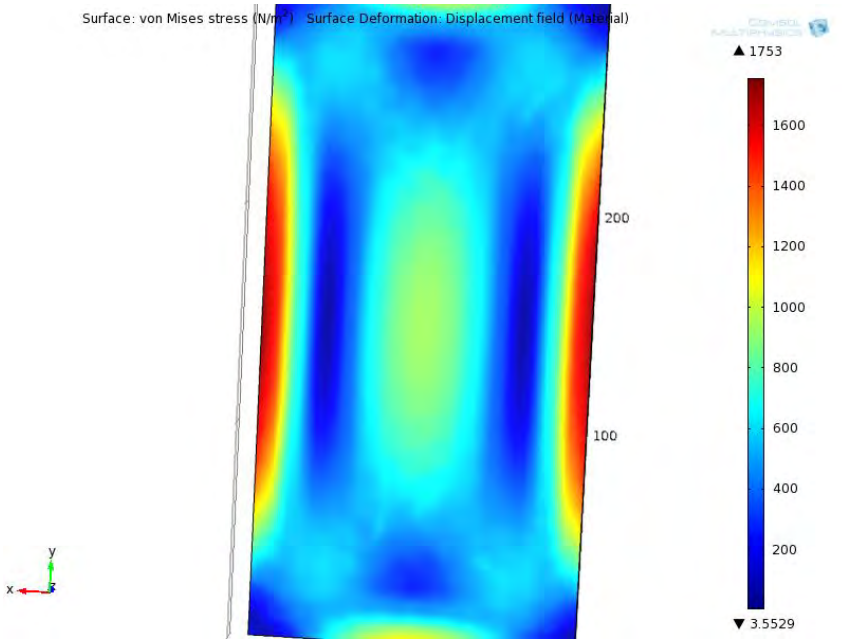

Figure 2.3. COMSOL plot of stress in FBAR plate.

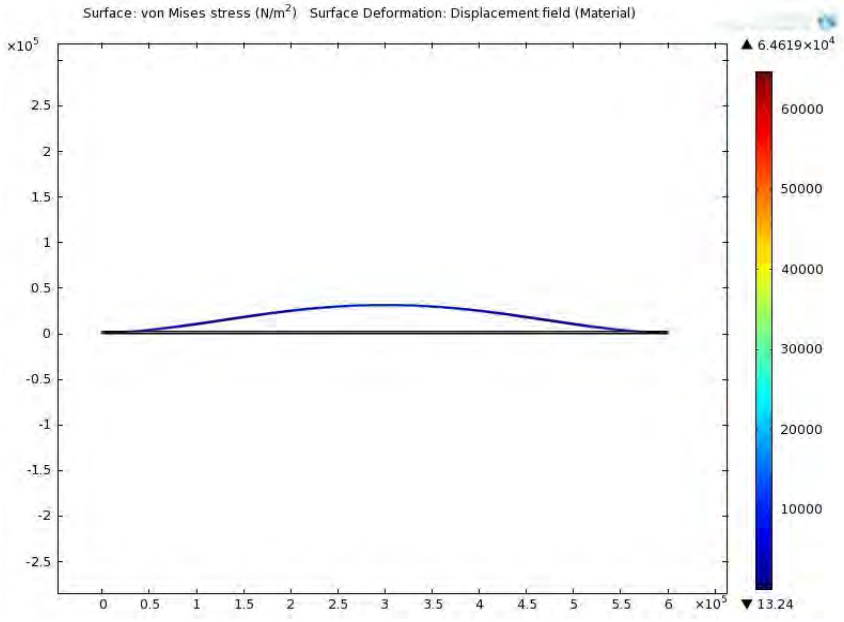

Figure 2.4. Surface deformation of FBAR diaphragm (from 2D model).

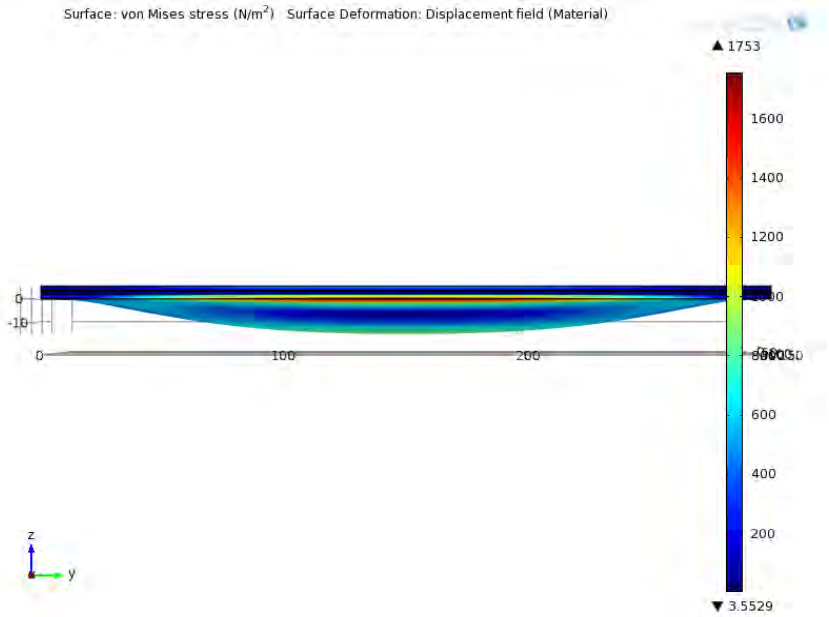

Figure 2.5. Surface deformation of FBAR diaphragm (from 3D model).

The effect of the PZT thickness on device resonance was also investigated. The higher the fundamental resonant frequency, the more sensitive the device will be. TFBAR devices are typically small and when coupled with a functionalized layer, their ability to detect mass loading provides a mechanism for direct *in-situ* sensing. The results of the simulations are shown in Figures 2.7-3.0. Using the COMSOL piezoelectric module, simulations were performed based on the assigned material mechanical and electrical properties entered and with voltages applied to the top and bottom electrodes. Piezoelectric film thicknesses were then changed in order to observe the effect on the resonant frequency of the device. The frequencies were measured in terms of impedance vs. frequency when a frequency domain sweep was performed on the device.

Early modeling and simulations focused primarily on BTO/STO multilayers, but this work was later switched to investigating PZT thin films as the piezoelectric layer because of ease of processing. The PZT thicknesses were varied from 150nm to 600nm in order to observe the effect on resonance. The first of these new simulations was conducted at 150nm and can be seen in Figure 2.6 (a). The effect of the resonant frequency for the other thicknesses can be seen in in Figures 2.6-2.8. Figure 2.8 shows the resonant frequencies for the TFBAR device at various studied thicknesses.

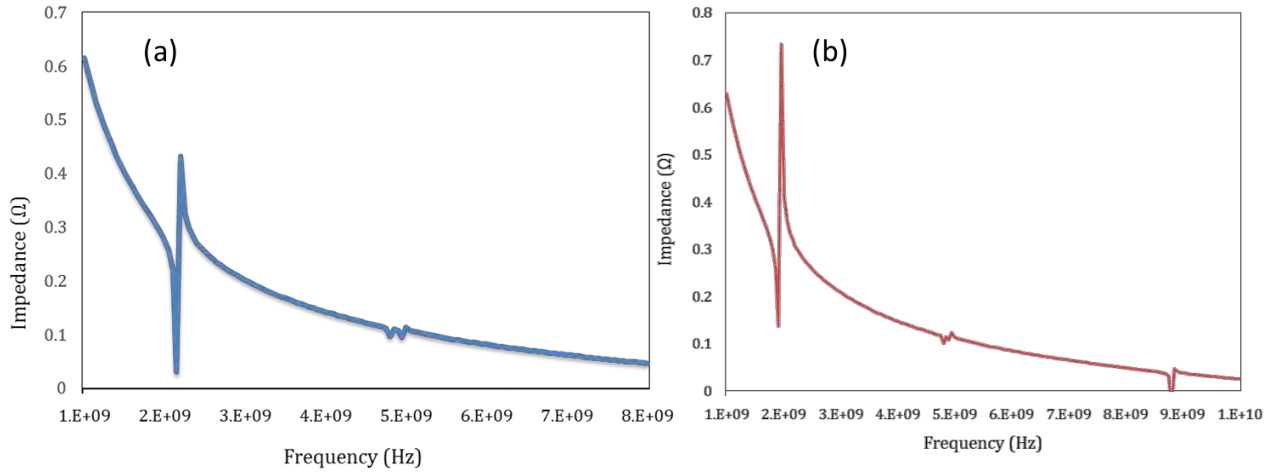

Figure 2.6. Resonant frequencies for TFBAR device with PZT thickness (a) 150nm and (b) 200 nm.

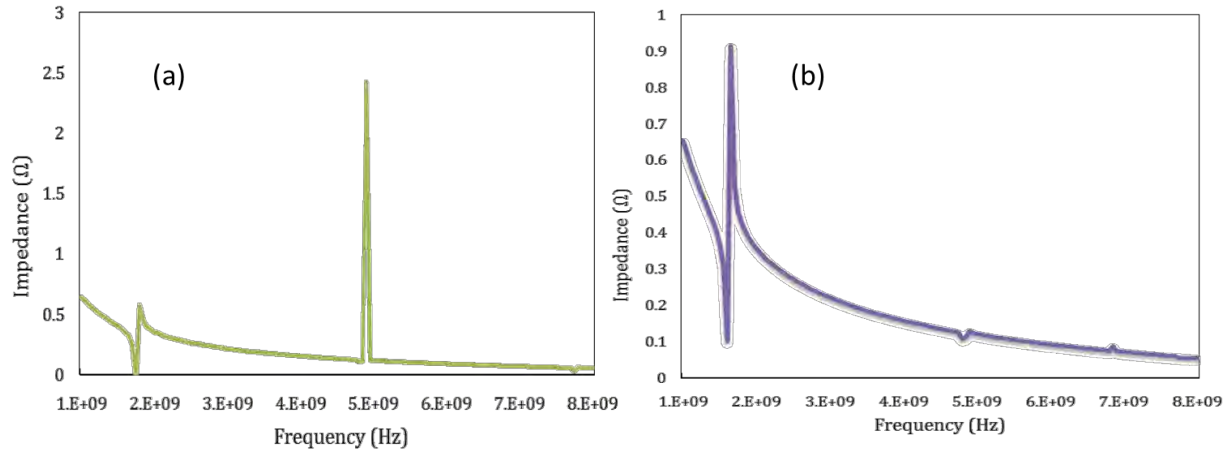

Figure 2.7. Resonant frequencies for TFBAR device with PZT thickness (a) 250nm and (b) 300 nm.

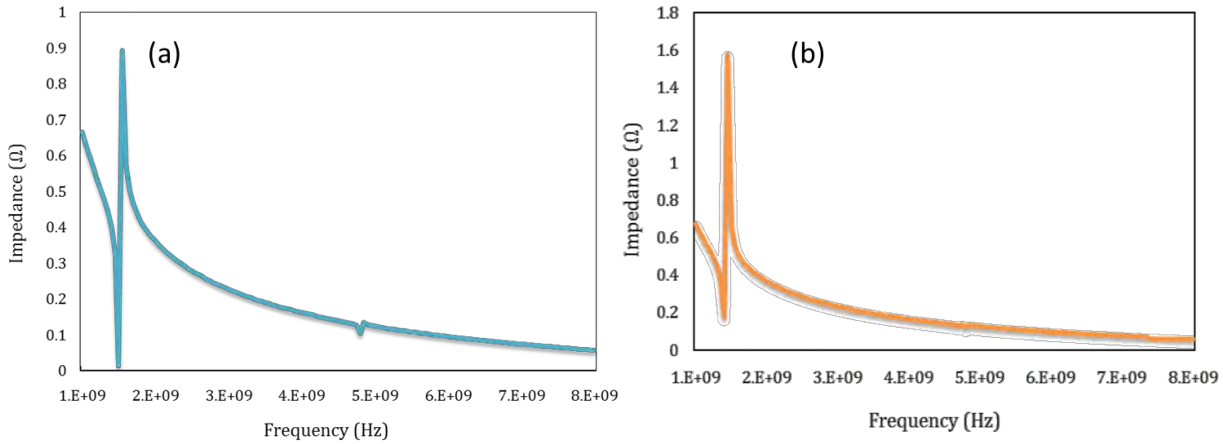

Figure 2.8. Resonant frequencies for TFBAR device with PZT thickness (a) 350nm and (b) 400 nm.

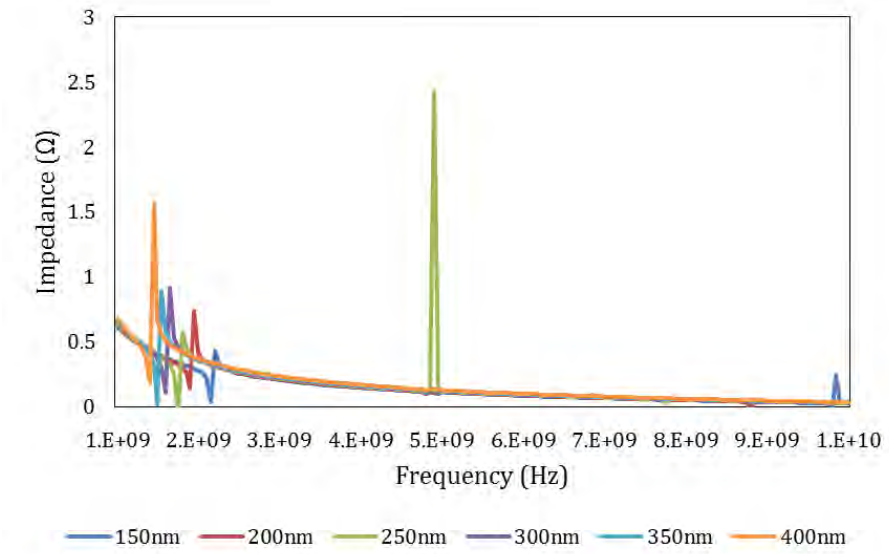

Figure 2.9. Resonant frequencies for TFBAR device at various thicknesses.

From these graphs, one can observe that the optimal thickness of the PZT is 150nm resulting in a higher resonant frequency. The effect of changes in the silicon dioxide (SiO_2) layer thickness on resonant frequency was also observed. These results are shown in Figure 2.10.

From the simulated results from COMSOL, it was determined that optimal resonant frequency of the device would be achieved with a PZT thickness of 150nm as well as a 150-200nm layer of SiO_2. This resulted in a simulated resonant frequency of approximately 3.2GHz.

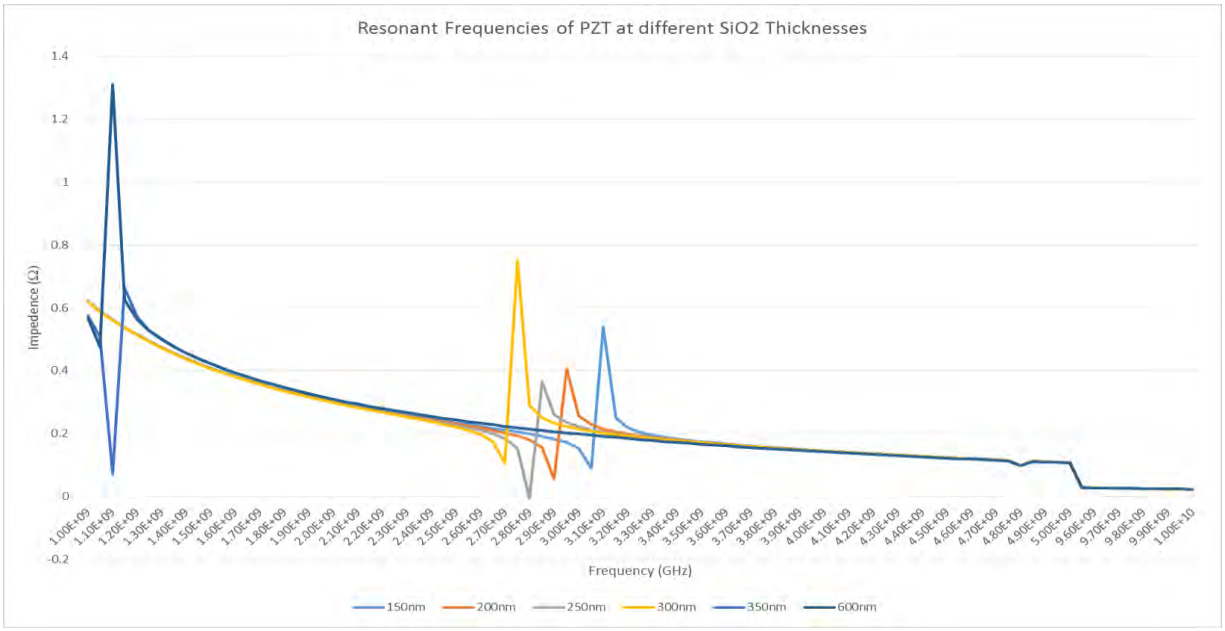

Figure 2.10. Resonant frequencies of TFBAR device at different silicon dioxide thicknesses.

Perovskite Materials Characterization

The thin film material being processed in this project is Lead Zirconate Titanate (PZT). This material has been proven to be of great use for MEMS and other electrical applications due its excellent ferroelectric and piezoelectric properties. It is essential to understand the ferroelectric properties of this film because it greatly affects its device performance.

In order to optimize the properties, advanced processing such as, RF Magnetron Sputtering is utilized. This processing/deposition creates the structure of the material. Since the structure greatly impacts the properties, careful growth of the film is needed. The parameters involved in the deposition of the film include temperature, pressure, Argon/Oxygen ratio, and RF power.

Since the growth of the film heavily relies on the growth temperature, we focused on studying dependence of the film quality on the growth temperatures. Once grown, the structure and crystallinity of the films were analyzed by XRD. Possible structures are single crystal, polycrystalline, or amorphous. The goal is to grow single crystal films to achieve the desired optimal properties. Optimal properties can be hindered by the appearance of a pyrochlore crystal structure after the film has been grown. If grown at the best-fixed deposition parameters (pressure, power, Argon/Oxygen Ratio), and by finding the optimal growth temperature, this pyrochlore structure can be minimized, leading to excellent ferroelectric properties.

The PZT deposited in this research effort maintained fixed parameters, except the temperature. By doing this, the temperature dependence of the film can be studied, as it relates to its structure and ferroelectric properties. The pressure, power, and Ar/O_2 flow rate ratio used were 2mTorr, 90W, and Ar: 10sccm/O_2: 5sccm, respectively. The thickness of all the samples were kept aroudn 150 nm.

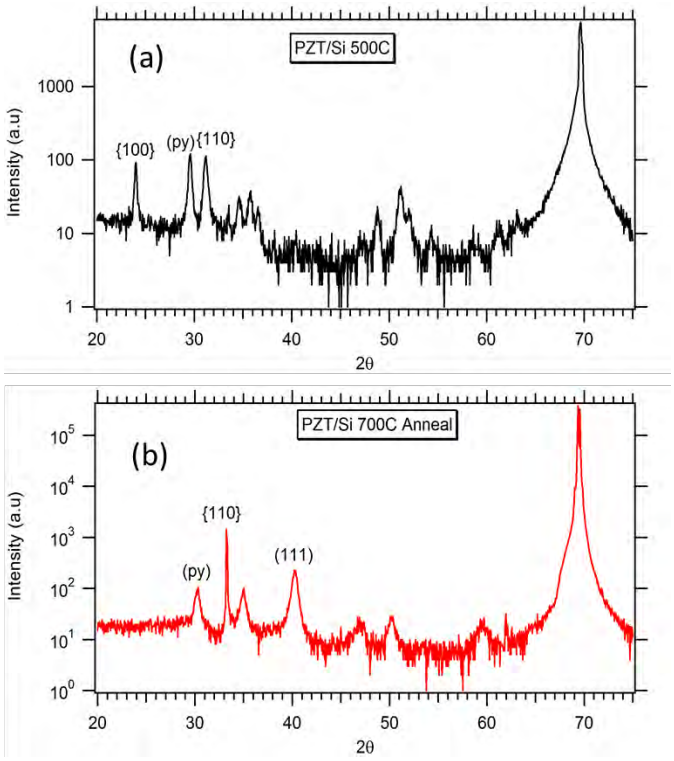

Figure 2.11. The XRD patterns of the grown PZT thin film where a basic acetone, methanol, and distilled water substrate cleaning technique is used. (a) represents as sample grown at 500 °C. (b) represents the film annealed at 700 °C for 20 min.

We studied several PZT films grown on silicon substrates at different temperatures ranging from 500°C to 700°C. The orientation for the grown PZT thin films is shown in Figures 2.11-

2.15 for different growth temperatures. Parameters such as grain boundaries and grain-size greatly influence the ferroelectric properties. Single crystal materials are usually identified by larger grain sizes and less grain boundaries. These grain boundaries indicate polycrystalline materials, which degrade device performance for this specific area of research.

Knowing the orientation helps determining the phase(s) of the film. In addition, much attention needs to be focused on the possible growth of the pyrochlore phase of PZT. This phase is not desired since it is not the preferred perovskite structure. The ferroelectric properties of the material will be damaged if there is any pyrochlore phases. The intensity of the pyrochlore phase, full width half max (FWHM), and the intensity percentage of the pyrochlore phase will be researched. The general trend observed is that, the pyrochlore phase diminishes in intensity for all grown samples by annealing as seen in XRD scans, Figures 2.11-2.15. The lowest pyrochlore phase intensity was observed for film grown at 500°C.

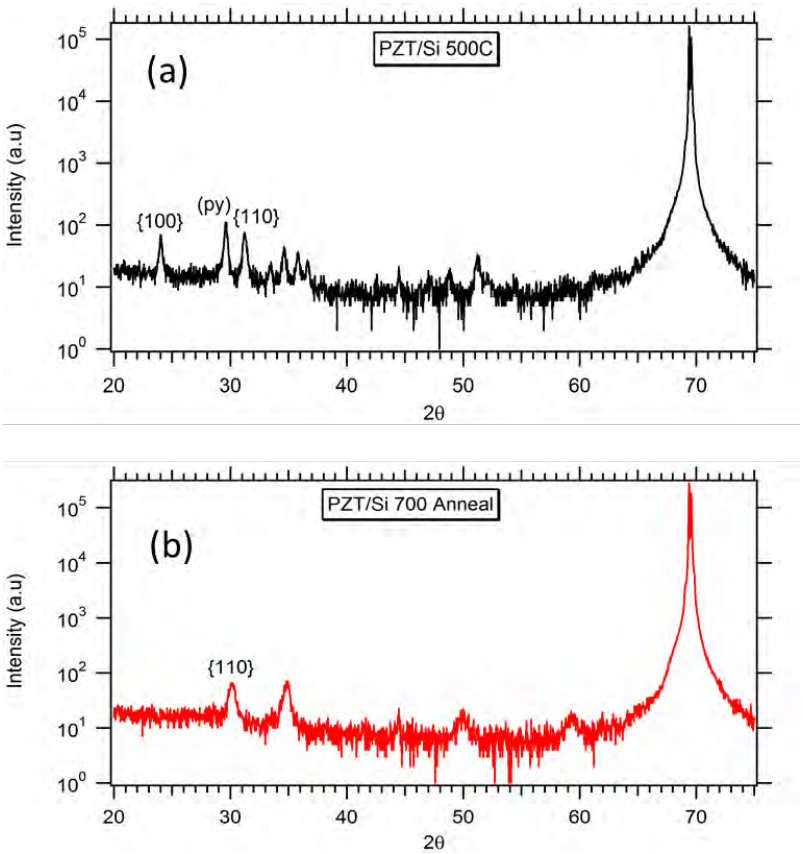

Figure 2.12. The XRD patterns of the grown PZT thin film where a standard RCA method of cleaning technique is used. (a) represents as sample grown at 500 °C. (b) represents the film annealed at 700 °C for 20 min.

We used two different cleaning methods of the substrate, (1) basic cleaning using acetone, methanol, and distilled water technique However, (2) popular RCA technique where the cleaning procedure has three major steps used sequentially:

a) Organic Clean: removal of insoluble organic contaminants with a 5:1:1 H_2O:H_2O_2:NH_4OH solution.
b) Oxide Strip: removal of a thin silicon dioxide layer where metallic contaminants may accumulated as a result of (1), using a diluted 50:1 H_2O:HF solution.

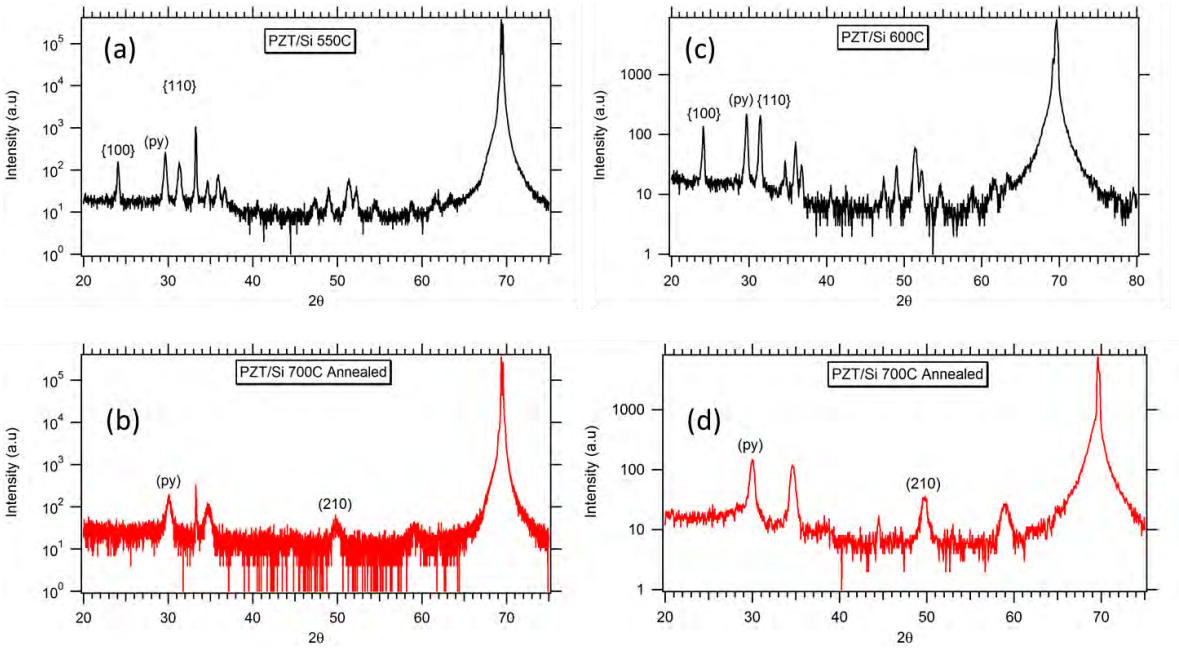

Figure 2.13. The XRD patterns of the grown PZT thin film where a standard RCA method of cleaning technique is used. (a) represents as sample grown at 550 ºC. (b) represents the film annealed at 700 ºC for 20 min. (c) represents as sample grown at 600 ºC. (d) represents the film annealed at 700 ºC for 20 min.

c) Ionic Clean: removal of ionic and heavy metal atomic contaminants using a solution of 6:1:1 H_2O:H_2O_2: HCl.

For the films grown at 500°C, we found that the undesired pyrochlore phase was diminished but still noticeable when the substrate is cleaned using the basic cleaning technique, Figure 2.11, and it is completely eliminated when the RCA cleaning method is used for the substrate, Figure 2.12. Consequently, we adopted the RCA cleaning technique for the remaining grown samples.

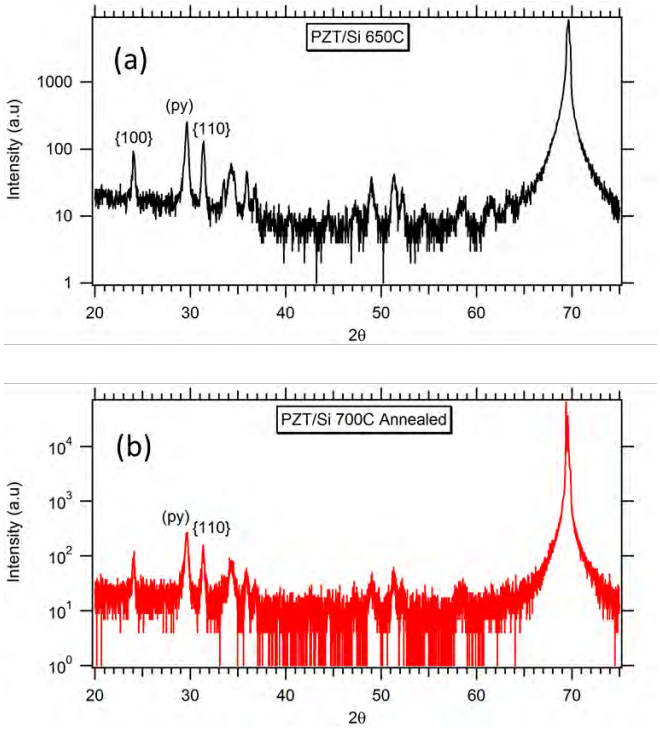

Figure 2.14. The XRD patterns of the grown PZT thin film where a standard RCA method of cleaning technique is used. (a) represents as sample grown at 650 ºC. (b) represents the film annealed at 700 ºC for 20 min.

However, MgO is buffered on Si (MgO was grown by the Pulsed Laser Deposition (PLD)), the pyrocholre phase was significantly suppressed as shown in Figure 2.15, starting with PZT on Si and followed by PZT on MgO buffered Si and with annealing.

The 2D and 3D 1μm Atomic Force Microscopy (AFM) scans for the grown samples at different temperatures are shown in Figures 2.16-2.18. From these scans, the largest grain size, about 100 nm is obtained for the sample grown at 500°C. This proves that the material is leaning toward more single crystalline nature. However, at this point all the samples are still in their polycrystalline phase.

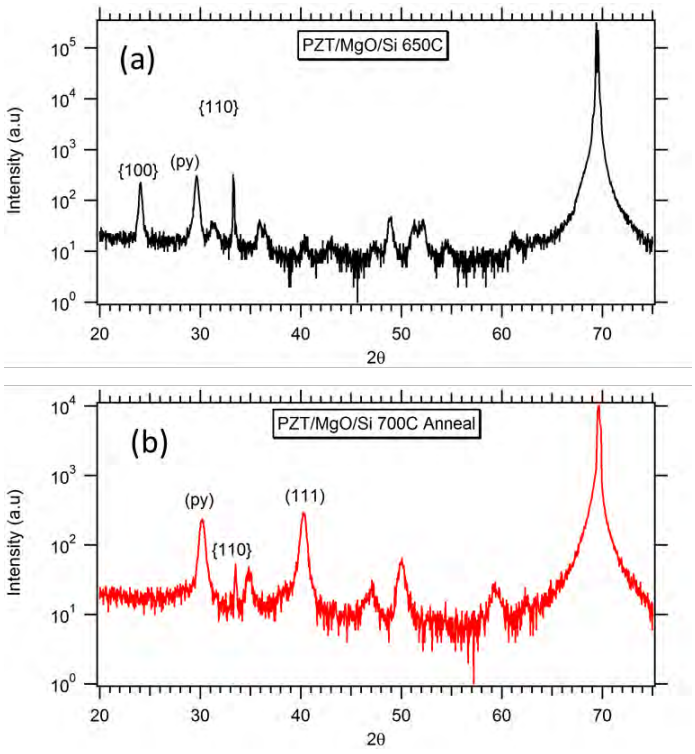

Figure 2.15. The XRD patterns of the grown PZT thin film thin film with MgO buffer layer where a standard RCA method of cleaning technique is used. (a) represents sample grown at 650°C. (b) represents the film annealed at 70 °C for 20 min.

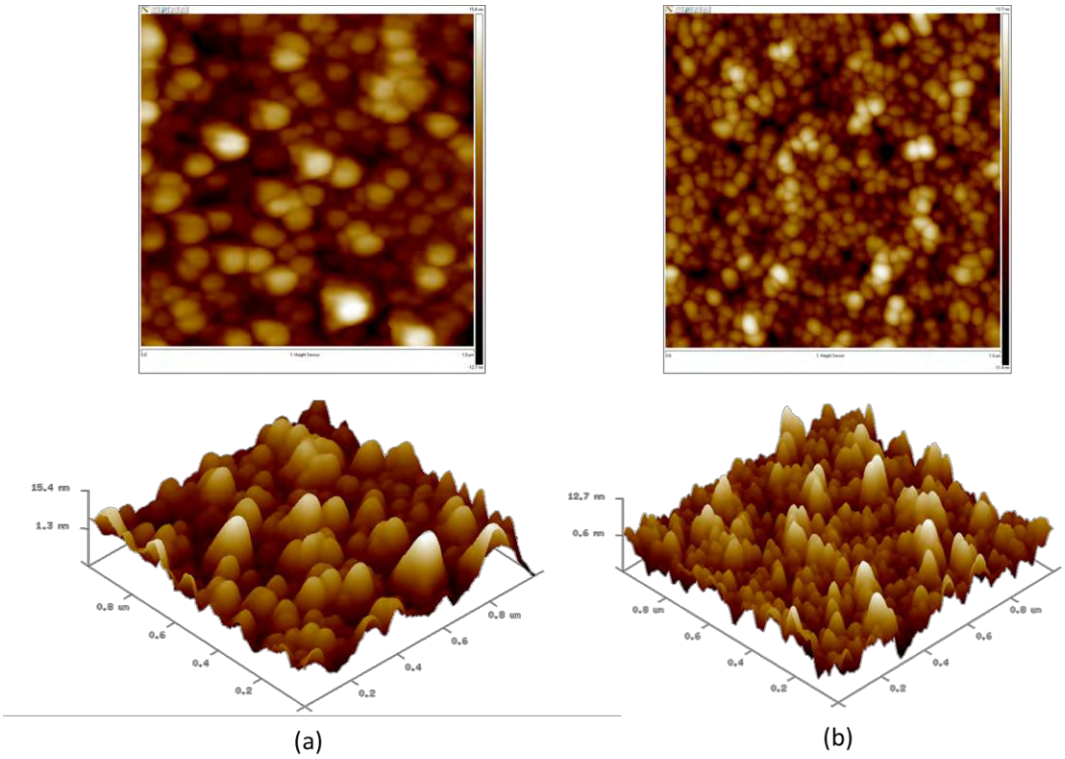

Figure 2.16. AFM 2D and 3D images of PZT thin film grown at 500 ºC (a) using basic cleaning technique for the substrate (b) using the RCA cleaning technique for the substrate.

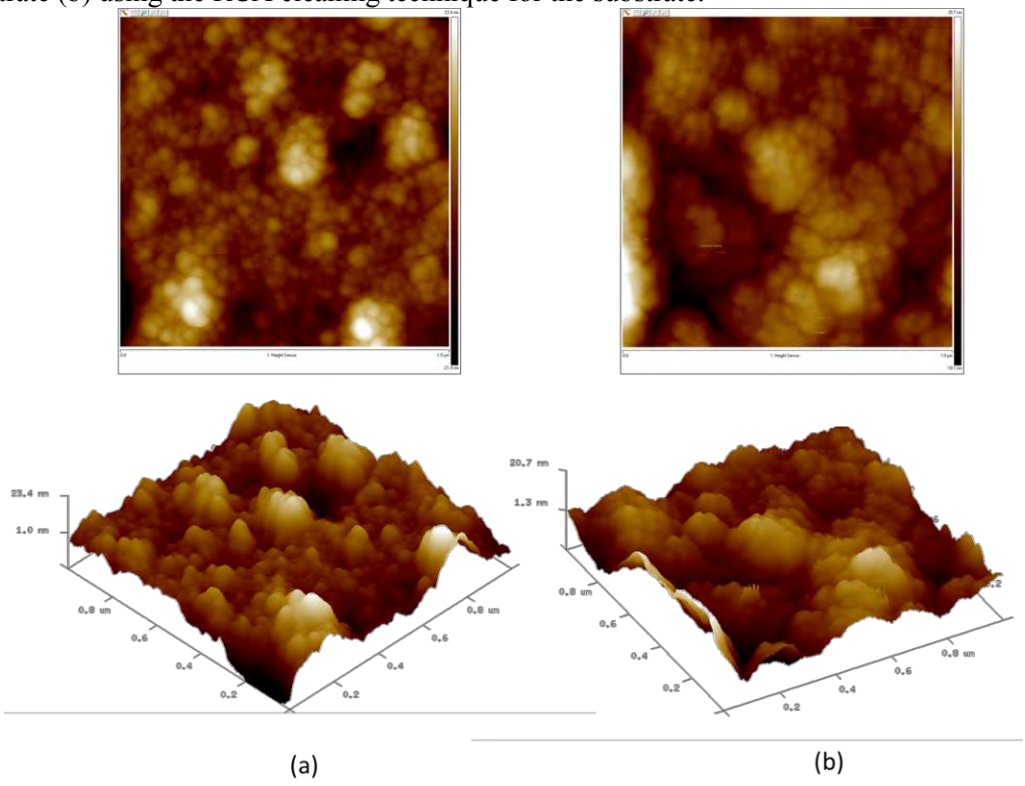

Figure 2.17. AFM 2D and 3D images of PZT thin film using the RCA cleaning technique grown at (a) 550 ºC and (b) at 600 ºC.

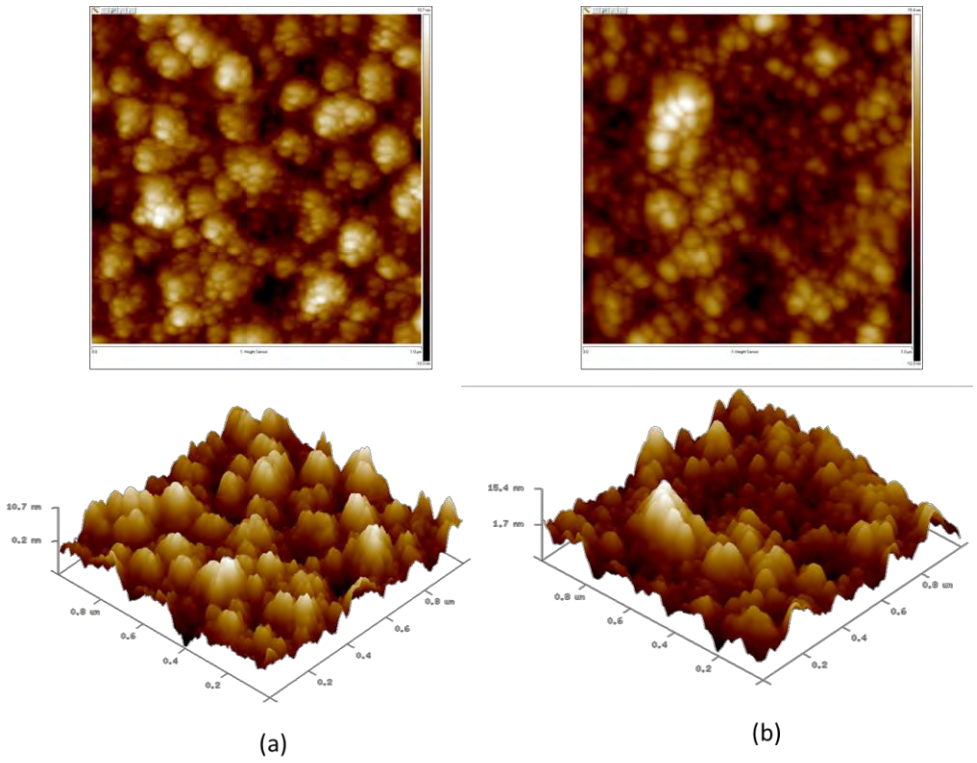

Figure 2.18. AFM 2D and 3D images of PZT thin film using the RCA cleaning technique grown at 650 ^{o}C (a) without buffer layer and (b) with MgO buffer layer.

Device Fabrication

The results from COMSOL and PZT film characterizations were then used to begin fabrication of the TFBAR device as outlined below. A process flow for fabrication was developed in order to determine the steps in which the device would be manufactured in the NSU cleanroom. The process flow beginning with the bare silicon wafer is outlined in Figure 2.19. To delineate the patterns and dimensions determined from the design developed, photomasks are used during the photolithography steps of the fabrication process. Thus, AutoCAD software was used in order to design the photomasks to be used. The design of the masks is shown in Figures 2.20 and 2.21. The device is currently being fabricated in the cleanroom at NSU.

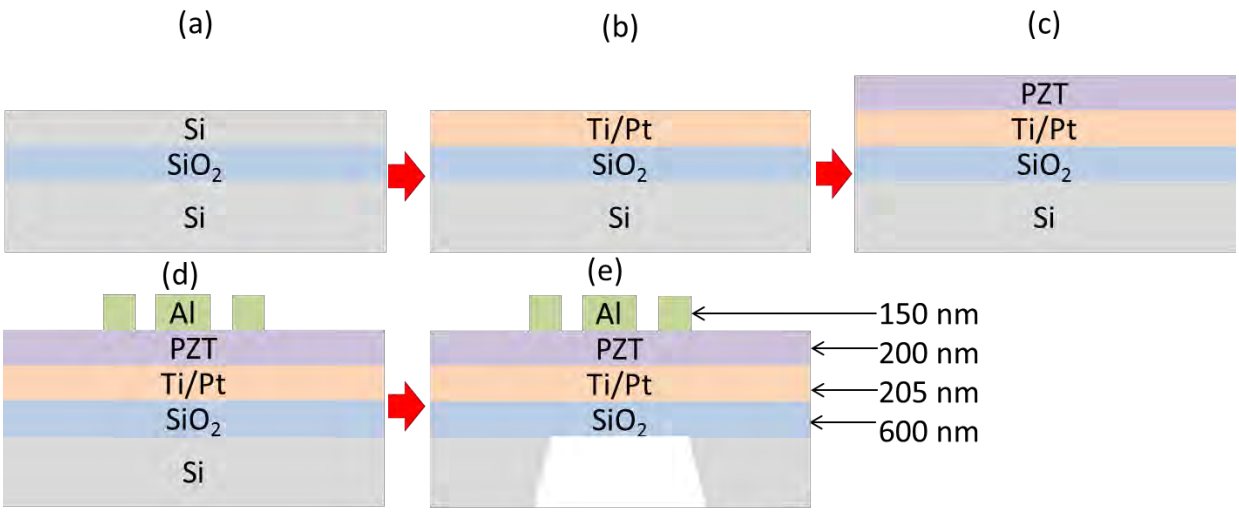

Figure 2.19. Device fabrication process. (a) Silicon deposition using PECVD. (b) Ti/Pt bottom electrode is then deposited using an e-beam evaporator. (c) PZT deposited using RF sputtering machine. An aluminum top electrode is then deposited after patterning the device using (d) photomask #1 and (e) photomask #2.

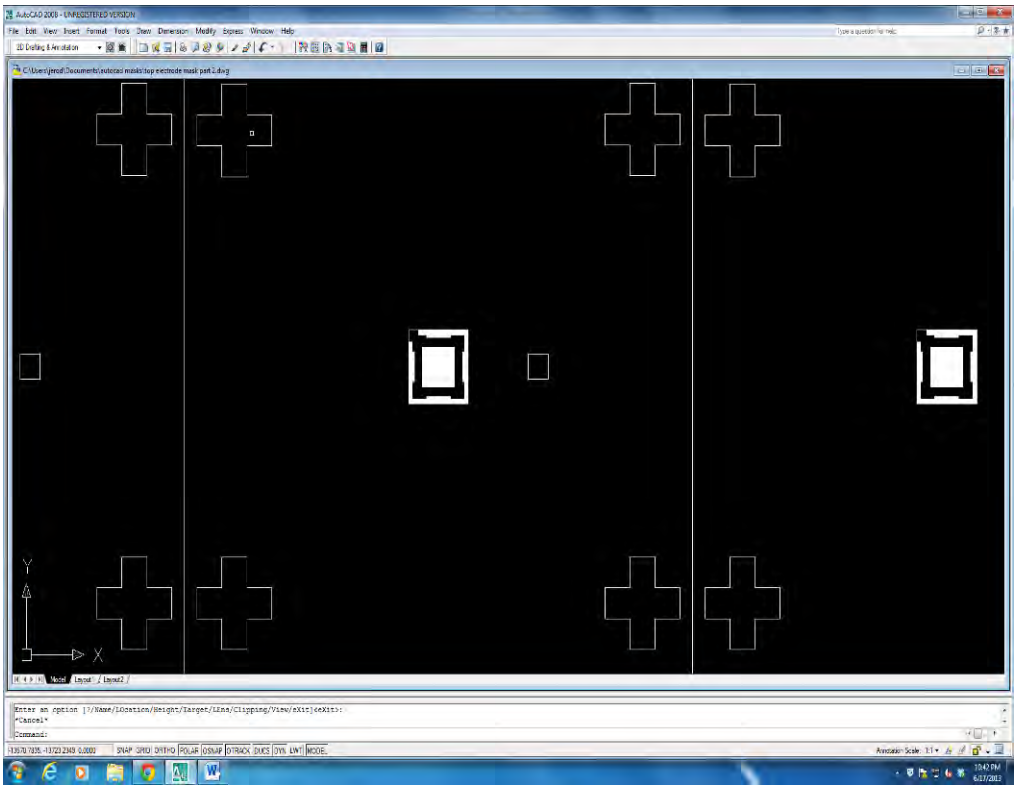

Figure 2.20. Top electrode mask (Mask #1).

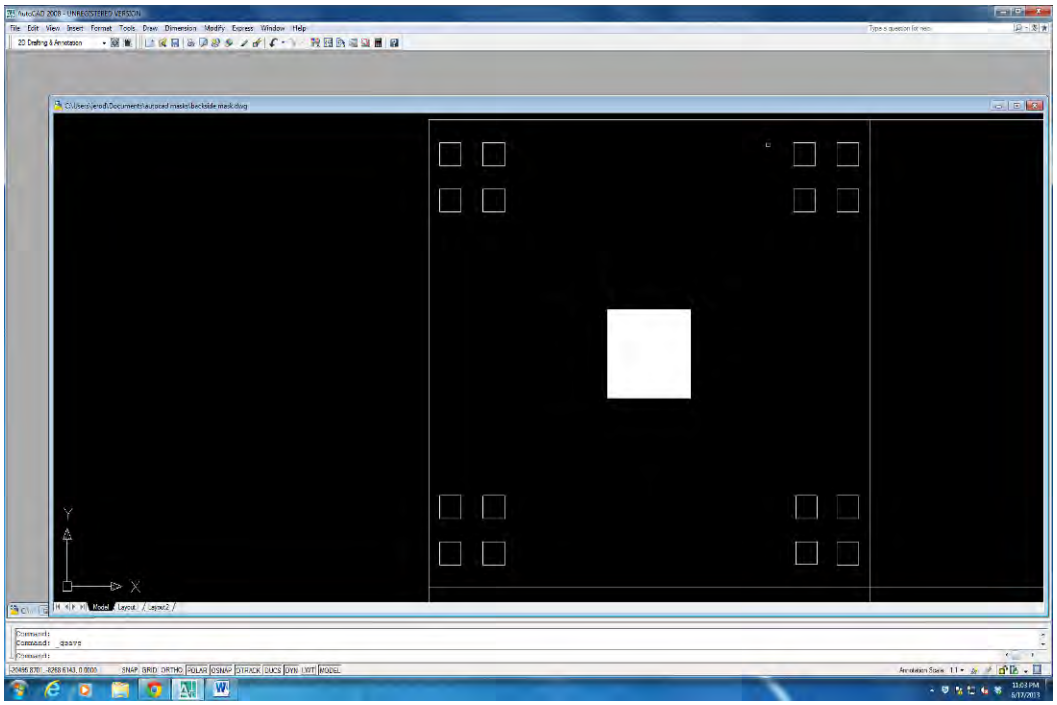

Figure 2.21. Backside diaphragm mask (Mask #2).

2.2 Design and Fabrication of a Functionally Modified Bimorph Actuator

A new project was also begun under this grant. The project is in collaboration with faculty from Clemson University and is to develop a functional modified bimorph MEMS actuator for micro- and nano- unmanned air vehicle (UAV) applications. UAV research has been increasingly popular over the last decade for potential reconnaissance and search and rescue applications. Current research is based on the development of devices that mimic the superior maneuverability of small birds and insects.

MEMS technology continues to play a dominant role in the miniaturization of devices in the industry. The advent of micro technology on the Unmanned Aerial Vehicles (UAVs) industry has caused a huge transition from drones to bio-inspired UAVs. UAVs are aircrafts that are self or remotely piloted to relay real time information to the operators. UAVs came to the spotlight as technological devices born out of necessity decades ago to support military operations. They carry equipment such as actuators for flying, accelerometer, gyroscope, barometer, ultrasonic sensors, global positioning systems (GPS), and on-board flight controller computers. The understanding of MEMS has inspired many researchers to replace complex and weighty mechanical components of UAVs that drive the device with a simple and less weight actuator.

A lot of research has been done to scale down the size of UAVs and improve their aerodynamics; nevertheless, optimization of UAVs' maneuverability with MEMS technology has not been fully explored. Application of an electric field to a traditional actuator produces a

linear displacement with one degree of freedom. This conventional design may require supplementary structural modification to control maneuverability of the device. The setback in this approach is that it adds to the payload of the device, and it does not produce optimum aerodynamics. The objective of this research work is to optimize the maneuverability and aerodynamics of a miniaturized UAV. The research involves the design of a functionally modified bimorph actuator and fabrication of anisotropic layers of PZT on a primary PZT layer with stainless steel substrate. It focuses on careful selection of process parameters and process materials to generate a bend-twist motion in the fabricated cantilever with active layers.

Dimensions of the device are stipulated by the optimized results obtained from finite element analysis software COMSOL analysis. The composite structure has 6mm x 36mm x 102 micron thick stainless steel as its substrate. 0.86 µm layers of PZT are deposited on both sides of the substrate. 1 µm of PZT forms the top PZT striped layer and is grown on the 0.86 µm PZT top layer. The PZT stripes are angled by 45˚ to the bottom PZT layer as shown in Figure 2.22. The dimensions of the top and bottom electrode are not factored in the design because their thickness has an insignificant effect on the performance of the device. The top and cross sectional (side) views of this device are shown in Figures 2.23 and 2.24.

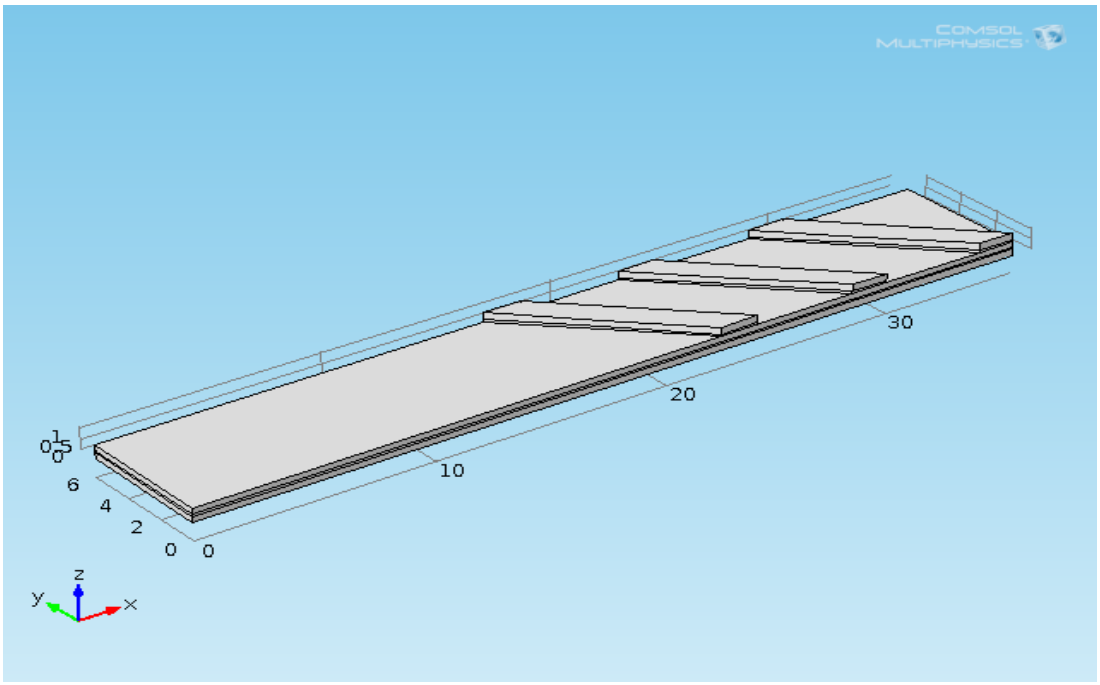

Figure 2.22. Functionally Modified Bimorph Actuator.

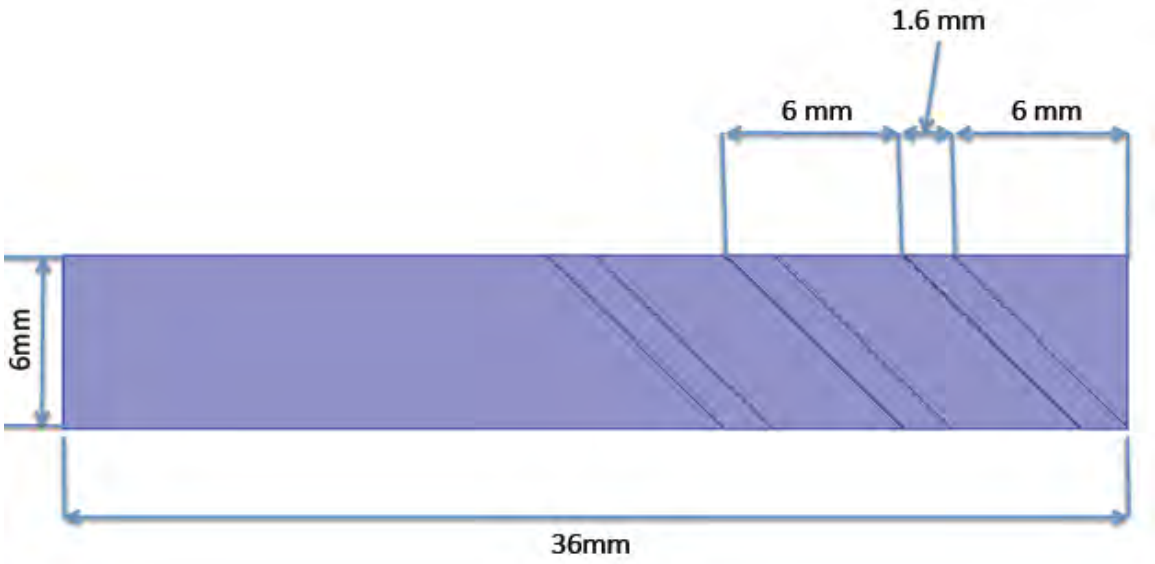

Figure 2.23. Top View of Functionally Modified Bimorph Actuator.

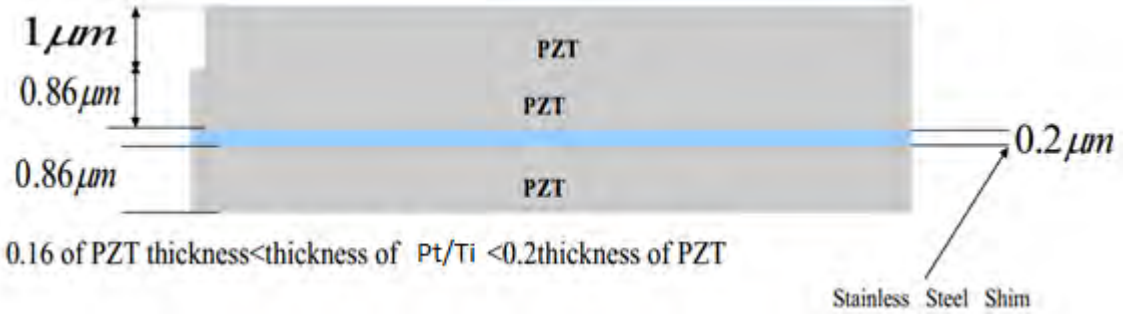

Figure 2.24. Side View of Functionally Modified Bimorph Actuator.

Autodesk Inventor Results

Fabrication of the device involves etching of PZT and deposition of electrodes on the selected parts of the PZT that are not etched. In order to actualize these two critical steps, two photomasks were needed during the lithographic process. The two masks were designed by Autodesk Inventor as shown in Figure 2.25.

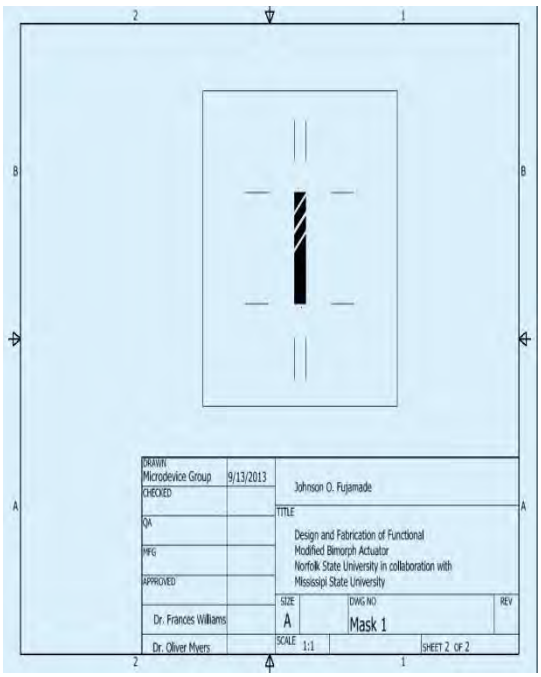

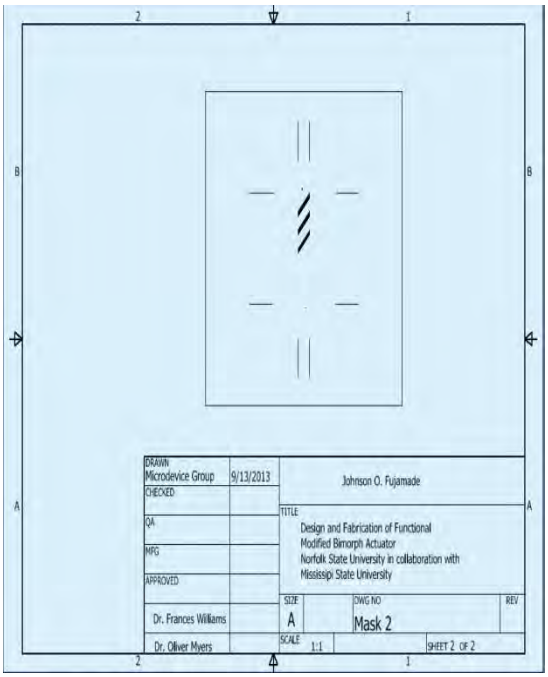

Figure 2.25. Mask 1 and Mask 2 Designed with Autodesk Inventor.

Device Fabrication

The fabrication of the device is carried out following careful selection of materials and process flow. The stainless steel (SS) substrate is thoroughly cleaned with a solution of sulphuric acid and hydrogen peroxide (piranha solution) to remove organic residue. Then the substrate is rinsed with de-ionized water.

Process Flow

Following a thorough review of related work and careful consideration of the best approach to fabricate the device, the process flow to create the functionally modified biomorph actuator was developed. A schematic diagram of the process flow used to grow the multilayered film is displayed in Figure 2.26. A description of the processing steps is detailed below.

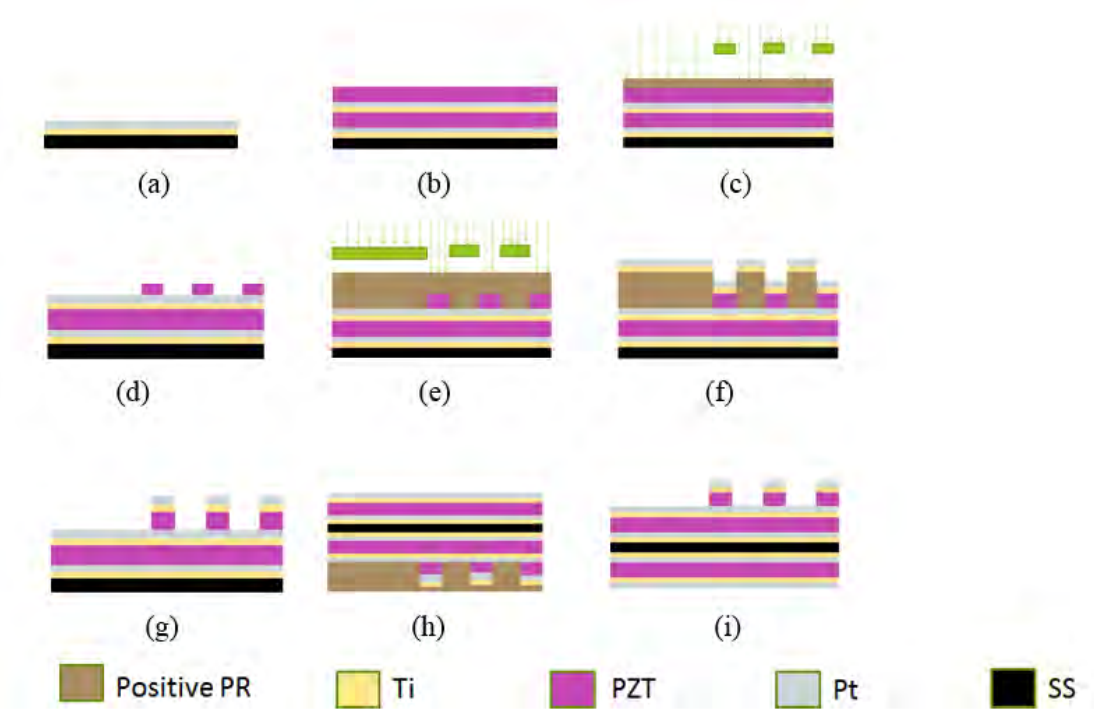

Figure 2.26. Process Flow.

Once the stainless steel substrate is thoroughly cleaned and air-dried, 500Å of titanium (Ti), an adhesion layer, is sputtered on the substrate using a DC sputterer. It is important to consider the heteroepitaxy effect to grow a good quality PZT film. Since platinum (Pt) has a lattice structure that is similar to PZT, growing PZT on Pt will help with the crystalline orientation of PZT. In order to promote lattice matching, Pt is used as a bottom electrode. The DC sputtering technique is also used to grow 2000 Å of platinum on titanium as shown Figure 2.26a. Deposition of platinum is followed by the deposition of 850 nm of PZT using the RF sputterer.

Table 2.1 shows the parameters used to grow the multi-layered films. The first layer of PZT film is annealed in RTP 600S at 700 ºC for 3 minutes to facilitate the transition of PZT crystalline structure from an amorphous phase to a perovskite phase. The thermal treatment is repeated after sputtering another 1µm of PZT before depositing the top Pt/Ti electrode as depicted by Figure 2.26g. The same parameters in Table 2.1 are applied in growing all of the thin films illustrated in the process flow in Figure 2.26. The PZT films are grown at room temperature.

Table 2.1 Deposition Parameters.

Machine	Film	Power (W)	Pressure (mTorr)	Ar:O_2	Thickness (kÅ)
DC Sputterer	Ti	300	5	1:00	0.5
	Pt	300	5	1:00	2
RF Sputterer	PZT	120	1.92	9:01	8.6/10
E-Beam	Ti	35%	-	-	0.5
Evaporator	Pt	35%	-	-	2

The photomasks were designed using Autodesk Inventor software. The first photomask was used during the lithography process for patterning of the photoresist as depicted in Figure 2.26c. The patterned photoresist was then used as a mask during the etching of the PZT as shown in Figure 2.26d.

Exposure and Etching

Studies have shown that etching PZT is challenging. Complications are due to the selectivity of the PZT in relation to the masks as PZT properties could be altered during either chemical or physical etching processes. Research shows that the bombardment of PZT with ionized atoms in a reactive ion etching process could have a damaging impact on the electrical properties of PZT material. Similarly, ion beam etching, which could have been a good physical etching alternative, can result in carbonization of photoresist that makes it difficult to strip off the photoresist after the photolithography process. The unmasked portion of the PZT in Figure 2.26d is etched in BHF: HCl: NH_4Cl (1:2:4:4) solution for 1 minute and then dipped in $2HNO_3$:$1H_2O$ solution for 15 seconds to remove any chemical residue and later immersed in DI water for 5 minutes and air dried. The photoresist is stripped off with acetone. Research shows that adding a chloride compound to the acidic PZT etchant will reduce undercut, and the complex lead chloride compound, which is a byproduct of the etching process, is made soluble after immersion in HNO_3.

Back-Side Processing

As the SS substrate is sandwiched between PZT and Ti/Pt layers on the front and backside, backside processing is required to deposit these layers on the back as shown in Figure 2.26h. The sample was flipped over and processing on the backside commenced with the deposition of Ti, Pt, PZT, Ti, and Pt (in that order) on the back.

Lift-off Process

Figure 2.27. A sample with Pt electrodes after etching.

Figure 2.28. Final Device.

Once the etching of the exposed part of PZT film was completed using the first mask, processing of the top Ti/Pt electrode continued with the deposition and patterning of the photoresist using the second photomask, as shown in Figure 2.26e. Since platinum is inert and very difficult to etch, patterning of the angled PZT on the top side is done by a lift off technique as shown in Figure 2.26g. An e-beam evaporator is used to deposit the top electrode (Ti/Pt). The Ti/Pt electrodes are patterned using a lift-off process which results in the segmented (angled) top electrodes as shown in Figure 2.26i. Figure 2.27 shows the microscopic view of the Ti/Pt electrode deposited on the angled PZT after etching the PZT film in the middle while Figure 2.28 shows the final device (top view).

Characterization of PZT Layers

In many cases, PZT is grown at a very high temperature to enhance the transition of its crystalline structure from pyrochlore to perovskite phase. The PZT films grown on the SS substrate are grown at room temperature. Therefore, to attain the perovskite structure, the composite structure is annealed for three minutes at 700 °C with a rapid thermal processing machine. It is essential to understand the ferroelectric properties of PZT because it has a big impact on the actuator performance. Once PZT is grown, the structure and crystallinity of the films were analyzed by X-ray Diffraction (XRD). Possible material structures are single crystal, polycrystalline, or amorphous. The goal is to grow a polycrystalline PZT with desired optimal properties. However, these valuable properties could be unrealistic if the grown PZT film has pyrochlore crystalline phase. The orientation for the PZT thin films grown is illustrated in

Figure 2.29 using XRD analysis of the SS/Ti/Pt/PZT layers after annealing at 700 ºC. As shown in Figure 2.29, the dominant peak is the preferred orientation of {110} that exhibits a high value of e_{311} (piezoelectric coefficient) which is highly favorable for our application.

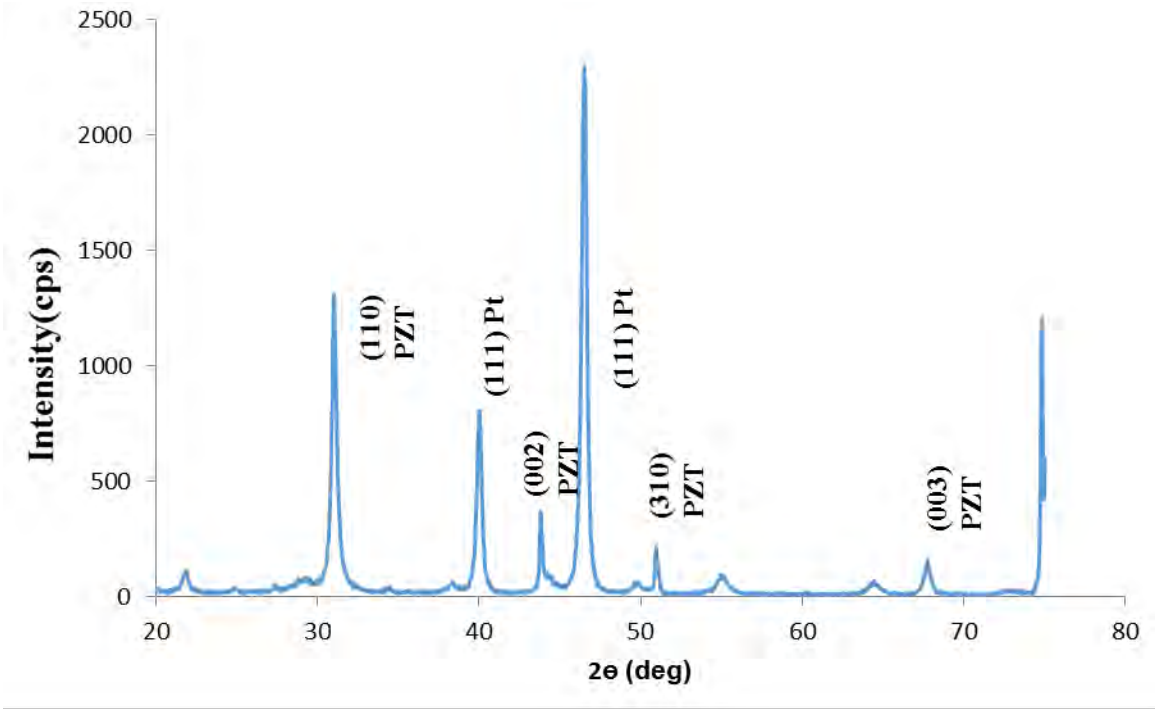

Figure 2.29. XRD Characterization of Grown PZT.

In addition, in order to validate the optimization of the applied deposition parameters, the I-V characteristics of 50 nm thick PZT on 4-inch by 4-inch stainless steel substrate and a Ti adhesion layer is examined (Figure 2.29). In order to validate the dielectric status of the grown PZT film, I-V (current versus voltage) test was carried using Keithley probe station. It was observed that the grown PZT layer has a very small leakage current and behaves as a dielectric material. This is validated by the result of the test shown in Figure 2.30.

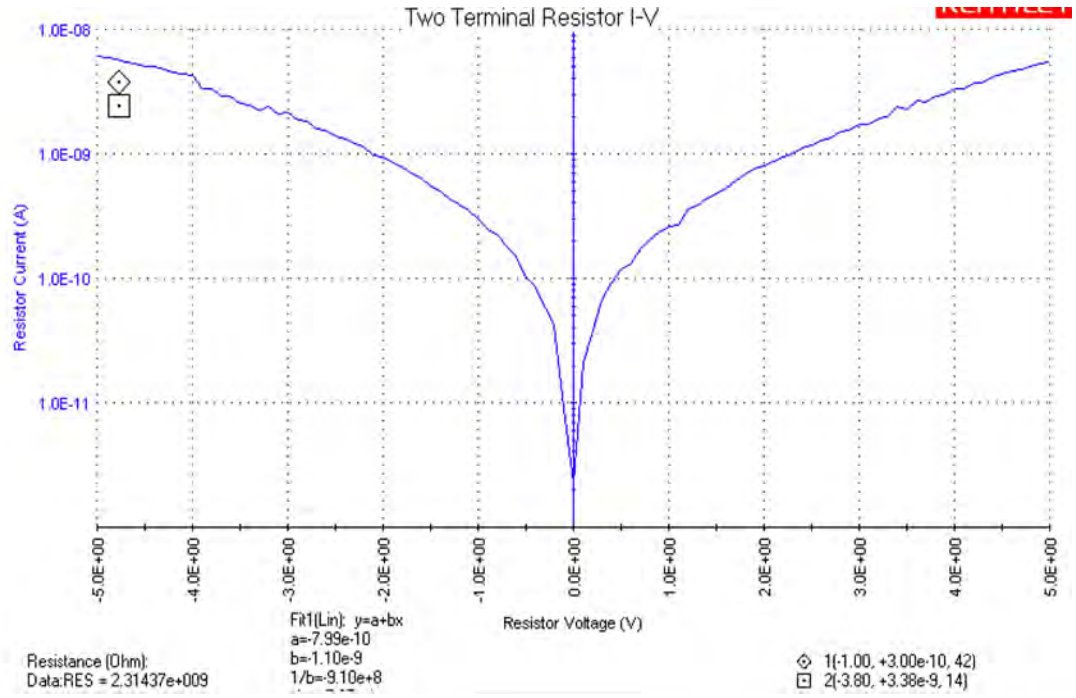

Figure 2.30. I-V Characteristics of PZT.

Device Measurement

The device measurement was carried out at the National Aeronautic and Space Administration (NASA) using a MicroEpsilon Displacement Sensor with 0.2 micron resolution as shown in Figure 2.31. A DC power supply was used to apply a voltage to the device, starting at 0 V and slowly increasing the voltage. Wires were attached using conducting epoxy to the electrodes on the striped PZT on the top Pt3 electrode, bottom electrodes Pt1, and the top electrode Pt2 for the first PZT layer as shown in Figure 2.32.

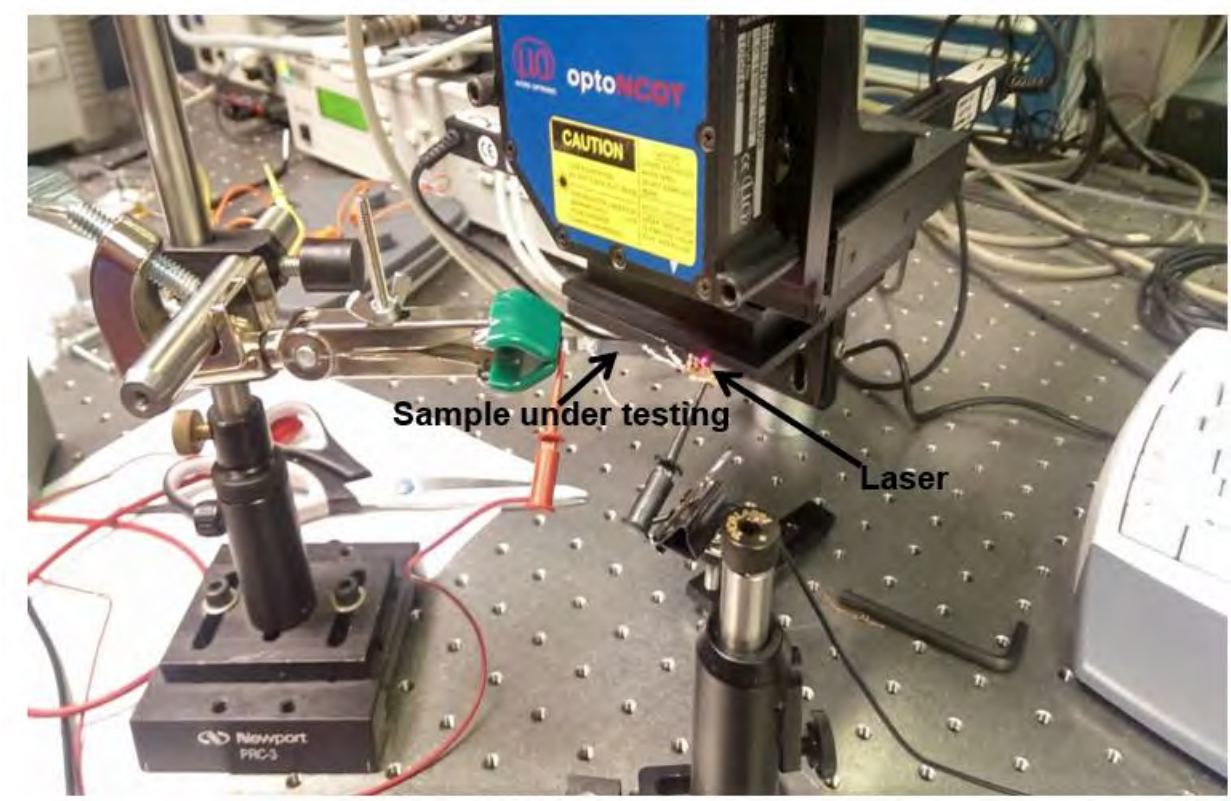

Figure 2.31. Measurement Set-Up.

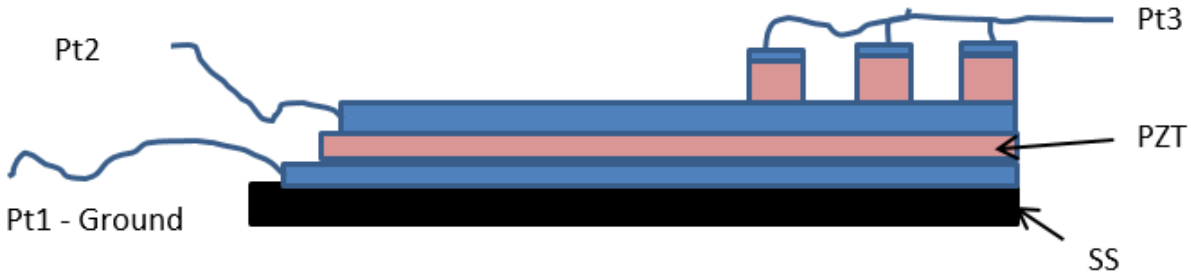

Figure 2.32. Wire Connections to the Sample.

The plot in Figure 2.33 shows the relationship between the applied voltage between Pt1 and Pt2 and the mechanical response. It also shows that the voltage applied is proportional to the displacement up to a voltage of ~0.6 V. Thereafter the deflection started to decrease and it appeared that other mechanisms were affecting the device performance. Testing was also performed where a voltage was applied between Pt1 and Pt3. For this measurement, a maximum deflection of 15 μm was observed at 3 V. The breakdown voltage was reached for voltages

above 3V. This is in compliance with the I-V curve which shows that the thin film will begin to approach breakdown voltage after 3 V.

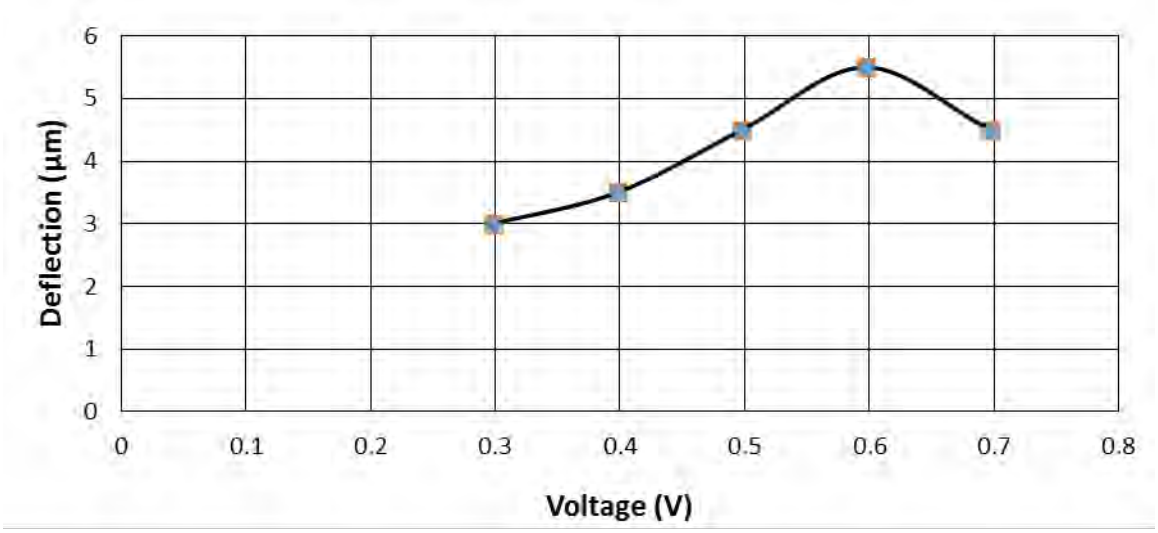

Figure 2.33 Measurement from the First PZT Layer. Deflection versus Voltage (measured between Pt1 and Pt2).

The voltage and displacement discrepancies observed (such as the deflections decreasing after a certain voltage) could be due to some factors such as:

a) Residual stress in the film which could be caused by the thermal effect and heating of the cantilever due to applied voltage.
b) Weight of the wires attached to the electrodes using conducting epoxy.

These issues need to be further investigated. Possible solutions include, coating the stainless steel with silicon dioxide to reduce the thermal expansion variation and to isolate the stainless steel from the platinum; increasing the thickness of the PZT layers; and enhancing the placement of the wire by using wire bonding and enhanced electrodes design.

3. EDUCATION AND TRAINING OF STUDENTS FROM UNDERREPRESENTED MINORITY GROUPS IN MEMS AND SENSOR DEVELOPMENT AND FABRICATION

3.1 EDUCATION AND CURRICULAR DEVELOPMENT

Dr. Williams (Co-PI) developed and taught a graduate course on semiconductor and MEMS processing techniques "MEMS" (EEN 650) for undergraduate and graduate students to lean the nano- and micro-fabrication necessary techniques for the sensors fabrication. More than a dozen of students were enrolled each year. Classroom teaching experiments have been developed and utilized for graduate and undergraduate classes of OEN 530 and OEN 360, and OEN 498/499.

Students training on the use of the Pulsed Laser Deposition (PLD) system for the growth of multi-layers films.

3.2 STUDENTS TRAINING

Undergraduate, graduate, and high school students have been trained through research experiences as well as classroom theory in biomedical and MEMS devices and semiconductor processing. The majority of the students are minority or female students.

Students being trained on the use of Atomic Force Microscopy (AFM).

The state-of-the-art class 100/1000 Cleanroom, Micro- and Nano-technology Center (MiNatC) at the Marie McDemmond Applied Research (MCAR) was used to train undergraduate and graduate students. All students are being trained in our state-of-the-art 6000 sq. ft. clean room. Students are being signed off in each instrument. This training complements the hand-on training for EEN 650, Microelectromechanical Systems (MEMS) course taught by Dr. William.

Dr. Williams provided training in Clean Room for students on the following systems

- RF Sputtering System Training for graduate students
- DC Sputtering System Training for graduate students
- E-beam Evaporator System Training for graduate students
- Thermal Evaporator System Training for graduate students
- Ellipsometry system Training for graduate/undergrad students
- Photolithography
- Electron Beam Lithography system
- Atomic force Microscopy

Training of students in the educational clean room.

3.3 PROFESSIONAL DEVELOPMENT

MRS Student Chapter activities

The first Materials Research Society (MRS) Student Chapter at NSU was launched by ten CMR students under the supervision of Dr. Pradhan and Dr. Bahoura. The MRS Students members are active in community outreach and are acquiring leadership skills in managing a chapter through meetings, developing bylaws, managing finances, learning communications skills though programs offered by MRS and by attending MRS Spring and Fall Meetings, inviting distinguished speakers; and competing for special project grants.

MRS Student Chapter poster competition announcement flyer.

The MRS Student Chapter organized poster competitions during the summer that attracted many students from all over the College of Science, Engineering and Technology (CSET) and local colleges. The posters were judged by prominent scholars such as Dr. Aklesh Lakthakia. Monetary prizes and certificates were given to the first three top posters.

Research Group Activities

The undergraduate and graduate students were mentored by the faculty and research associates. During the weekly research group meetings, the students presented their research progress and received feedback about their research and tips on how to present efficiently their results in public. In addition, references to ethics and responsible research conduct were made in these meetings.

MRS Student Chapter poster competition event.

Professional Development Seminars

The students took advantage of the series of professional development seminar series hosted by the Center for Materials. Expert in industry, academia and national laboratories, including former NSU students and international scholars were invited to give talks about the state of the art of their cutting edge research as well as professional development topics.

The seminar of Dr. Lakhtakia.

The scientific seminars covered a wide range of topics in materials science and new trends in the fields of metamaterials, radiation detectors, polymer solar cells, and piezoelectric materials. For example, Professor Akhlesh Lakhtakia, Pennsylvania State University, gave an outstanding lecture about the state-of-the art research and development in the areas of nanotechnology and metamaterials.

The professional development seminars included the following topics: resume, CV and cover letter, non-traditional careers, tips on networking, job search tips, postdoctoral appointments and internships, interviewing and mock interviewing, first year on the job- government careers, First

year on the job-Industrial careers, intellectual property and patents, and how to start a business. For example, Dr. Gurusamy, from SC Johnson Company talked about the industrial jobs, how to apply for them, how to write a successful resume, the differences between academic and industrial jobs, choosing right industry/field, what to look for, where to get info, the importance of networking, planning before interview, effective presentation skills-interview, critical success factor, non-verbal techniques, critical after interview, key elements of Success. This presentation was interactive and engaged all the students, especially the students graduating soon.


Dr. Deepam Maurya presenting at the seminar.

Also, we invited Dr. Jayfus Tucker Doswell Ph.D., President/Chief Executive Officer of Juxtopia, LLC, a biomedical and information technology (BIO-IT) company and an innovative leader in the design and development of human performance products, based in Virginia. Dr. Jayfus Tucker Doswell gave a presentation on entrepreneurship and on how to start a company and do business with government agencies. The talk attracted many undergraduate and graduate students who asked many relevant questions and were inspired by the entrepreneurship and leadership of the presenter.

Our students benefited from a two day professional development interactive workshop for resume reviews and mock interviews. This workshop was free to all graduate students.

The list of the seminars is shown in the table below:

Date	Title	Presenter
Sep. 14, 2012	Opto-electronic Properties of Atomic Layer Deposited Al-doped ZnO Films with Varying Carrier Concentration for Multifunctional Applications	U.N. Roy, Brookhaven National Laboratory
Oct. 12, 2012	Optical Floating Zone as a Scientific Tool for Creating Crystals of New Oxides	Hanna A. Dąbkowska, Brockhouse Institute of Materials Research, McMaster University, Canada
Oct. 19, 2012	Development of polarimetric imaging OCT and laser radar systems	Dr. Renu Tripathi, Optical Sciences Center for Applied Research (OSCAR), Delaware State University
Mar. 8, 2013	Industrial jobs - Why? How?	Gurusamy (Mani) Manivannan, SC Johnson Company

July 19, 2013	Thin Films and other NanoTales	Akhlesh Lakhtakia, Pennsylvania State University
October 18, 2013	Engineering the coherent, thermal and quantum state of light using metamaterials	Dr. Zubin Jacob, Department of Electrical and Computer Engineering, University of Alberta, Canada
November 15, 2013	Understanding the Structure and Behavior of Polymer Gels as host for nano solutes – a photonics recipe.	Dr. Kimani A. Stancil, Department of Physics and Astronomy, Howard University, Washington DC
September 13, 2013,	Crystal growth and characterizations of radiation detector materials	Dr. Pijush Bhattacharya, Department of Physics, Fisk University, Nashville, TN
September 27, 2013	Toward high performance polymer solar cells	Prof. Xiong Gong, University of Akron, Akron, OH
February 21, 2014	Laboratory for Advanced Nitride Device Design, Fabrication and Synthesis	Lourdes Salamanca-Riba and Mario Dagenais, University of Maryland, College Park, MD
March 7, 2014	Nanomaterials for Energy Applications	Dr. Sivaram Arepalli, VP of Education & Outreach, National Institute of Aerospace, Hampton, VA and Department of Energy Science, Sungkyunkwan University, Suwon, Korea
March 21, 2014	Beyond the Material Limits for Mid-Infrared Wavelength Devices	Gregory Triplett, PhD, Associate Professor and Director of Undergraduate Studies Electrical and Computer Engineering, University of Missouri
April 18, 2014	Recent Advances in MRI Cell Tracking Using Nanoparticle Probes	T. Kevin Hitchens, Assistant Director, Pittsburgh NMR Center for Biomedical Research Carnegie Mellon University, Pittsburgh, PA
June 13, 2014	High Performance Textured Lead-Free Piezoelectric Materials	Dr. Deepam Maurya, Bio-inspired Materials and Devices Laboratory (BMDL), Center for Energy Harvesting Materials and Systems (CEHMS), Virginia Tech
August 13, 2014	Thermal Spray Processing of Ethylene Methacrylic Acid and Polymer-Ceramic Composites	Michael Xie, Energy Storage Department Pacific Northwest National Laboratory, Richland, WA

October 17, 2014	Blinded by light	Mark Boland, Science and Art at the Australian Synchrotron
October 31, 2014	Collective resonant energy transfer in plasmonic structures	Alexander N. Poddubny *Ioffe Institute, St. Petersburg, Russia, ITMO University, St. Petersburg, Russia*
November 20, 2014	Properties of 3d transition metal point defects used to stabilize hexagonal BaTiO3 at room temperature	Sanjeev K. Nayak *Institute of Physics, Martin Luther University Halle-Wittenberg, Germany*
November 21, 2014	Delivering a sustainable and Revolutionizing Solar Energy	Reginald Parker, 510nano Inc. President and CEO
January 23, 2015	Building Your Professional Skills/Building the CMR Reputation for Outstanding Science Education /Outreach and Training to Communicate Science to Diverse Audiences	Dr. Suely M. Black, *RISE Project Education Coordinator, CMR, NSU*
April 10, 2015	Time Management	Janna Lamey, Assistant Dean for Graduate Student Life at Cornell University
April 17, 2015	Understanding Blazars - Nature's Particle Accelerators	Jedidah C. Isler, Ph.D., *Department of Physics, Syracuse University, Syracuse, NY*
April 24, 2015	Coupling and Control over Electronic and Plasmonic effects in Plasmonic Nanostructures and Metamaterials	Maxim Durach, *Department of Physics, Georgia Southern University,Statesboro, GA*
June 17, 2015	Research in the National Ignition Facility and Photon Science Directorate (NIF&PS), Lawrence Livermore National Laboratory (LLNL)	Dr. P. Jeffrey (Jeff) Wisoff, Principal Associate Director, NIF & Photon Science Directorate Lawrence Livermore National Laboratory

Graduate Students Seminars

In addition to the weekly presentations of the research update of the undergraduate and graduate students during the group meetings, the graduate students participated in the series of seminars organized by the center. This opportunity allowed the students to reach a wider audience

including all of the Center's faculties and students as well as university wide audience. The newly established seminar feedback rubrics grading system proven to be beneficial to the students in sharpening their communication skills and improving their overall presentations.

3.4 STUDENTS' ACHIEVEMENTS

Benjamin Osoba: an African American undergraduate student supported by this grant. He graduated with a Bachelor of Science, Electronics Engineering (minor Mathematics) in May 10, 2104. He was admitted to the M.S./Ph.D. program in the Department of Electrical Engineering and Computer Sciences at University of California Berkeley; he also received the Chancellor's Fellowship for Graduate Study and the GEM University Fellowship, prestigious awards which will both cover his costs for graduate studies and provide internship opportunities.

Mr. Benjamin Osoba, graduated with Bachelor of Science, Electronics Engineering (minor Mathematics) and supported by this grant.

Fellowships/Awards: 2014 Chancellor's Fellowship; 2014 GEM University Fellowship; 2014 Berkeley Excellence Award.

Franiece Bennett: an African American undergraduate student supported by this grant. She graduated with a Bachelor of Science, Electronics Engineering (minor Mathematics) in May 10, 2014. As a senior she received multiple job offers from Sandia National Labs, Ball Aerospace, and Booz Allen Hamilton. She has been accepted to numerous universities to further her education including: the University of Michigan-Ann Arbor, the University of Rochester, Queen Mary University-London, and King's College-London, and Middlesex University-London. In fall 2014, she accepted an offer of admission from the University of California, Berkeley and is currently a MS/PhD student in Electrical Engineering with a focus on Micro/Nano Electro Mechanical Systems.

Ms. Franiece Bennett graduated with Bachelor of Science, Electronics Engineering (minor Mathematics) and supported by this grant.

Fellowships/Awards: Graduate Assistance in Areas of National Need (GAANN) fellowship for the academic 2014-2015 year. This fellowship is funded by the U.S. Department of Education. GEM University Fellow, Awarded the NSF Fellowship, 2014.

More details about these two outstanding students can be found at this URL:

https://www.nsu.edu/cset/engineering/Events/class-of-2014

Calvin Nellum: an African American undergraduate student supported by this grant. He graduated with a Bachelor of Science, Physics in May 10, 2104. He was, recently, chosen as a Woodrow Wilson Michigan Teaching Fellow, a national fellows program that prepares science, technology, engineering and mathematics (STEM) graduates to teach in high-need secondary schools. The Michigan program is supported by the W.K. Kellogg Foundation and will allow Calvin to attend Wayne State University and participate in an intensive master's level education program.

Mr. Calvin Nellum, graduated with Bachelor of Science in physics and supported by this grant.

Calvin Nellum, native of Fairfax, Virginia, said that "NSU gave me the foundation to be able to apply for and be accepted into the program. My professors always believed in me. They were consistently telling us about attending graduate school and gave us research opportunities. I feel like NSU gave me the foundation to be prepared for this. I'm committed to teaching three years in a high-need school in Detroit. When you do what you love, it doesn't seem like a job. I'm really excited about getting in the classroom and hopefully changing kids' lives."

Kameron George: an African American undergraduate student supported by this grant. He dual majored in electronics engineering and mathematics. Graduated in May 2015 and received the 2nd place senior project final presentation award at NSU. He is a 4 years track and cross country athlete.

Javon Knox: an African American undergraduate student supported by this grant. Majored in physics and graduated Summa Cum Laude in May 2015. He is the recipient of the prestigious Dozoretz National Institute for Mathematics and Applied Sciences (DNIMAS) Scholar and Member of NSU Honor College. He was accepted for the graduate school at Florida State University, where his field of study is condensed matter physics.

Zachary Walls: an African American undergraduate student supported by this grant. Majored in electronics engineering and graduated in May 2015. Mr. Walls is the recipient of the following honors and scholarships:

- NSU Dean's List/Honor Roll
- Alpha Lambda Delta Honor Society
- Golden Key International Honor Society Science and Technology Honors Program for Retaining and Advancing Majors (STEAM) Scholarship
- Office of Civil Rights (OCR) Scholarship
- Honors College Scholarship

- British Aerospace (BAE) Systems FIRST Scholarship

Other students' achievements include the following:

- Christian Carvajal: Best Poster (First) at Local OSA Chapter, 2014
- Irving Cashwell: 3rd position at Local OSA Chapter, 2014

3.5 Students' Graduations

We supported 21 undergraduate students from STEM disciplines including physics, engineering and biology. Among them 5 females and 20 African Americans and 1 Asian students. During the period of the grant, 13 students graduated: 10 males and 3 females and all of them were African Americans. Among these graduated students about 84% will pursue a graduate degree, about 77% of them will intend to work for the Department of Defense, about 38% achieved a GPA equal or higher than 3.5/4.00, about 84% achieved a GPA equal or higher than 3.0/4.00, and about 46% of them will receive scholarship to further their studies in STEM fields.

We supported 10 graduate students, among which three graduated with M.S. degree in electronics engineering, Mr. Johnson Fujamade and Mr. Irving Cashwell, and one in Materials Science Mr. Casey Gonder. There were 6 male students and 4 females among them 8 African American and one Hispanic student.

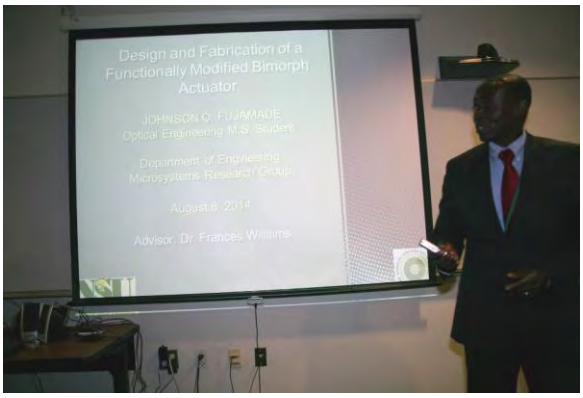

Mr. Johnson Fujamade defending his MS thesis, 8/14.

Mr. Irving Cashwell defending his MS thesis, 7/15.

Mr. Casey Gonder defending his MS thesis, 7/15.

3.6 FACULTY AWARDS AND RECOGNITIONS

The summary of the faculty awards and recognitions is as follows:

- Dr. Messaoud Bahoura:
  - Received the "Excellence Award for Outstanding Service in the Center for Materials Research", for the academic year 2013-2014, May 5th, 2014.
  - Received the "Excellence Award for Outstanding Service in the Engineering Department", for the academic year 2014-2015.
- Dr. Frances Williams:
  - Received the 2013 State Council of Higher Education for Virginia (SCHEV) Outstanding Faculty Award. The Outstanding Faculty Award is the Commonwealth's highest honor for faculty at Virginia's public and private colleges and universities and recognizes superior accomplishments in teaching, research and public service. Dr. Williams is one of 12 recognized statewide.
- Dr. Aswini Pradhan:
  - Received the 2015 State Council of Higher Education for Virginia (SCHEV) Outstanding Faculty Award.
  - Was elected as editorial board for Nature Journals, 2015.

3.7 OUTREACH EFFORTS

The education and outreach activities in STEM areas for underrepresented minorities are an integral part of our efforts. Outreach activities aimed to:

- Raise awareness of the importance of STEM education from early ages and for a diverse population.
- Encourage under-represented populations, including women and minorities, to pursue STEM careers.
- Build a strong STEM pool of talents at different levels that would benefit the nation as a whole.

Through multiple and focused outreach activities, including hands on activities and summer

research experience, we raised awareness of the importance of STEM education from early ages and for a diverse population. These efforts aim to educate, inspire and engage K-12 students and encourage under-represented populations, including women and minorities, to pursue STEM education and be the next generation of scientists and engineers. This will build a strong STEM pool of talents at different levels and will help in maintaining a diverse pipeline of U.S. citizens who are interested in participating in DoD programs and STEM careers.

Our outreach and educational activities were numerous and proven to be successful. We reached populations from K-undergraduates and within the grant duration we reached more than 6,000 individuals, including many women and underrepresented minority students in the Hampton roads area. Dr. Bahoura, with the assistance of undergraduate and graduate students led these efforts organized and hosted several educational and outreach activities for the graduate, undergraduate and K-12 students in STEM areas.

The table below summarizes these activities and details are given in sections below.

Date	Event	Activities	Attendance	Location
April 7th, 2012	2012 NanoDays	Nanotechnology Hands on activities	>500	Children's Museum of Virginia
April 28-May 10th, 2012	STM 101 Course	Developed and delivered a Nanotechnology Module hands on activities	>50	Virginia Beach Higher education Center
May 30 to July 20, 2012	Undergraduate Summer Research	Research on Project tasks	22	CMR, NSU
June 25 to July 20, 2012	High School Summer Research	Phys-Chem- Bio Hands on activities	22	CMR, NSU
June 25-28th, 2012 and August 13-17th, 2012	Nano Summer Camps	Nanotechnology Hands on activities	8+9=17 (5th graders)	Children's Museum of Virginia
September 29, 2012	Science is Alive Day	Nanotechnology activities and demonstrations	300 girl scouts	NSU
October 6, 2012	Cooperating Hampton Roads Organizations for Minorities in Engineering (CHROME)	Hands on experiments to engage students in STEM	20 Elementary, Middle and High school teachers	NSU
March 28th, 2013.	Annual S.T.E.M. Career Fair	Display and exhibit of nanotechnology hands on experiments	More than 200 K-5 students	Compostella Elementary, School of Science, Technology, Engineering & Math
April 6th, 2013	2013 NanoDays	Nanotechnology Hands on activities	1,200	Children's Museum of Virginia

May 11, 2013	NSU-STEP STEM Day	Introduction to Nanotechnology experiments	50	NSU
May 29-July 19, 2013	Summer 2013 Undergraduate Summer Research	Research on Project tasks	16	CMR/ NSU
June 14th- 28th, 2013	Health and Science Summer Academy 2013: "Summer of Inquiry"	Hands on activities with quizzes: High School Students from Hampton Roads area	34	NSU Campus
June 17-19, 2013	"Gear up for college", Gear up summer academy 2013"	nanotechnology hands on experiments: high school students from Phoebus and Hampton high schools	100	June 17-19, 2013
June 24 to July 19, 2013	High School Summer Research	Building and characterizing dye sensitized solar cells	23	CMR/NSU
July 31st, 2013	STEM activity "Urban Youth Summer Academy"	"Exploring Nanotechnology"	55 rising 6th graders	NSU Campus
October 19th, Nov. 9th, 23rd 2013 and May 3rd 2014	CSET Saturday Scientists	"Exploring the Nanoworld"	20 HS students	NSU
January 25th, 2014	FTC Eastern Virginia Qualifier, FIRST Tech Challenge (FTC) (organized by Dr. Mead)	Robotic competition: High School and Middle School robotics teams from across Virginia	Few hundreds	Joseph G. Echols Hall, NSU

April 5th, 2014	2014 NanoDays	Nanotechnology Hands on activities	>500	Children's Museum of Virginia
April 11th, 2014	the Campostella Elementary School STEM Career fair	Hands on activities for elementary school students	> 100	Campostella Elementary School, Norfolk
June 23-July 18, 2014	High School Summer Research	Building a Macro Atomic Force Microscope and testing, taking scans and analyzing results	22	CMR/NSU
June 8th- June 10th, 2014	Health and Science Summer Academy 2014	Experimental hands on activities	27	NSU
July 15, 2014	The Amazing World of Science	Nanotechnology hands on experiments	200	Hampton Roads Convention Center, Hampton, VA
September 27, 2014	2014 Science is Alive Day	Nanotechnology activities and demonstrations	70	NSU
October 2, 2014	"Bite of Science Program" for Hampton Roads area high school science teachers sponsored by the Center for Excellence in Education (CEE), Virginia Space Grant Consortium, and the College of Science, Engineering, and Technology.	"Nanotechnology for high school teachers" Seminar with hands on activities. Teacher enrichment program, with presentations focusing on educational approaches and methods in the science classroom that are creative and unique	35	NSU

October 6, 2014	Recruiting and outreach at King's Fork High School	Presentation of Engineering and STEM activities at NSU	>100	Suffolk
November 12, 2014	Richmond Public Schools (RPS) Governor's Career and Technical Education (CTE) Academy for Science, Technology, Engineering, and Mathematics (STEM) in Richmond	Presented nanotechnology and physics hands activities	>20	NSU
November 15, 2014	FirstView	Presented overview of the engineering program to protective NSU students and their parents	15	NSU
March 18, 2015	Engineering Department Open house	Presented nanotechnology and physics hands activities	>10	NSU
March 31st, 2015	Grassfield High School Visit	Presented Hands on activities of physics and nanotechnology	35	NSU
March 16-April 16, 2015	STM 101 Course to 8 Virginia Beach public Schools	Taught the Nanotechnology Module	31	Virginia Higher Education Center
April 2nd, 2015	The annual Career Day Fair at Ruffner Middle School.	"Nanotechnology is Fun" set of engaging hands on activities	>800	Ruffner Middle School, Norfolk

April 5, 2015	2015 NanoDays outreach event	Presented more than 40 hands on activities, nearly 60 volunteers to visitors: 2 y.o.-adults	>500	Children's Museum of Virginia, Portsmouth
May 1, 2015	Campostella Elementary School Career Fair	Presented nanotechnology and physics hands activities	>575	Campostella Elementary School, Norfolk
May 16, 2015	STEM Symposium	Nanotechnology and Physics hands on experiments	>30	Performance Arts and Teen Center, Hampton, VA
June 5, 2015	Career Fair at John Tyler Elementary (Portsmouth)	Physics hands on experiments	>150	John Tyler Elementary School, Portsmouth, VA
Total audience reached				>6,000 individuals

Undergraduate Summer Research

We run a successful undergraduate summer research each year where we hosted couple dozen of students coming from different universities. The majority of these students are underrepresented minorities, including females and African Americans.

The duration of the program is 8 weeks during which the student will receive safety training and laboratory guidelines and protocols. After passing the safety training the student will be cleared to work in the designated laboratory of her/his choice with graduate students and co-principal investigators. The student is required to present weekly research progress report and bimonthly presentation to the research group where he/she will receive feedback on the research and the quality of the presentation. During the summer research experience the student receives a competitive stipend of $3,500 (from another grant) to cover meals and transportation costs.

The 21 undergraduate summer research students of 2014 came from the University of Virginia, Virginia Commonwealth University, George Mason, Virginia Tech, Elizabeth City State University, University of Pittsburg, and Coastal Carolina. Among them there were 7 females and 14 males, and 14 of them were minorities.

Undergraduate students working on the synthesis and characterization of nanomaterials.

Undergraduate student working in the cleanroom.

Summer Research Undergraduate Presentations

Undergraduate students presenting their research progress during the bimonthly meeting, 2013.

Second group of undergraduate students presenting their research progress during the bimonthly meeting, 2013.

In 2014, the undergraduate summer research students presented their research at the Washington Baltimore Hampton Roads-Louis Stokes Alliance for Minority Participation (WBHR-LSAMP) 13th Annual Undergraduate Research Symposium, Tuesday July 15, 2014 at Hampton University. The WBHR-LSAMP symposium theme is "Empowering the 21st Century STEM Professional Through Undergraduate Research."

The Washington Baltimore Hampton Roads-Louis Stokes Alliance for Minority Participation (WBHR-LSAMP) is committed to the goals set by the National Science Foundation, that is, to increase the number of underrepresented minorities who receive bachelor degrees in science, technology, engineering, and mathematics (STEM) fields and to encourage students to pursue graduate degrees. To achieve this goal WBHR-LSAMP has developed strategies to emphasize and facilitate recruitment, retention, and tutoring throughout the undergraduate STEM programs.

The program members include: Howard University as the lead institution with Bowie State University, the University of the District of Columbia, Hampton University, Morgan State University, Norfolk State University and Virginia State University as partners.

WBHR-LSAMP symposium participants, 2014.

Summer Research Closing Ceremony

Our summer research undergraduate students and high school students participated in the summer research closing ceremony under Science and Technology Academicians on the Road to Success (STARS) Program. This catered ceremony included all undergraduate and high school students' summer research experience participants. The ceremony schedule included greetings by Dean or Associate Dean Michael Keeve (Associate Dean), opening remarks by a faculty, and reflections from high school program, undergraduate student reflection, reflective /moment presentation by Dr. Bahoura and closing remarks STARS director. Each participating student received a certificate of participation in the program.

Undergraduate students summer research experience participants their certificate of participation from Dr. Pradhan and Dr. Bahoura.

Group picture of all undergraduate students participating in the 2013summer research program at NSU.

Group picture of the 2014 STARS Summer Research Experience for undergraduate Students after the closing ceremony.

High School Summer Research

One of our major education and outreach efforts, is to reach to high school students and introduce to STEM fields through a thoughtful and well organized summer research opportunity on our campus. The majority of the applied students were female and minorities.

Program Goals:

- Broaden the student's experimental experience.
- Develop critical thinking through reasoning, inquiring, and problem solving.
- Gain independence and confidence in performing lab work.
- Work in a team environment.
- Learn by doing.

These goals will be accomplished by teaching students how to:

- Perform lab work in a safe and organized manner.
- Keep a legible and accurate description of procedure, observations, and results in a lab note book.
- Manage time efficiently in lab.
- Maintain a positive attitude toward lab work.
- Be ethically and effectively prepared for college and research.

2012 High school summer research program participants.

2013 High school summer research program participants.

2014 High school summer research program participants.

In 2012, we supported 22 High School (HS) students from as far as Texas for a 5 week summer research experience this year. There were 11 females, 11 males, including 14 minorities (African American and Hispanics), three admitted to college: Virginia Tech, VCU, and University of Pittsburgh.

For 2013, we supported 23 HS students from 17 local high schools in the Hampton Roads area. There were 12 females, 11 males, including 20 minorities (African American and Hispanics), one of the student were admitted to the marine biology program at UNC. And for the 2014 program, we admitted 22 HS students from 17 local high schools in the Hampton Roads area and one from Petersburg, VA. Among them 13 females, 9 males and 17 minorities including African American and Asians.

The table below summarizes the statistics of participants.

Year	*Female*	*Male*	*Minorities*	*Total*
2012	*11*	*11*	*14*	***22***
2013	*12*	*11*	*20*	***23***
2014	*13*	*9*	*17*	***22***

The duration of the summer research program is 5 weeks and the students received a stipend of $1,500 (from another grant) upon completion of the program. The students were mentored by Dr. Bahoura with the assistance for graduate and undergraduate students. Laboratory Safety Training were provide by the Center's safety officer and students must pass a safety quiz to be allowed to work in laboratories.

Hands on Experiments and Programs

In the 2012 program, the students were introduced to different areas of physics, chemistry, biology, and electronics. The students worked in groups on different topics and took measurements. They were trained on how to take measurements, how to read measurement, how to report data in a lab notebook and how to present the results to the public.

The list of the activities is as follows:

- Investigating the mpemba effect.
- From dull to dazzling.
- Electrolyte challenge.
- How much sugar is in that soda?
- Forensic science.
- Crime scene chemistry.
- Understanding lactose intolerance.
- Develop your own soda pop recipe.
- Build your own crystal radio.
- Build a photo receptor.
- Build an electric field detector.
- Build a simple motor.

2012 HS summer Research: High school students carrying out hands on experiments: taking measurements and taking notes using lab notebooks.

Dr. Bahoura delivering an interactive lecture about responsible conduct of research and ethics to the high school summer research students.

2012 HS summer Research: High school students presenting their research at the Science and Technology Academicians on the Road to Success (STARS) Research Symposium at NSU.

The 2013 HS summer research topic was building a Dye Sensitized Solar Cell and compare its performance to a Silicon solar cell. The students' learning outcome for this activity is that the students will be able to:

- Explain how a dye-sensitized solar cell (DSSC) works.
- Prepare a DSSC using crushed blackberries and raspberries, to serve as the source of sensitizer molecules.
- Take absorption data of the dyes used.
- Explain why sensitizer molecules are required for successful operation of the DSSC.
- Explain why high surface area TiO_2 is vital to the successful operation of the DSSC.
- Explain why I^-/I_3^- electrolyte is needed.
- Graph IV and PV curve.
- Estimate efficiency of the solar cell they built.

Nanotechnology Hands on Activities

Dr. Bahoura presenting nanotechnology lectures and hands on demonstration and experiments. Students answering nanotechnology quizzes.

High school students building their experiments: from top left: super-sensitive electric field detector; light Bulb; low-power AM radio transmitter and homemade turbidity meter.

High school students presenting their literature search about solar cells during the second week of the program.

Leaning Basic Electronic Circuitry


High school students learning about resistance, current and voltage and how to make electrical measurement using digital millimeters.



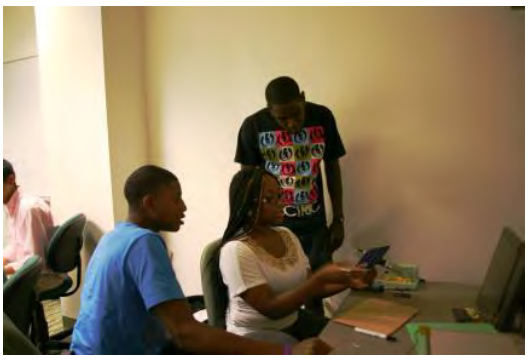


Graduate student explaining the principles of solar cells to the high school students. High school students learning how to solder the busbar interconnects of the solar cell.

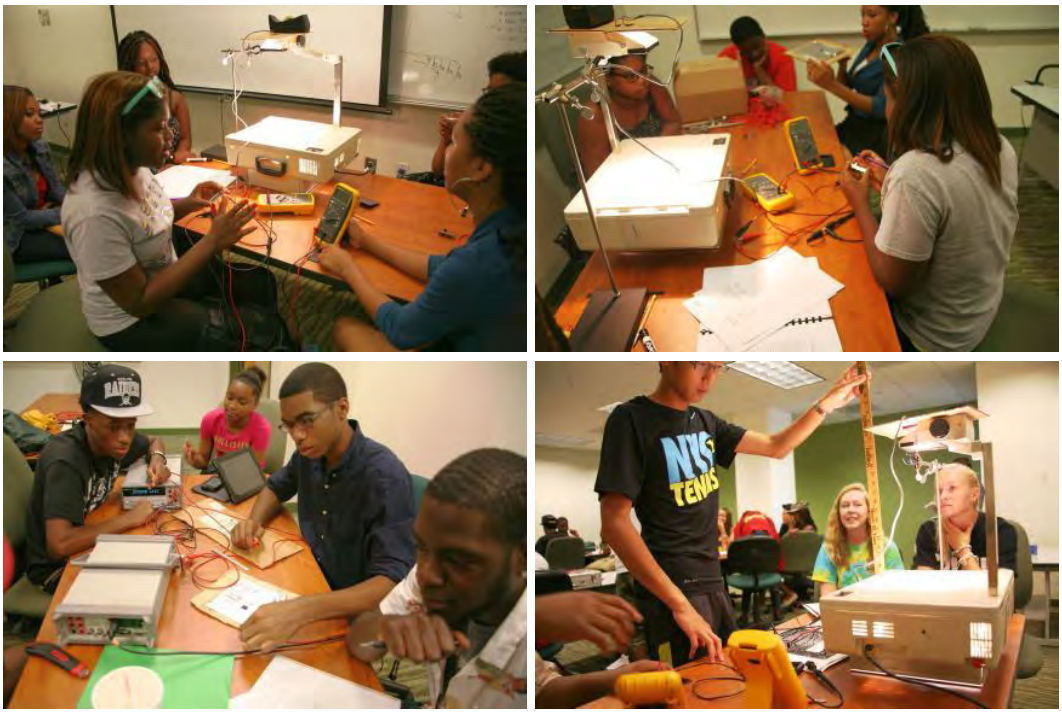

High school students setting up their silicon solar cell electrical characterization.

High school students taking absorption spectra of their dye using UV-VIS photo spectrometer.

High school students building the dye sensitized solar cells in the chemistry laboratory while supervised by Dr. Bahoura.

Testing the Built Solar Cell using Ambient Light and a Projector Light

High school students measuring the electrical output characteristics for the dye sensitized solar cells they built.

2013 Poster Session and Closing Ceremony

On July 18th, 2013, our summer research undergraduate students and high school students participated in the summer research closing ceremony under Science and Technology Academicians on the Road to Success (STARS) Program. The high school students presented their posters to the public on the main campus. NSU graduate, undergraduate and faculty attended the poster session and asked the students questions about their work and experience. Dr. Akhlesh Lakhtakia, professor of Engineering Science and Mechanics at the Pennsylvania State University, was invited to judge the high school students posters and to give the high school students the certificates of participation at the summer research closing ceremony.

HS students presenting their poster to the public. Faculty and students' families were present.

High school students receiving their certificate of participation from Dr. Akhlesh Lakhtakia

The 2014 HS summer research experience we have chosen Building "Macro" Atomic Force Microscopy as a project for the HS students. We adapted the activity "Building "Macro" Atomic Force Microscopy For High School Classrooms by Paul Fedoroff and Tom Pittman (Burnt Hills-Ballston Lake High School, Burnt Hills, NY 12027) and Chang Y. Ryu and Linda Schadler

(Nanoscale Science and Engineering Center Rensselaer Polytechnic Institute, Troy, NY 12180).

This activity was chosen because it related to nanotechnology and to materials research. The high school students were split, randomly, into three groups of 7-8 students each. The students were provided with all the needed parts and step-by-step instructions how to build a Macro-Atomic Force Microscopy. The students were introduced to three modes of the Atomic Force Microscope (AFM).

Building "Macro" Atomic Force Microscopy Learning Outcomes:

- Upon utilizing the Contact-mode "Macro-AFM", the high school students will enhance their understanding on bending, forces and light reflection.
- Upon utilizing the Tapping "Macro-AFM", the high school students will enhance their understanding on resonance, standing waves, simple harmonic motion, and light reflection.
- Upon utilizing the Magnetic "Macro-AFM", the high school students will enhance their understanding on magnetic forces and fields and light reflection.
- Upon building the Macro-AFM, the high students will strengthen their skills in using technical tools and building an integrated technological apparatus.

Assembling and constructing the AFM

The high school using electrical power tools to drill holes or to screw screws in woods to assemble their AFM setup.

Understanding and measuring the resonance frequency of the system

In class explanation of waves and resonance frequency. High school students finding the resonant frequency for their AFM setup in tapping mode.

Lecture on professional ethics and responsible research conduct

Dr. Skuza (CMR) presenting a talk to the high school students about professional ethics and responsible research conduct followed by a quiz.

High school students taking measurements and scanning different objects using the three modes of the AFM.

High school students taking quizzes.

High school students presenting their literature search about how the Atomic Force Microscope works and how it is used to scan objects.

Dr. Haines (Biology Department) gave a presentation to the high school students about how to present their results in an oral communication or poster setting. Students taking a quiz about what they just have learned.

High school student being trained on Vecco Atomic Force Microscope by graduate student Mundle. The students took real scans at the micro and nano levels for few objects that they included in their posters.

High school students' experimental results using the Macro Atomic Force Microscopy system they built

	Contact mode		Tapping Mode		Magnetic Mode	
Group A						
Group B						
Group C		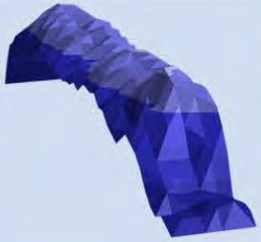		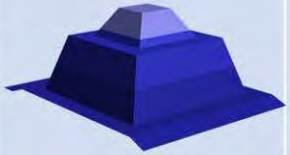	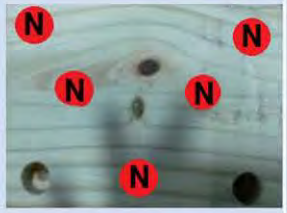	

High school students' experimental results using a Vecco Atomic Force Microscope

	Object	AFM Scan
Group A	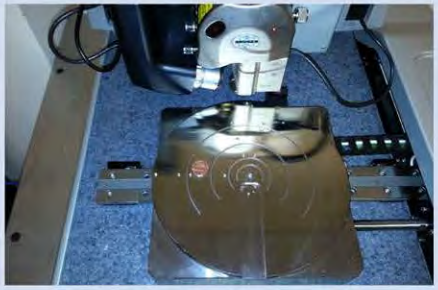	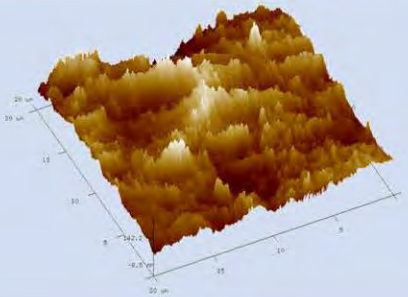
Group B		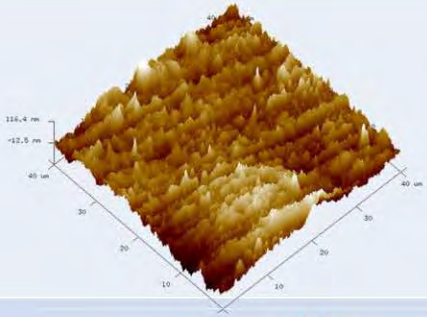
Group C	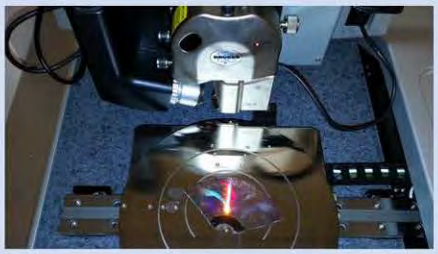	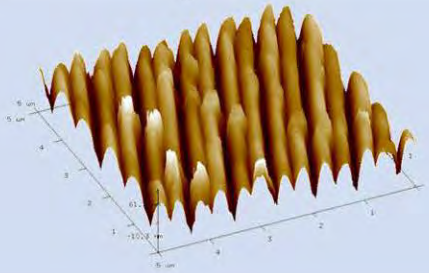

Summer Research Poster Session and Closing Ceremony

The summer research experience closing ceremony was held on July 18th, 2014 at the NSU's Student Center. This ceremony included all undergraduate and high school students' summer research experience participants under Science and Technology Academicians on the Road to Success (STARS) Program.

The high school students presented their posters to the public on the main campus. NSU graduate, undergraduate and faculty attended the poster session and asked the students questions about their work and experience.

High school students presenting their posters to the public. Faculty and students' families were present.

NanoDays Outreach Event

NanoDays is a nationwide outreach event, created by the Nanoscale Informal Science Education Network (NISE) with support from an NSF grant. In 2008, Dr. Bahoura initiated a partnership between NSU, Children's Museum of Virginia (CMV), Portsmouth, VA and NISE to disseminate informal science education through outreach events year along using the resources provided by NISE. Since 2008, Dr. Bahoura has been organizing the Nanodays outreach event at the CMV. The aim of NanoDays is increases public awareness, engagement and understanding of the nanoscale, engineering and technology, informs the public about scientific advancements, and shares the passion of science with the community. NanoDays activities bring university researchers together with science museum educators, creating unique learning experiences. NanoDays engages people of all ages in a miniscule world where materials have special properties and new technologies have remarkable promise.

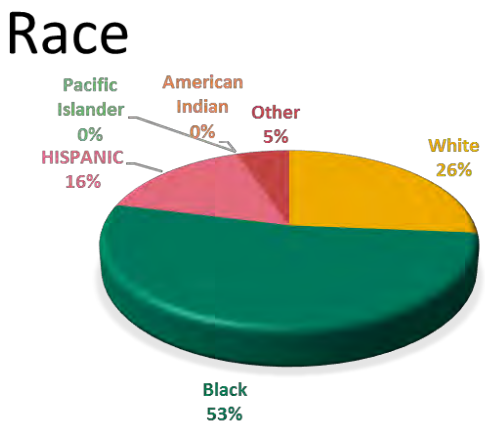

The Nanodays outreach event brought undergraduate and graduate students, faculty, staff, educators, and volunteering from different departments at NSU, Old Dominion University, College of Williams, and Jefferson Laboratory to bring these exciting hands on activities to the Children Museum year after year. In 2015, the number of volunteers was nearly 60. We used NanoDays kits, courtesy of the NISE network and the hands on activities were complemented by informative posters throughout the museum. As incentive to participate in all activities, we developed a short scavenger hunt in which visitors must visit certain stations to participate in the experiments, learn the answers, and then could submit their completed hunt for a prize. The prizes included NanoDays T-shirts (paid from another grant), maze pens, and tattoos as prizes for successful answers to the scavenger hunt. Booklets of "Nanotechnology Big Things from a tiny

world" and "Nanotechnology and Energy-Powerful things from a tiny world" courtesy of the National Nanotechnology Coordination Office (NNCO) were given to visitors as an introduction to Nanotechnology.

Audience: From 2012-2015 we reached more than 2,700 visitors, ages 5 to grandparents. Special care was dedicated to about a dozen of visitors with mental or physical disability. This included instructing volunteers to allow these visitors extra time to interact with the activities, to be patient and accommodating and to address their special needs. The Children's Museum of Virginia (CMV) is the largest children's museum in Virginia and serves the metropolitan area of Hampton Roads. The CMV strategic location in Portsmouth allowed reaching out to a diverse and multicultural audience, notably underserved students from Portsmouth are African American, of low socio-economic status. On average, about have of the visitors are age 7-22.

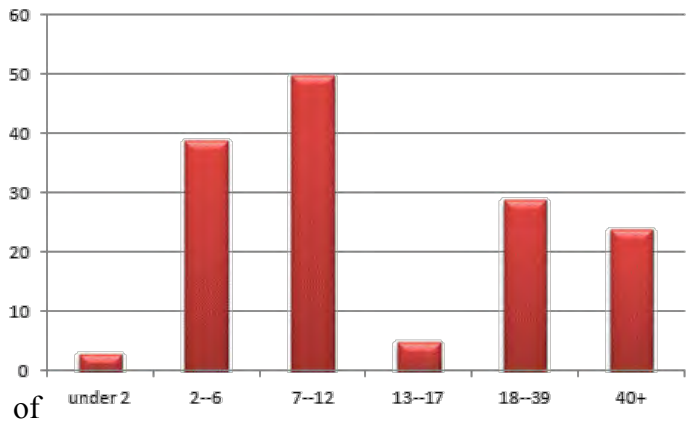

The snapshot view of the 2015 Nanodays outreach event is shown below.

Audience	Activities	Volunteers	Giveaway	Duration	Budget
• More than 500 visitors.	• 40 Hands-on Nanotechnology activities	• About 60 undergrad and grad students (from the CMR, Engineering, Physics, and Chemistry). • 3 faculty from NSU , 1 f from ODU • 3 Staff members from W&M • Over 10 educators from the Museum.	• NanoDays T-shirts • Maze Pens and Buckyballs • "Nanotechnology Big Things from a tiny world" booklets	• Half day.	• $1,100 (t-shirts)

Hands on Activities

The hands on activities included the main ideas about how nanotechnoloy scale is different from the macro scale using simple to undertsand experiments. The table below shows the covered activities.

Activity Type	Activity	Activity Type	Activity
Exploring Size	• Moving Molecules • Scented Balloons • Ball Sorter • Powers of Ten • Measure Yourself	**Exploring Properties**	• Invisibility • Capillary Action • UV Bracelets • Electric Squeeze
Exploring Materials	• Graphene • Ferrofluids • Oobleck • Memory Metal • Hydrogel • NanoGold • Nanosand	**Exploring Tools**	• SEM-Special Microscopes • Mystery Box • Mitten Challenge • 3D tools
Exploring Products	• Computer Hard Drives • NanoFabric • Sunblock • Liquid Crystal Displays	**Exploring Forces**	• Static Electricity • Gravity and Cups
Exploring Structures	• Morph Butterfly wing	**Exploring Fabrication**	• Electroplating • 3D printing
Nano-Game	• I spy Nano!	**Fun Chemistry**	• Chemistry nano experiment
Neuroscience	• Neural probes	**Exploring Nano & Society**	• You Decide! • Would You Buy That? • Space Elevator

The 2015 NanoDays audience pictures are shown below:


Diverse audience


Children doing experiments!
Explorando materiales: metal con memoria
Exploring Materials— Memory Metal


Children doing experiments!


The young ones having a blast!


Having a lot of fun!


Engaging volunteers!


One of the room at the Museum
William and Mary 3D printer


Families at the Museum


Dress like a NanoScientist!
Ultimate Prize: Nanodays T-shirt!
NanoDays

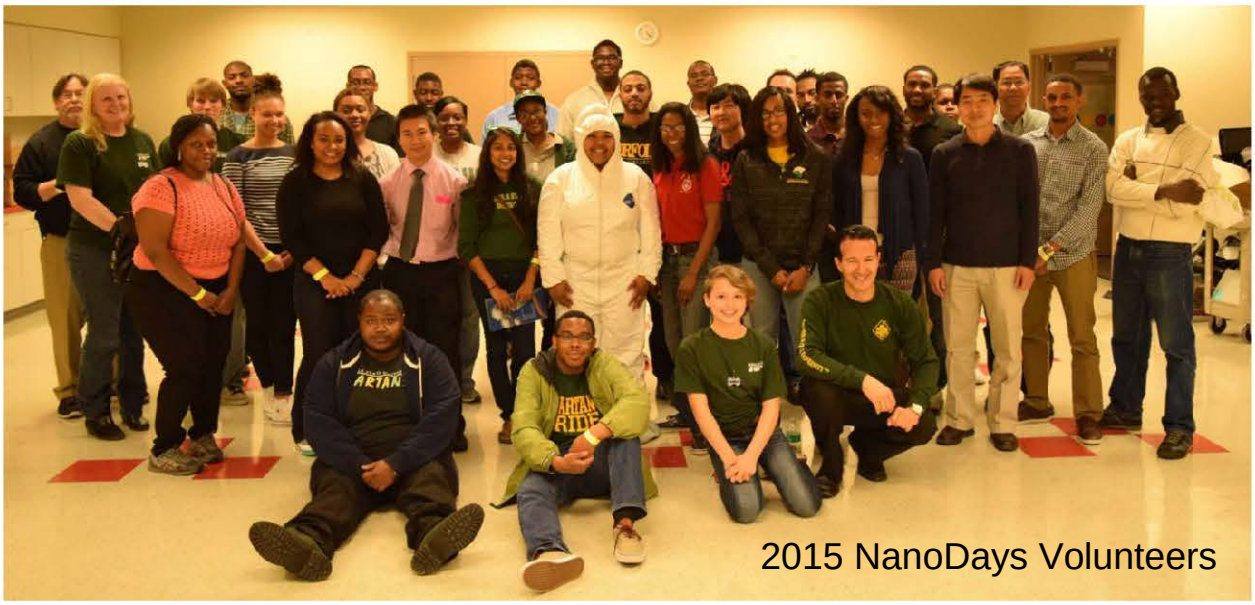
2015 NanoDays Volunteers

Public Feedback

The visitors, children, parents, and grandparents, enjoyed this annual outreach event. Many of them requested us to visit their schools and present such activities during the year. The parents found the volunteers engaging, the topics age-appropriate the commended us for such a successful event. We received an overwhelming support from children, parents and educators for this event.

Summative Evaluation-Likert Scale of the event: Most of the visitors completed an evaluation forms about the event each year. As an example, the survey results are shown below:

The analysis of our NanoDays surveys, averaged over the number of participants are shown below:

Strongly agree:4;	Agree: 3;	Disagree: 2;	Strongly disagree: 1

Administrative / Logistics	Average Score
The topics were interesting to me	3.9
Presenters and Content	**Average Score**
The presenters provided useful information about the topics	3.8
The presenters were engaging	3.6
I understood the concepts presented	3.2
Course Design	**Average Score**
The presentations were about the right length	3.7
The logistics for this event (registration, parking, finding the room, etc.) went smoothly	3.6
The setting for this event was comfortable	3.9
I enjoyed this event	3.4
Perceived Impact	**Average Score**
I would recommend future events like this to my friends and colleagues.	3.8

Each year, parents and visitors express their gratitude the outstanding work our volunteer do to make the NanoDays event fun, interactive and stimulating. Please find below a letter send by one of the parent (Rear Admiral, Denny Moynihan) to the President of our institution about NanoDays:

WASHINGTON, DC 20350-1200
dennis.moynihan@navy.mil

Dennis Moynihan
7834 Greeley Blvd.• Springfield, VA 22152
Phone: 757-560-0227• E-Mail: dirniswl@me.com

OFFICE OF THE PRESIDENT
RECEIVED
2012 APR 16 PM 1:12

11 April 2012

Dr. Tony Atwater
Office of the President
Norfolk State University
700 Park Avenue Unit 2568
Norfolk, VA 23504

Dear President Atwater:

This past weekend my wife and I visited Norfolk for a quick spring break vacation. Our children are ages seven and nine, so much of our time was spent visiting places that would appeal to them.

One of visits was to the Portsmouth Children's Museum on Saturday. It happened to be Nano Day, a series of displays and experiments on nanotechnology conducted by graduate students from your university.

To make a long story short, your students were incredible ambassadors for your institution. They were engaging, professional, and easily connected with kids. They were also very proud to be part of the Norfolk State family. At the end of our four-day visit my kids said Nano Day was the highlight of our visit to Hampton Roads.

Kudos to you and your team for creating a positive environment that produced the engaging students who represented Norfolk State University at the Portsmouth Children's Museum last weekend. My family and I are all the better for meeting your students.

Sincerely,

Denny Moynihan

DENNIS J. MOYNIHAN
REAR ADMIRAL, U.S. NAVY
CHIEF OF INFORMATION

1200 NAVY PENTAGON
ROOM 4B453
WASHINGTON, DC 20350-1200
E-MAIL: dennis.moynihan@navy.mil

TEL: (703) 697-7391
DSN: 227-7391
CELL: (703) 407-3765
FAX: (703) 697-8921

Visitors expressed their appreciation, support and positive feedback at the end of the event. Below are some visitors' comments for the 2014 event:

What did you like most about these presentations?

- I love how patient the guys were
- The kids got to do all the hands on activities
- Learned a lot
- The helpers were very engaged
- The education
- Engaging and informational for my 6 ½ yr 1st grader
- The enthusiasm of the presenters and how they broke down the meanings
- Staff
- Everything/ ex: nano hydrogel
- Good amount of topics
- The experiments
- *I loved that the presenters provided age appropriate exhibits. They talked directly to the kids and showed real concern for their answers. I loved the great interaction and all of the participants were friendly, energetic, and knowledgeable.*
- The interactive activities
- I liked the creation of a hydrogel
- *Demonstrations presenters answered questions for the kids and were very engaged with them.*

What should we change if we hold similar events in the future?

- Nothing, all was great
- More exhibitions
- Great presentation
- Nothing, great
- Advertise! We happened to come to museum, but were so glad we came today!
- Better demos
- Nothing xxx
- Have the presenters talk more to the age of the audience
- Maybe a coloring book to take home to share with friends. Seriously, the staff did a wonderful job and I have no complaints.

Please share any additional comments

- I was very impressed!
- From a 4th grade teacher's viewpoint, this was excellent! My grandkids were too young for some concepts but excellent for older kids!
- Great. Would like something like this more in the future
- I absolutely enjoyed
- The event was marketed and carried out wonderfully. Thank you NSU for making learning fun. We had a wonderful time. We hope to see you again.

Great job!

Development and Delivery of a STEM course to 8 Public High Schools of Virginia Beach

The Virginia Beach City Public Schools (VBCPS) received a federally funded grant from Opportunity Inc. to provide after-school Science, Technology, Engineering, and Math (STEM) programs for the fourth year in a row.

Students from the VBCPS have the opportunity to participate in the STEM After-School Program which will enhance their knowledge, education, experience, and career options in the STEM field. The STEM After-School Program consists of 2 options in which a student may participate in one or both.

- ***STEM Robotics Club (SRC):*** Student will work with a team to construct a robot in which he/she will compete at the annual STEM Robotics Competition in June. If selected and eligible for the program, your child will receive a $700.00 stipend for his/her participation. Stipend is based upon their active attendance.
- ***STEM 101 Course:*** Student will digitally interact with professors from Norfolk State University in a spring semester course that will introduce students to fields such as Computer Science, Electrical Engineering, Nano-Technology, and more. Upon successful completion, student will receive a 3-hour transferrable elective college credit.
- ***Entrepreneurial Saturdays:*** One Saturday a month, students will have the opportunity to prepare for their futures both professionally and financially through exciting entrepreneurial activities.

STEM 101 Course

- Student digitally interact with professors from Norfolk State University in a Spring semester
- Introduction to fields such as Computer Science, Electrical Engineering, Nano-Technology, and more.
- Upon successful completion, student will receive a 3-hour transferrable elective college credit.

- This course, in which VBPCS is funding students' tuition, will be taught via distance learning at each school's home site on Mondays/Wednesdays beginning **January 28, 2015**.
- Students will receive an iPad to *borrow* for the entire semester and receive a $250.00 stipend at the end of the course. *Stipend based upon active attendance*

STEM After-School Programs Performance Evaluation

- Student will master 90% of the SRC and/or STEM 101 course competencies.
- Student will maintain 90% attendance rate at the SRC and/or STEM 101 sessions (*Stipends for SRC and grades for STEM 101 are based upon attendance and active involvement*).
- Student will maintain good behavior.
- Student must obey and follow guidelines of VBCPS Student Code of Conduct. If student is found in violation of Student Code of Conduct, student will be dismissed from the STEM After-School Program and could face repercussions at his/her respective high school.

Norfolk State University, each year, offered 8 hands on module for the STEM 101 course, including: nanotechnology, computer science, physics, chemistry I and II, technology, mathematics and biology. Dr. Bahoura developed and delivered a Nanotechnology Module hands on activities for STEM 101 to 8 Virginia Beach Public High schools serving more than 50 students each year. The course was delivered, simultaneously, to the 8 high schools from one location using real time teleconferencing tools. The students of one of the high schools were present at central the location where the professor gave the lectures and the demonstrations. ***To our knowledge, this is the first STEM course in its kind in the U.S.***

The nanotechnology module does not require any previous knowledge of the field of nanotechnology and therefore was open to students from all backgrounds. The module is hands-on; application based and it gives a broad overview to nanoscience/nanotechnology as a field with many career opportunities. The students were able to gain a comprehensive understanding about nanotechnology through activities that introduce them to the unique properties at the nanoscale. The module included video demonstrations and interactive media. The students were exposed to the interdisciplinary aspect of Nanotechnology/Nanoscience with other disciplines. In addition, the module included discussion groups on societal and ethical implications of nanoscience/nanotechnology.

STEM 101 Course: Nanotechnology Module

Topics:

- Introduction to Nanoscience and Scale of Objects.
- Unique Properties at the Nanoscale
- Tools of Nanotechnology
- Applications of Nanotechnology

Pedagogy:

- The objective is to spark student's interest in nanoscience, introduce them to common terminology, and get them to start thinking about issues of size and scale.
- Students participated in learning activities that are designed to help them to establish an understanding of the nature of nanoscale science, the relative size of objects, unique properties of nanosized particles, and applications of nanoscience.
- Students were introduced to two of the most widely used new probe imaging tools.
- This lesson introduced students to applications of nanoscience, explores how nanoscale science and engineering could improve our lives, and described some potential risks of nanotechnology.

Assessment:

- Students are assessed through graded quizzes and homework after each session.

STEM 101 Nanotechnology module lectures and hands on activities delivered by Dr. Bahoura, 2012.

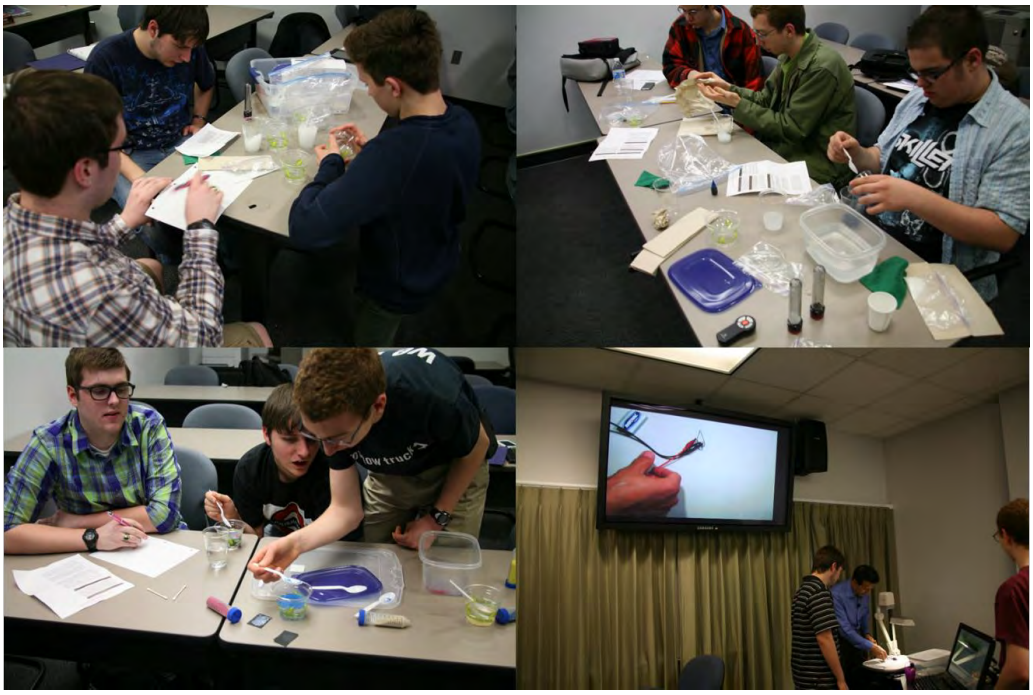

2015 STEM 101 Nanotechnology course: students carrying out experiments.

STM 101 closing ceremony. Parents and students were invited. Testimonies of students and educators. Awards and certificate ceremony, 2012.

FIRST Tech Challenge (FTC) Eastern Virginia Qualifier

In addition, our students and faculty served as volunteers for the annual FIRST Tech Challenge (FTC) Robotics Tournament, held early this year at Norfolk State University each year. FIRST (For Inspiration and Recognition of Science and Technology) is a world-wide effort that impacts more than 200,000 students. Participants are ideal candidates for STEM careers, and the rate of STEM matriculation is about three times that of the general population. The FTC tourney was held in collaboration with VirginiaFIRST, BAE Systems, and Booz-Allen-Hamilton. The tournament featured several high school robotics teams, over 200 students plus parents and teachers, from across the Commonwealth of Virginia.

FIRST Tech Challenge (FTC) is designed for students who want to compete head to head, using a sports model. Teams of up to 10 students are responsible for designing, building, and programming their own robots to compete in an alliance format against other teams. Teams, including coaches, mentors and volunteers, are required to develop strategy and build robots based on sound engineering principles. Awards are given for the competition as for well as for community outreach, design, and other real-world accomplishments.

This event is free and open to the public. High School and Middle School robotics teams from across Virginia compete to win a place at the FTC State Championship in March.

Students get to:

- Design, build, and program robots.
- Apply real-world math and science concepts.
- Develop problem-solving, organizational, and team-building skills.
- Compete and cooperate in alliances and tournaments.
- Earn a place in the State, Eastern Super Regional, and World Championships.
- Qualify for nearly $19 million in college scholarships.

Our undergraduate and graduate students and faculty served as volunteers and referees for the annual FIRST Tech Challenge (FTC) Robotics Tournament, held in January at Joseph G. Echols Hall, Norfolk State University. The FTC tourney is organized by Dr. Mead (Engineering Department) in collaboration with VirginiaFIRST, BAE Systems, and Booz-Allen-Hamilton.

In 2014, the tournament featured 45 high school teams from across the state. There were about 400 mostly high school students, and about 25 middle school students.

Norfolk State University's official addressing the attendees: from the top left: Dr. Moore (NSU Interim President), Dr. DeLoatch (Provost), Dr. Mattix (Interim Dean), Dr. Mead (Professor and Event Coordinator).

Few of the several high school students' teams in the competition. Each robot has several tasks to perform in a set time.


Many of the volunteers and referees were undergraduate and graduate students from the Center for Materials Research.


Local TV Station, Chanel 13 interviewing Dr. Mead, event coordinator. Parents and spectators attending the competition.

S.T.E.M. Career Fairs Outreach Events

We were invited to provide outreach activities and hands on experiments for many STEM career fairs at local K-12 Hampton Roads public schools. Those schools included, Campostella Elementary, School of Science, Technology, Engineering & Math in Norfolk, Ruffner Middle School, Norfolk, and John Tyler Elementary, Portsmouth.

Campostella Elementary, STEM Career Fairs

The table below summarizes our outreach events at this elementary school over the past 3 years:

Year	Date	Audience
2013	March 28th, 2013.	More than 200 minority K-5 students
2014	April 11th, 2014.	More than 100 minority K-5 students
2015	May 1st 2015.	575 Students, > 40 teaching and school staff personnel

Dr. Bahoura introducing the students to the basic concepts of Science though interactive activities and question-answer debate, 2013.

Our hands on activities were the most popular activity at the event. Teachers asked us to visit their schools, 2013.

Graduate students attending the annual STEM career fair and teaching the K-5 students concepts of nanotechnology through hands on activities, 2014.

Dr. Bahoura demonstrating hands STEM activities during the Campostella Elementary School STEM career day, 2015.

We have also reached out to Ruffner Middle School in Norfolk and John Tyler Elementary, Portsmouth.

Ruffner Middle School STEM Career fair

Event:	Ruffner Middle School STEM Career fair
Activity:	Nanotechnology is FUN!
Audience:	> 800 Students
Location:	Ruffner Middle School, Norfolk, VA
Date:	April 2nd, 2015

John Tyler Elementary Career Fair

Event:	John Tyler Elementary Career Fair
Activity:	STEM Hands on Activities
Audience:	> 150 elementary students
Location:	John Tyler Elementary, Portsmouth, VA
Date:	June 5th, 2015

Nano Summer Camp at the Children's Museum of Virginia

In 2013, Dr. Bahoura received a mini grant from NSF-Nanoscale Informal Science Education Network (NISE-funded through the National Science Foundation under Award Number 0940143) to develop a Nano Summer camp at the Children's Museum of Virginia (CMV).

Goals of the Program

- Integrate nanoscience activities into existing summer camps of our partner institution, the Children's Museum of Virginia.
- Introduce students to the basic knowledge of nanotechnology.
- Expose students to interactive and hands on experiments where they become active.
- Shed the light on why the physics of nanotechnology is different from that of macroscopic world.

- Introduce students to the tools used in nanotechnology and discuss the societal, economical and ethical issues and impact of nanotechnology.

Schedule

Our project consisted of two one -week summer camps, incorporating nano activities into the CMV summer camp framework. One week was offered to an underserved 5th grade class from a school in Portsmouth, VA, which had previously struggled in passing standardized science tests. Those students scoring at a certain level were offered a chance to register for camp. The NISE grant funded the transportation from the school to the museum, and returning to school.

The camp ran Monday through Thursday from 9 am -12 pm for a maxium of 15 students. The second week of camp was a nano-oriented camp open to the general public, ages 9-12 years. This camp ran Monday through Friday, 9 am -12 pm for 9 students.

Audience Description

The CMV is the largest children's museum in Virginia and serves the metropolitan area of Hampton Roads. The CMV strategic location in Portsmouth allowed reaching out to a diverse and multicultural audience, notably underserved students from Portsmouth are African American, of low socio-economic status. They are 11-12 year olds with extended family being the primary caregivers. Campers in the public camp were 9-12 years of age, of varying ethnicity and socio-economic backgrounds. Half of the campers have previously attended a science camp at the museum.

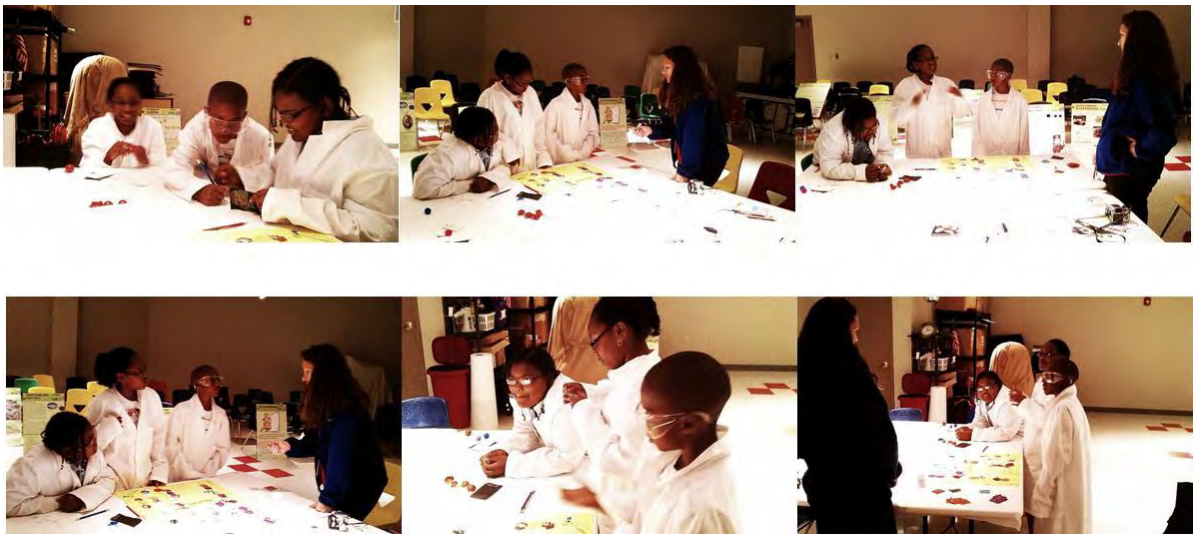

First Nano Summer camp at the Children's Museum of Virginia, 2013.

Second Nano Summer Camp at the Children's Museum of Virginia, 2013.

Science is Alive Day

In September 29, 2012, Dr. Bahoura presented Nanotechnology activities and demonstrations to girl scouts at the "Science is Alive Day", NSU, We reached more than 300 girl scouts.

Dr. Bahoura with a group of girl scouts after the end of the hands on demonstrations.

Dr. Bahoura explaining the scales and why the blue morph butterfly has blue wings. The girl scouts were surprised by the magic sand and the nano-sun screen behavior.

Dr. Bahoura demonstrating a hydrogen car and the infectiveness of gravity at the nanoscale.

Girl scouts learning about the tools used in nanotechnology such as Atomic Force microscope and playing nano-interactive game.

In 2014, we participated at the same event and we reached 70 girl scouts.

Event	Science Alive
Activity	Display and exhibit of nanotechnology hands on experiments
Audience	70 Girls Scouts' ages 4-17
Location	Student Center , Norfolk State University
Date	September 27th, 2014.

Cooperating Hampton Roads Organizations for Minorities in Engineering

Dr. Bahoura presented hands on Nanotechnologies related activities to more than twenty Elementary, Middle and High school teachers attending the *CHROME transformers-STEM, The Annual Cooperating Hampton Roads Organizations for Minorities in Engineering (CHROME) Sponsor Launch.* NSU, *October 6, 2012.*

Dr. Bahoura instructing teachers on how to explain nanotechnology concepts through hands on activities.

Dr. Bahoura showing teachers on how to incorporate nanotechnology into their STEM curricula.

NSU-STEP STEM Day

NSU hosted the NSU- STEP, STEM Day on campus on May 11, 2013.This is a STEM educational program for junior and senior high school students. It provides the students with opportunities to broaden, enhance, and develop an increased interest in the science, engineering, and technology fields. Activities such as SAT Prep courses and college tours are designed to expose the students to the various processes required for college admissions and college success. Students participate in an on-campus internship experience during the summer months.

Dr. Bahoura presented 15 hands on activities about "introduction to Nanotechnology" for more than 50 middle and high school students.

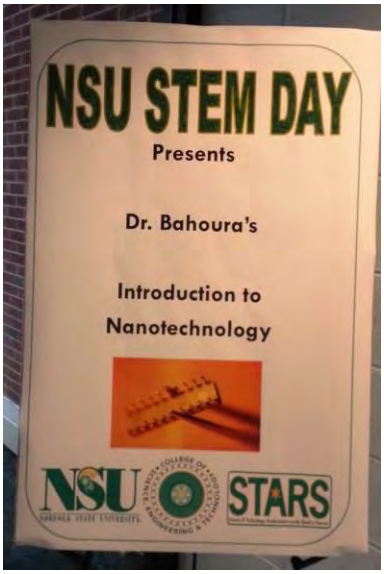

Dr. Bahoura demonstrating hands on activities to the participating students.

Demonstration using simulation and multimedia.

Students participating in activities.

"Gear up for college", Gear up summer academy 2013"

NSU hosted the "Gear up for college" summer academy where close to 70 minority high school students from Phoebus and Hampton high schools spent three days on the NSU campus to take a closer look at college, June 17-19, 2013, 8am-3pm. Besides exposing students to science, technology, engineering and mathematics (STEM), students also get a taste of campus life, learn about financial aid, academic degrees and the admissions process.

Dr. Bahoura, Ms. Anderson (Chemistry) and two graduate students presented a variety of hands on activity about nanotechnology and showed the students what is unique about some materials at the nano-scale. Activities included demonstration about size scales and understanding how small the nanometer is using a nanometer ruler and size comparison to objects they know. The unique properties at the nanoscale were introduced to the students by having them think about the action of gravity and electrostatic electricity on different sides of beads as well as the action of gravity in water in a regular cup and in miniature cup.

The students were very engaged and having fun learning about nanotechnology. When we asked them about their plans after high school graduation, the majority said that they will go to college and they will consider NSU as first choice.

Students learning about application of nanotechnology in water filtration and discovering bracelets that contain photochromic dye and change colors when exposed to ultraviolet light.

Dr. Bahoura demonstrating a Hydrogel material in which students discover how a super absorbing material can be used to move a straw. They learn that hydrogels can be used on the nanoscale in a similar fashion to manipulate tiny structures.

Dr. Bahoura demonstrating electrostatic electricity principles to the students.

Students experimenting with the nano sand and its ability to not get wet

Students putting together a car that runs on hydrogen using a tank of water. Students are intrigued about the fact that, tiny scent molecules will be leaking out of balloons.

Students investigate the hydrophobic properties of pants made from nano fabric and ordinary fabric. Dr. Bahoura explaining why nanoparticles of gold can appear red, orange or even blue. They learn that a material can act differently when it's nanometer-sized.

Health and Science Summer Academy

The Health and Science Summer Academy is a two-week non-residential academic enrichment program for motivated middle and high school students. It provides academic and laboratory activities and field trips. We participated in the 2013 and 2014 Health and Science Summer Academy hosted to NSU.

Year	Dates	Audience
2013	June 14th- June 28th	32 minority high school students
2014	July 7th- 17th	27 minority middle school students

Dr. Bahoura developed structured nanotechnology module for the participating high school students based on a series of lectures and interactive hands on activities. The nanotechnology module does not require any previous knowledge of the field of nanotechnology and therefore is open to students from all backgrounds. The students were able to gain a comprehensive understanding about nanotechnology through activities that introduce them to the unique properties at the nanoscale. The module included video demonstrations and interactive media. The students were exposed to the interdisciplinary aspect of Nanotechnology/Nanoscience with other disciplines. In addition, the module included discussion groups on societal and ethical implications of nanoscience/nanotechnology.

Topics covered

- Introduction to Nanoscience and Scale of Objects.
- Unique Properties at the Nanoscale
- Tools of Nanotechnology
- Applications of Nanotechnology

Outcomes of the module

- The module sparked student's interest in Nanoscience, introduced them to common terminology, and got them to start thinking about issues of size and scale.
- Students participated in learning activities that are designed to help them to establish an understanding of the nature of nanoscale science, the relative size of objects, unique properties of nanosized particles, and applications of nanoscience.
- Students were introduced to two of the most widely used new probe imaging tools.
- This lesson introduced students to applications of nanoscience, explores how nanoscale science and engineering could improve our lives, and describes some potential risks of nanotechnology.

Assessment: Students were assessed through in class quizzes and homework.

The two groups of high school students, 2013.

Dr. Bahoura giving a talk about what nanotechnology is, its unique properties, the tools used in nanotechnology and applications in real life, 2013.

Dr. Bahoura demonstrating "magic sand". Students explore how water behaves differently when it comes in contact with nano sand and regular sand, 2013.

Dr. Bahoura demonstrating electrostatic electricity versus gravity force at the nanoscale, 2013.

Students exploring the color changing of nano gold, lean about the application of nano-sized whiskers can protect clothing from stains, comparing sunblock containing nanoparticles to ointment, and experiment with UV bracelets that change color when exposed to UV light, 2013.

Students discover how a super absorbing material "hydrogel" can be used to absorb 40 times its own weight, 2013.

For the 2014 Health and Science Summer Academy, we hosted 27 minority middle school

students, split into two groups. There were two sessions a day for each group for 3 days period.

The two groups of middle school students, 2014.

The scale and sizes concepts were introduced to the students through the scented balloons and ball sorter activity. In scented balloons activity students use their sense of smell to explore the world on the nanoscale. They learn that we can smell some things that are too small to see, and that a nanometer is a billionth of a meter. In the ball sorter activity, the students use sieves with different-sized holes, to sort balls by size. They learn that researchers are developing new technologies that can sort nano-sized things, including filters with nano-sized holes, 2014.

The students learned that size can affect the way a material behaves by performing the exploring forces activity, 2014.

The students explored the properties at the nanoscale by understanding the concepts of surface area. Another activity, UV Bracelets, where the students uses ultraviolet light to change the color of beads that contain photochromic dye, 2014.

Students explored examples of nanomaterials. In the "Magic Sand" activity, students learned how changing nanoscale changes in a material can affect how that material behaves at the macroscale. In another example, students explored Hydrogel and discovered how a super absorbing material can be used to move a straw. The students also explored the properties of a memory metal spring (NitTiNol) to an ordinary spring, 2014.

When the students were asked to build a Lego structure while wearing mittens they learned that is difficult to build small things when your tools are too big. Then, the students were introduced to the concept of a scanning probe microscope (SPM) though the use of a flexible magnet, 2014.

CSET Saturday Scientists

The Saturday Scientists program was developed by the College of Science, Engineering and Technology (CSET) in 1993 to improve student performance and foster student interest in biology, chemistry and physics through practical applications. The program aims to prepare high school students for college. The participants are high school junior and senior students selected for participation through their teacher's recommendation. Students are assigned to a CSET academic area based on their current high school course schedule. This is an eight session program where the students meet two Saturdays per month during the semester. The students meet in the classrooms and laboratories on the campus of Norfolk State University to participate in college level enrichment activities and hands-on laboratory work.

The objectives of the program are:

- To develop student's appreciation for science and technology while encouraging them to declare such as a major.
- To give students the opportunity to experience university academics while facilitating mentoring relationships between university scientists and program participants.
- To promote academic achievements in math, science and computer literacy while introducing them to the use of educational technologies that complement and strengthen their course curricula.

Dr. Bahoura presented hands on activities entitled “Exploring the Nanoworld” for the CSET Saturday Scientists to 18 High school students on October 19th, Nov. 9th, 23rd 2013 and May 3rd, 2014 at NSU. The students were introduced to principles of nanotechnology using presentations and animations as well as interactive activities using hands on experimental kits.

Dr. Bahoura presenting the fundamentals of nanotechnology though presentations, animations and questions/answers to the high schools students.

The students carried out experiments and measurements related to nanotechnology concepts such AFM, surface to volume area, and they were introduced to the dominant objects, tools, models and forces at different scales.

Dr. Bahoura showing the students how Nitinol spring returns to its original shape when heated but the steel spring doesn't. Also, how changing nanoscale changes in a material can affect how that material behaves at the macroscale. Dr. Bahoura introduced the students to renewable energies by demonstrating a hydro car on clean hydrogen that runs on fuel using a PEM fuel cell.

The Amazing World of Science

The Amazing World of Science is a free opportunity for children ages 6-12 to learn about STEM in a fun way. This outreach event was held on July 15th from 10am-5 pm. at the Hampton Convention, Hampton, VA. The event attracted more than 200 visitors ages 4-70 years old, from different background and ethnically diverse. We presented hands on activities about the amazing world of nanotechnology where the visitors experimented with the "magic" nonosand, played with ferrofluid, explored the color of blue morph butterfly, and they wrote their names in binary language using magnets. The visitors rotated through each station with a time frame of 30 minutes per station. The visitors were curious and asked many questions and many parents asked us to come to their children's schools to deliver these types of STEM outreach activities. The event concluded with drawings and prizes for the children.

Event:	The Amazing World of Science
Activity	Display and exhibit of nanotechnology hands on experiments
Audience	More than 200 children as young as 4
Location	Campostella Elementary, School of Science, Technology, Engineering & Math
Date	April 11th, 2014.

Group pictures of children attendees with many military parents.

Children and parents participating in hands on activities of various stations.

Bite of Science Program

Dr. Bahoura was invited by the Center for Excellence in Education (CEE) to give a workshop for the "Bite of Science Program" to 35 high school teachers from different Hampton Roads area public schools on October 2, 2014. This is a teacher enrichment program, with presentations focusing on educational approaches and methods in the science classroom that are creative and unique. Dr. Bahoura introduced the teachers to nanotechnology and shared with them resources and best practices to include and embed STEM activities in their classrooms. This program sparked the interest of many high school teachers and new partnerships were formed.

Public schools visits to NSU

In addition to providing outreach activities off campus, we delivered activities to high school students visiting the NSU campus. In 2014 we hosted the Richmond Public Schools (RPS) Governor's CTE Academy for STEM students and in 2015 the Grassfield High School students.

Richmond Public Schools (RPS) Governor's CTE Academy for STEM

Event	**Richmond Public Schools (RPS) Governor's CTE Academy for STEM Visit**
Activity	STEM and nanotechnology hands on experiments
Audience	> 20 Students
Location	Center for Materials Research, Norfolk State University
Date	November 12th, 2014.

Grassfield High School Visit

Event	**Grassfield High School Visit**
Activity	STEM hands on experiments
Audience	35 Students: Freshmen, Juniors and Seniors
Location	Center for Materials Research, Norfolk State University
Date	March 18th, 2015

Time out 4U STEM Symposium

Event:	**Time Out 4U STEM Symposium**
Activity:	STEM Hands on Activities
Audience:	> 30 5th-9th Graders
Location:	Performance Arts and Teen Center, Hampton VA
Date:	May 16th, 2015

4. IMPACT OF INFRASTRUCTURE DEVELOPMENT

This grant allowed us to acquire an Electron Beam Evaporation (EBE) system from AJA International Inc., Model ATC-2400H, which is the best system that would meet our research needs and was within our budget. The EBE system facilitates the growth of high-performance films and multilayers over large area substrates.The system that we have chosen from AJA is outfitted with a Thermal Evaporation Source that is needed to deposit metallic films and contacts for electrical measurements. The AJA Evaporation System has the following unique features:

- The chamber has an integral removable base plate that can accommodate alternative base plates with different deposition components (Thermal/Sputtering). This modular feature ensures it versatility in a multi user facility.
- Modular system design allows addition of multiple components to be implemented after purchase including load-lock, 6-position cassette, and different types of substrate holders (H_2O, LN_2, heating).
- All bought in components (e-guns, power supplies, vacuum pumps, gate valve) are state of the art, top level equipment made from the leading manufacturers in the industry.

- The AJA substrate heater allows simultaneous, heating, rotation, biasing, z-motion and deposition at up to 850°C in a pure oxygen environment. Stability is +/- 1 degree C, Uniformity over 4" is better than +/- 1.4 percent.
  Graduate students and undergraduate students were trained on the operation and maintenance of the EBE system by an AJA International Inc. field service engineer. The students are able to run the system and grow different materials with little supervision. To enhance collaboration with other groups at the Center for Materials Research, the EBE system has been used, under our supervision, by students and researchers from other groups to advance their materials deposition and growth. The EBE system enhanced the existing capability of the CMR as it is the only system of its kind on Campus.

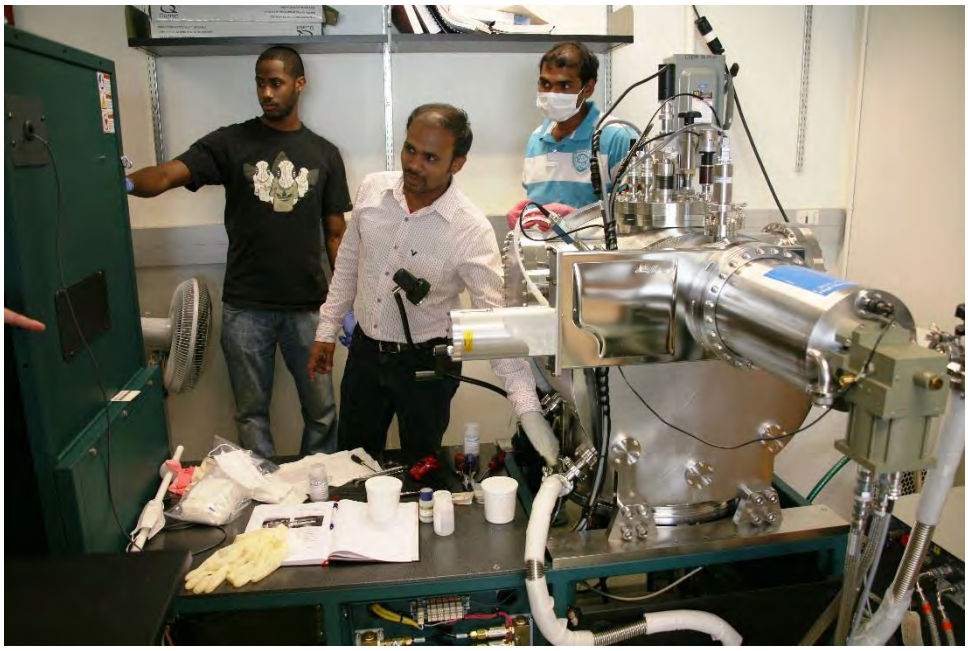

Graduate students, from left, Casey Gonder, Rajini Konda and Hareesh Dondapati using the EBE system.